This is to certify that the
thesis entitled

ESTIMATING THE NATURE AND DISTRIBUTION OF
SHALLOW SUBSURFACE PALEOSOLS ON FLUVIAL FANS
IN THE SAN JOAQUIN VALLEY, CALIFORNIA

presented by

GEORGE LUTHER BENNETT V

has been accepted towards fulfillment
of the requirements for the

Master of Science degree in Geology

Major Professor's Signature

13 November 2003

Date

PLACE IN RETURN BOX to remove this checkout from your record.
TO AVOID FINES return on or before date due.
MAY BE RECALLED with earlier due date if requested.

DATE DUE	DATE DUE	DATE DUE

6/01 c:/CIRC/DateDue.p65-p.15

ESTIMATING
PALEOSOLS C

ESTIMATING THE NATURE AND DISTRIBUTION OF SHALLOW SUBSURFACE PALEOSOLS ON FLUVIAL FANS IN THE SAN JOAQUIN VALLEY, CALIFORNIA

By

George Luther Bennett V

A THESIS

Submitted to
Michigan State University
in partial fulfillment of the requirements
for the degree of

MASTER OF SCIENCE

Department of Geology

2003

ESTIMATING T
PALEOSOLS O

Fluvial fa
sediment sequen
et al. 2002). The
pedogenically a
believed to be
and 2) continu
during glacial
the Kings, Me
is a regionally
paleochannel
identified in t
different fact
drainage are
between the

ABSTRACT

ESTIMATING THE NATURE AND DISTRIBUTION OF SHALLOW SUBSURFACE PALEOSOLS ON FLUVIAL FANS IN THE SAN JOAQUIN VALLEY, CALIFORNIA

By

George Luther Bennett V

Fluvial fans in the San Joaquin Valley, California are composed of multiple sediment sequences separated by unconformable surfaces (Weissmann, 1999; Weissmann et al. 2002). The individual sequences are composed of channel, overbank, and pedogenically altered sediments. The pedogenically-altered deposits (paleosols) are believed to be 1) laterally continuous sequence stratigraphic bounding unconformities and 2) continuous with the exception of discrete breaks caused by paleochannel activity during glacial times. Using ground-penetrating radar and digitized county soil surveys on the Kings, Merced, and Tuolumne River fluvial fans we show that the Riverbank paleosol is a regionally laterally continuous feature and that discrete erosional breaks due to paleochannel activity do exist in the Kings River fluvial fan. Erosional breaks were not identified in the Merced or Tuolumne River fluvial fans. It is believed that a number of different factors including, basinal subsidence differences, stream base-level, Sierran drainage area, and sediment supply play a role in the morphological differences observed between the Kings, Merced, and Tuolumne River fluvial fans.

This resea
Chemical Society
Baker and the ge
and data provided
the work done at
possible without
of Geological S
thank Karen Bu
USGS whom I
this project. Co
in the understan

I wish t
and Phanikuma
keep me moti
met so many
here. Yet for t
I am now. I sh
were always
Norris for he

ACKNOWLEDGMENTS

This research was supported by the Petroleum Research Fund, American Chemical Society (PRF #37731-G8). I benefited greatly from discussions with Greg Baker and the geophysics students at SUNY, Buffalo. In addition, conversations with, and data provided by Thomas Harter and Sevim Onsoy greatly improved the caliber of the work done at the Kearney Agricultural Center. Also, this work would not have been possible without the GPR equipment provided by Dr. Detlef Warnke and the Department of Geological Sciences, California State University, Hayward. Lastly, I would like to thank Karen Burrow, Barbara Dawson, Jill Judy-Densmore, and Mike Wright of the USGS whom I worked with during an internship following the GPR data collection for this project. Conversations with and data provided by Karen Burrow and the USGS aided in the understanding of this work.

I wish to sincerely thank my thesis committee, Gary Weissmann, Dave Hyndman, and Phanikumar Mantha. Their enthusiasm for this project, especially Gary's, helped to keep me motivated while slogging through our enormous data set. I feel blessed to have met so many wonderful people here at MSU that I regret I am unable to mention them all here. Yet for those of you who read this, know that in some way you helped me get where I am now. I should also acknowledge our office staff, Loretta, Cathy, and Jackie, who were always helpful and supportive. Last, but by no means least, I wish to thank Sarah Norris for her never-ending support.

TABLE OF CONTENTS

Table 2.1 Approxim
materials. (Data fron

Table C1 Table listi
and location in Degr

LIST OF TABLES

LIST OF FIGURES

(Images in this thesis are presented in color.)

The fluvia
in the Central Va
for irrigation and
architecture contr
shown that the typ
sequences separat
2002a). The indiv
river forming the
or floodplain dep
formation proces
et al. 2002a). Th
the unconformab
Additionally, the
aquifers since th
distributed over
Weissmann et al

Ground-
lateral continuit
(TRF), and the
tool when attem

CHAPTER ONE

INTRODUCTION

The fluvial fans located along the western margin of the Sierra Nevada Mountains in the Central Valley of California contain aquifers that are significant sources of water for irrigation and municipal use. In these fluvial hydrologic systems, the sediment's architecture controls fluid flow. Recent work on the Kings River fluvial fan (KRF) has shown that the typical framework for the fluvial fan deposits consists of multiple sequences separated by unconformable surfaces (Weissmann, 1999; Weissmann et al. 2002a). The individual sequences are composed of channel sediments from the primary river forming the fluvial fan, overbank sediments which result from levee, crevasse splay, or floodplain deposition, and pedogenically-altered deposits, which result from soil formation processes during times of depositional hiatus (Weissmann, 1999; Weissmann et al. 2002a). The pedogenically-altered deposits, or paleosols (ancient soils), represent the unconformable surface (depositional hiatus) that separates the sequences. Additionally, they probably exert a profound control on fluid flow within the fluvial fan aquifers since they are composed of clay rich (low conductivity) sediments and are distributed over large areas and are acting as confining layers (Weissmann, 1999; Weissmann et al. *in press*).

Ground-penetrating radar (GPR) was utilized in this study to estimate the regional lateral continuity of the near-surface paleosols on the KRF, Tuolumne River fluvial fan (TRF), and the Merced River fluvial fan (MRF). GPR has been shown to be an effective tool when attempting to track the lateral extent of silt and clay layers in KRF by Burrow et al. (1997). In th

techniques (GPR

methods, provide

framework of the

continuity of a ne

paleosol that repr

al. (2002a).

Additional

the KRF. We beli

facies) at the Kear

Parlier, CA on the

as a tool in facies

Huggenberger, 19

GPR and a series

Harter et al. (199

above the near su

Lastly, in a

the KRF, TRF, an

TRF exhibit subtl

significance when

fluvial aquifers. T

act as groundwate

head builds up, be

et al. (1997). In their study, Burow et al. (1997) showed that surface geophysical techniques (GPR and Seismic Reflection), combined with geologic coring and borehole methods, provided a means to more extensively characterize the sedimentological framework of the KRF. Using GPR, Burow et al. (1997) successfully mapped the continuity of a near-surface fine-grained layer, which we believe to be the near surface paleosol that represents a sequence stratigraphic boundary hypothesized by Weissmann et al. (2002a).

Additionally, we evaluated the application of GPR to recognize the radar facies in the KRF. We believe that GPR may be used for the recognition of facies patterns (radar facies) at the Kearney Agricultural Center (KAC), a small-scale study site southeast of Parlier, CA on the KRF. Various studies in the past have shown the applicability of GPR as a tool in facies interpretation (e.g. Beres & Haeni, 1991; Jol & Smith, 1991; Huggenberger, 1993; Jakobsen & Overgaard, 2002). In this portion of the study we used GPR and a series of closely spaced wells cored and described for a vadose zone nitrate by Harter et al. (1999) in an attempt to extrapolate hydrogeologic facies to a depth of 6 m above the near surface paleosol at the Kearney Field Station.

Lastly, in attempting to evaluate the lateral extent of the near surface paleosols on the KRF, TRF, and MRF it is observed that the near surface paleosols on the KRF and TRF exhibit subtle topography. The implications of this observation may be of significance when attempting to estimate the locations of significant recharge in these fluvial aquifers. Topographic lows in the surface of this near surface confining layer may act as groundwater collection areas (depression storage) and thus, once the hydraulic head builds up, be the locations where water is forced through the confining layer into deeper aquifer u

developing futur

The follo

1) Near-s

featur

2) Breaks

distrib

3) Mean w

paleoc

4) GPR al

near-su

We will al

the KRF, TRF, an

including, but not

and Sierran draina

To test the

geologic well borin

Burrow et al. (1997

deeper aquifer units. Future groundwater models may want to consider this when developing future models to characterize these systems.

THESIS HYPOTHESES

The following hypotheses are the primary focus of this work:

1) Near-surface paleosols on the KRF, TRF and MRF are laterally-extensive features, on a regional scale.

2) Breaks exist in these near-surface paleosols which can be attributed to distributary paleochannels that are active early during aggradational events.

3) Mean widths and geometries (width and orientation) of the identified paleochannels can be estimated from the GPR data.

4) GPR allows for the recognition of facies patterns in the sediments above the near-surface paleosol (Radar Facies) on the KRF.

We will also comment on and evaluate any morphological differences between the KRF, TRF, and MRF, which could be attributed to a number of different factors, including, but not limited to, basinal subsidence, channel morphology and sedimentation, and Sierran drainage area.

METHODS

To test the first three hypotheses, large-scale GPR surveys combined with geologic well borings and interpreted county soil surveys were utilized. It was shown by Burrow et al. (1997) that a combination of geophysical techniques, along with standard hydrologic met

aquifer systems

GPR su

lateral extent of

Profiles were ru

volume on the u

towed behind a

1.1). Once colle

well logs. Post p

contrast betweer

paleosol layer w

widths of the bre

Figure 1.1 Ground
console, laptop com
and 100 MHz anten
rechargeable 6-V ba
charge, while doing

hydrologic methods, produce a more extensive understanding of sediment architecture in aquifer systems situated in fluvial settings.

GPR surveys were collected along km scale profiles that attempted to track the lateral extent of the near-surface paleosol as well as identify breaks in its continuity. Profiles were run along roads that provided long uninterrupted stretches and low traffic volume on the upper portions of all three fluvial fan surfaces. The GPR equipment was towed behind a car, and, in one case, a tractor, to facilitate rapid data acquisition (Figure 1.1). Once collected, the data were processed, plotted and compared with soil surveys and well logs. Post processing of the GPR data was limited and focused on enhancing the contrast between areas of shallow and deep signal penetration. Widths of breaks in the paleosol layer were measured and plotted to gain a better understanding of the mean widths of the breaks for later use in geostatistical groundwater modeling.

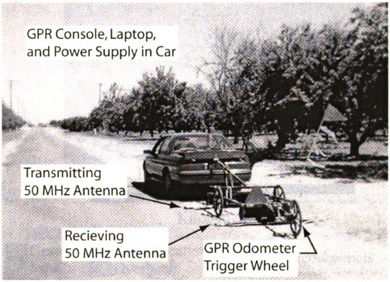

Figure 1.1 Ground penetrating radar system field setup in profiling mode. The system includes a console, laptop computer, 12-V battery power source (all located in car), and interchangeable 50 and 100 MHz antennae (50 MHz attached in photo). The GPR antennae were powered using two rechargeable 6-V batteries (chargers in trunk of car). Operational life of the batteries at full charge, while doing long profiles (km length) averaged approximately 45 minutes.

County

paleochannels

iocations could

increased depth

Figure 1.2 C-

paleochannel

County soil surveys were used to highlight the location of "outcropping" paleochannels on the KRF, TRF, and MRF. Using the C-horizon textures, paleochannel locations could be identified (Weissmann et al., 2002a) and compared with areas of increased depth of penetration observed in the GPR profiles (Figure 1.2).

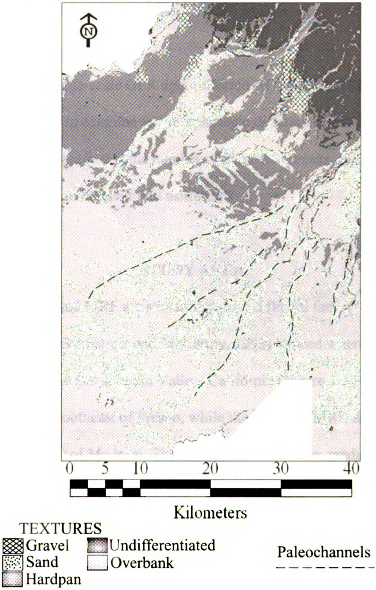

Figure 1.2 C-horizon texture map of the upper KRF. Dotted lines indicate interpreted paleochannel locations. (Map modified from Huntington, 1971).

Geologic

by Gary Weissm

(UCDavis) at nur

lithologic well lo

(hypothesis four)

paleosols in that s

Comparin

provides the oppo

fluvial fans. We h

and location on th

The KRF,

"braided river fan"

the Sierra Nevada

the San Joaquin Va

Valley east and sou

0.002 on the KRF a

southwest on the K

and TRF areas are a

(Burow et al., 1999

personal communic

Geologic well log analysis consisted of lithologic cores collected and described by Gary Weissmann (MSU), Thomas Harter, Sevim Onsoy, and Katrin Heeren (UCDavis) at numerous sites on the KRF (Harter et al., 1999; Weissmann, 1999). These lithologic well logs provided the groundtruth necessary to verify the radar facies patterns (hypothesis four) as well as the presence or absence and average depth of the near-surface paleosols in that specific location.

Comparing the large-scale GPR data collected on the KRF, TRF, and MRF provides the opportunity to examine any morphologic differences between the three fluvial fans. We hope to show that the number of identified breaks, their mean widths, and location on the fan can be identified using GPR.

STUDY AREA

The KRF, TRF, and MRF are stream-dominated fluvial fans ("losimean fan" to "braided river fan" after Stanistreet and McCarthy, 1993) located where their rivers leave the Sierra Nevada into the San Joaquin Valley, California (Figure 1.3). The KRF enters the San Joaquin Valley southeast of Fresno, while the TRF and MRF enter the Central Valley east and southeast of Modesto. The fluvial fans are of low gradient (approximately 0.002 on the KRF and 0.003 on the TRF and MRF), with the drainages trending west to southwest on the KRF and MRF, while drainage on the TRF trends more west. The KRF and TRF areas are also the sites of ongoing hydrostratigraphic characterization studies (Burow et al., 1999; Weissmann et al., 1999, 2002b; Weissmann and Fogg, 1999; Burow, personal communication).

Figure 1.3 Locatio
abandoned paleoc
30m Digital Eleva

Repeated
has created reco
Marchand, 1977
Harden, 1987; V
preserve those f
2002a). Variabl

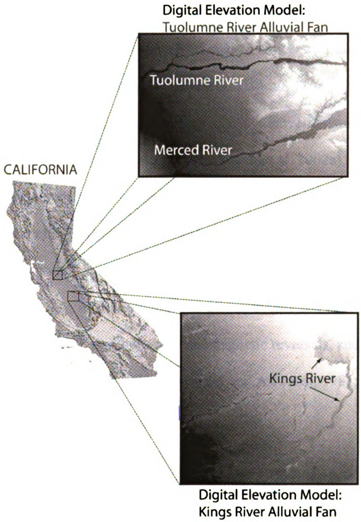

Figure 1.3 Locations of KRF, TRF and MRF within the San Joaquin Valley of California. (Note abandoned paleochannels visible on KRF digital elevation model) Background map are USGS 30m Digital Elevation Models.

Repeated glaciation and deglaciation of the Sierra Nevada during the Pleistocene has created recognizable cycles (sequences) of sediment deposition (Janda, 1966; Marchand, 1977; Huntington, 1980; Marchand and Allwardt, 1981; Lettis, 1982, 1988; Harden, 1987; Weissmann et al. 2002a) with San Joaquin basin subsidence acting to preserve those fan deposits (Lettis, 1982; Lettis and Unruh, 1991; Weissmann et al., 2002a). Variable subsidence rates for the northern and southern San Joaquin Valley, as reported by Lett

TRF and MRF 1.

KRF (0.2 m ka a

been recognized

(Huntington, 197

sequences descri

Marchand, 1977;

Weissmann, pers

eastern San Joaqu

based on fossil ev

dating (Arkley, 1

Lettis, 1982, 198

Weissman

the KRF. In this

the repeated Pleis

approach, stratigr

where the sequen

related strata bou

conformities" (M

on the TRF and M

reported by Lettis and Unruh (1991), may affect the morphology of the fluvial fans. The TRF and MRF lay further north and have experienced a slower subsidence rate than the KRF (0.2 m/ka and 0.4 m/ka respectively) (Lettis and Unruh, 1991). Sequences have been recognized on the KRF through subsurface analysis as well as soil mapping (Huntington, 1971,1980; Weissmann, 1999; Weissmann et al. 2002a), with similar sequences described on other eastern San Joaquin Valley fluvial fans (Janda, 1966; Marchand, 1977; Marchand and Allwardt, 1981; Harden, 1987; Lettis, 1982, 1988; Weissmann, personal communication). These sequences have been correlated along the eastern San Joaquin Valley, with correlations to glacial events and approximate ages based on fossil evidence, soil morphology, paleomagnetic reversals, and limited ash dating (Arkley, 1962; Huntington, 1980; Marchand and Allwardt, 1981; Harden, 1987; Lettis, 1982, 1988).

SEQUENCE STRATIGRAPHY

Weissmann et al. (2002a) proposed a sequence stratigraphic conceptual model for the KRF. In this work, they related the episodes of aggradation and erosion on the KRF to the repeated Pleistocene glaciations of the Sierra Nevada (Figure 1.4). Using this approach, stratigraphic successions are framed within chronostratigraphic *sequences*, where the sequence is defined as "...a relatively conformable succession of genetically related strata bounded at its top and its base by unconformities, or their correlative conformities" (Mitchum, 1977, p.210). Similar sequences have recently been recognized on the TRF and MRF (Weissmann, personal communication).

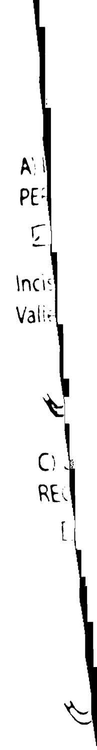

Figure 1.4 Sequen
A) Low accumula
Decrease in accur

In each
sediment seque
during intergla
during the san
recognized or
and Allwardt,
Laguna, Turl
Allwardt, 19
TRF represe
will later be

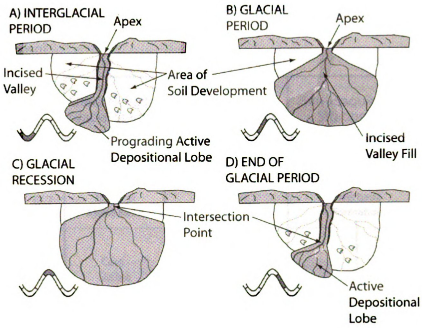

Figure 1.4 Sequence stratigraphic cycles on the KRF as interpreted by Weissmann et al. (2002). A) Low accumulation space. B) Increase in accumulation space. C) High accumulation space. D) Decrease in accumulation space. (Modified from Weissmann et al. 2002)

In each of the fluvial fans the unconformity that bounds the top and base of the sediment sequences are represented by a paleosol that developed on the fluvial fans during interglacial periods (Figure 1.4A), as well as the base of incised valleys formed during the same period. Five episodes of aggradation and progradation have been recognized on the Kings River fluvial fan (Marchand, 1977; Huntington, 1980; Marchand and Allwardt, 1981; Lettis, 1982, 1988). From oldest to youngest these include the Laguna, Turlock Lake, Riverbank, Modesto, and post-Modesto deposits (Marchand and Allwardt, 1981; Lettis, 1988) (Figure 1.5). What we see exposed today on the KRF and TRF represents the post-Modesto interglacial period, therefore, the soils developing today will later become a sequence boundary once a new glaciation begins. GPR profiles from

Figure 1.5 Stratigra
1958) showing the
Weissmann et al. (2

While wor
understand the co
(controlled by eus
accumulation, also
accommodation sp

this study focused one of the near-surface sequence bounding unconformities, the Riverbank paleosol.

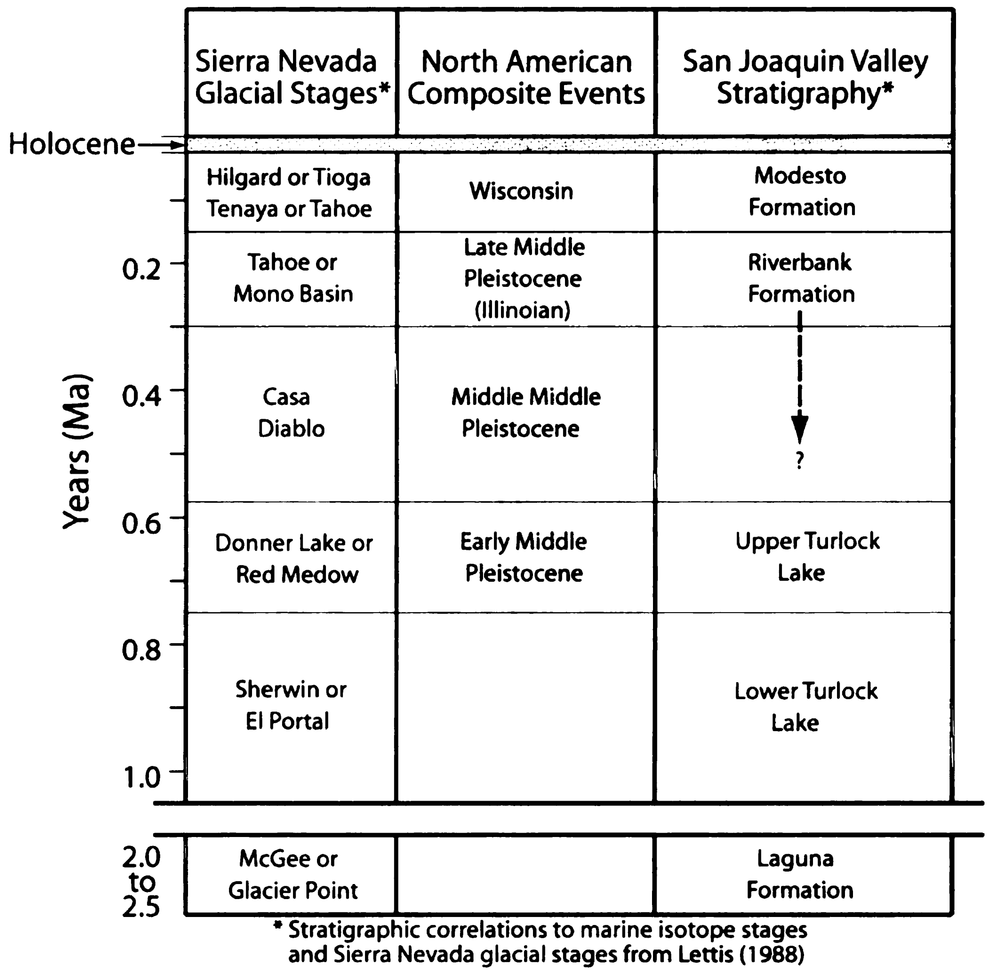

Figure 1.5 Stratigraphic column for the KRF (based on Marchand and Allwardt, 1981; Lettis 1988) showing the five "sequences" described by Weissmann et al. 2002. (Modified from Weissmann et al. (2002))

While working within the sequence stratigraphic framework, it is important to understand the controls on sequence development. In a marine setting, relative sea level (controlled by eustatic sea level and tectonics) defines the space available for sediment accumulation, also known as accommodation space. In the fluvial continental setting, accommodation space should be viewed as a combination of two different concepts, *accumulation sp*

system. *accumu*

where this ratio

Accumulation sp

accumulation sp

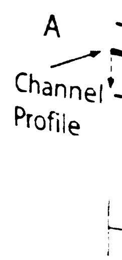

Figure 1.6 Accum
features. (Modified

In the fluv

accumulation fron

accumulation space and *preservation space* (Blum and Törnqvist, 2000). In a fluvial system, *accumulation space* is controlled by the ratio of sediment supply to discharge, where this ratio controls whether the system is aggrading, degrading, or at grade. Accumulation space exists while aggradation occurs in the system, while negative accumulation space exists when degradation is occurring.

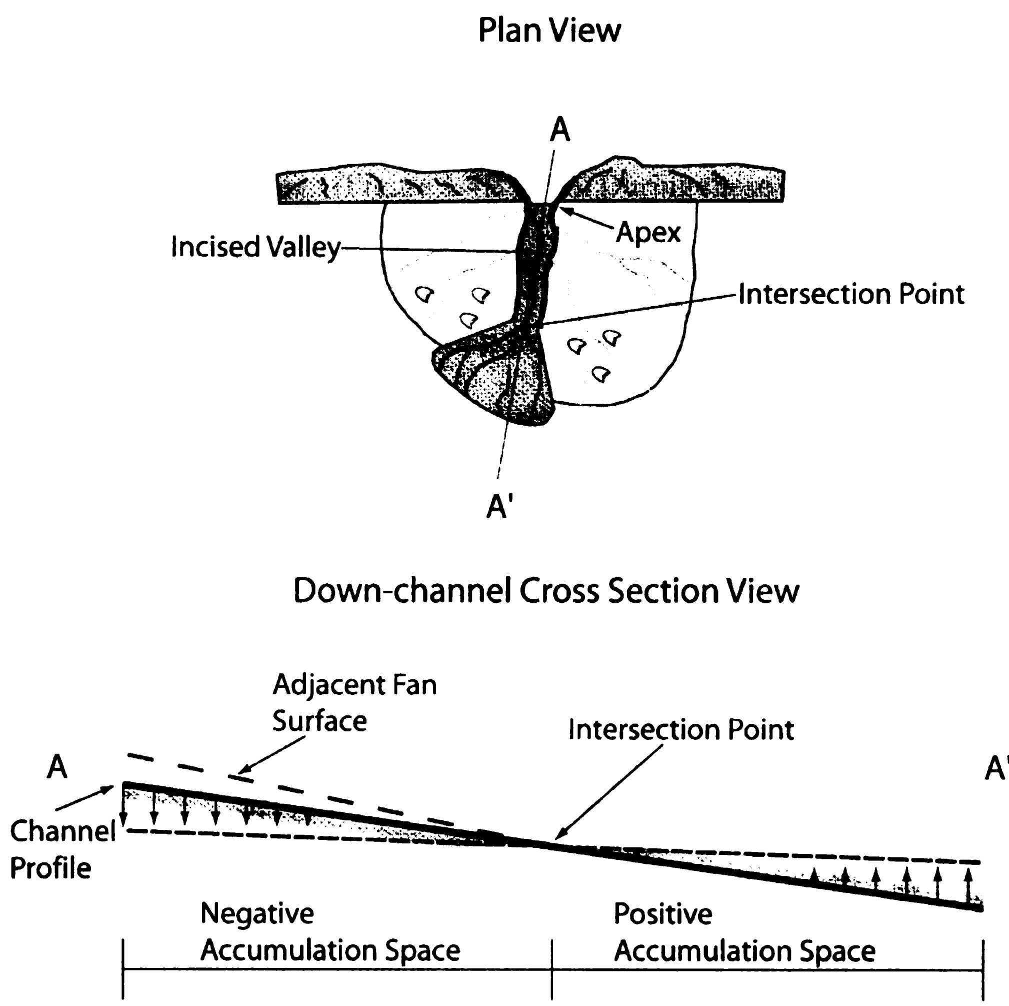

Figure 1.6 Accumulation space on fluvial fans relative to the fluvial fan surface and other fan features. (Modified from Weissmann et al. (2002))

In the fluvial fan setting, the morphologic feature that separates areas of positive accumulation from areas of negative accumulation is the intersection point (Figure 1.6)

(Weissmann et

exists, as shown

the intersection

indicating positi

intersection poin

sediment supply

accumulation spa

near the apex of

deposition occur

space (interglaci

which the river

to upper fan reg

What is signific

bases that devel

sequence bound

Blum a

as occurring "..

and removal".

in fluvial settin

preserved in th

This document

(Weissmann et al., 2002a). Above the intersection point, negative accumulation space exists, as shown by the fact that the river is constrained within an incised valley. Below the intersection point, aggradation occurs in the form of an active depositional lobe, thus indicating positive accumulation space. Over the life of the eastern valley fluvial fans, the intersection point has changed position in response to the changing ratio of discharge to sediment supply of the primary river forming the fluvial fan. During times at which accumulation space was at its highest (glacial periods), the intersection point was located near the apex of the fluvial fan (Figure 1.4B & C). During these times, open-fan deposition occurred over large areas of the fan surface. During times of low accumulation space (interglacial periods), the intersection point moved toward the toe of the fan, above which the river became entrenched in an incised valley (Figure 1.4A & D). Thus, the mid to upper fan regions were exposed to soil development, erosion, and eolian reworking. What is significant about this time in the fluvial fans history is that the soils and valley bases that develop during this time will later mark the unconformities that form the sequence boundaries.

Blum and Törnqvist (2000, p.20) describe the development of *preservation space* as occurring "... when subsidence lowers these deposits below possible depths of incision and removal". Therefore positive accumulation space allows the stratigraphic sequences in fluvial settings to form, while the development of preservation space allows them to be preserved in the stratigraphic record.

THESIS OUTLINE

This document is divided into three main sections with subsequent appendices:

- The firs
  run on t
  review o
  chapter
- The seco
  during th
  KAC stu
  discussio
  groundw
  GPR pro
- The thir
  the wor
- The fol
  -
  -
  -
  -
  -
  -

- The first section, covered by Chapter Two, covers the large-scale GPR surveys run on the KRF, TRF and MRF and presents the results of these surveys. A brief review of sequence stratigraphy and GPR methodology is also presented. This chapter also forms the draft of a manuscript that will be submitted for publication.
- The second section, covered by Chapter Three, covers other observations made during the course of this work, including GPR facies pattern recognition at the KAC study area, groundtruth of the paleosol at the KAC using borehole logs, a discussion on near-surface paleosol topography and its implications to future groundwater modeling, as well as a brief discussion of our attempt to automate GPR profile interpretation using MATLAB scripts.
- The third section, covered by Chapter Four, revisits conclusions reached during the work conducted for this thesis.
- The following appendices are attached:
    - Appendix A contains all large-scale raw GPR profiles.
    - Appendix B contains all small-scale raw GPR profiles from the Kearney Site.
    - Appendix C contains all CMP surveys used to determine near-surface GPR signal velocities.
    - Appendix D describes GPR data collection methodology as well as a description of data processing and analysis.
    - Appendix E contains all Matlab scripts developed during work.
    - Appendix F contains metadata and sources for GIS coverages produced to aid in the visualization of this project.

Since its

effective imagin

of near surface s

& Smith, 1991; S

Overgaard, 2002

subsurface that a

In a prev

showed that a ne

tracked using GI

represents a dep

now hypothesiz

sequence stratig

that influences g

al., *in press*) and

transport by pro

determination o

groundwater flo

We inter

CHAPTER TWO

INTRODUCTION

Since its introduction, ground-penetrating radar (GPR) has allowed for quick and effective imaging of the stratigraphy, internal structure, and, in some cases, the lithology of near surface sands and gravels (e.g., Davis & Annan, 1989; Beres & Haeni, 1991; Jol & Smith, 1991; Smith & Jol, 1992; Huggenberger, 1993; Beres et al. 1995; Jakobsen & Overgaard, 2002). GPR produces nearly continuous high-resolution profiles of the subsurface that are similar to those produced using seismic-reflection methods.

In a previous study on the Kings River fluvial fan (KRF), Burrow et al. (1997) showed that a near-surface laterally continuous fine-grained layer could be successfully tracked using GPR. This fine-grained layer was later identified as a paleosol that represents a depositional hiatus on the KRF (Weissmann, et al. 2002a). That paleosol is now hypothesized to be a sequence stratigraphic boundary (Weissmann 2002a). This sequence stratigraphic boundary is hydrologically significant because 1) it is an aquitard that influences groundwater flow and solute transport (Weissmann, 1999; Weissmann et al., *in press*) and 2) breaks in the sequence boundary influence groundwater flow and transport by providing permeable pathways into deep portions of the aquifer. Therefore, determination of break geometry and the causes of these breaks are significant for groundwater flow and contaminant transport modeling.

We intend to show through the use of GPR the following:

1) Tha
and
regi
2) Brea
distr
fluvi
be es
maps
In additio
fluvial fans (TR
morphological d
but not limited t
of data collectio

The KR
"braided river f
leave the Sierra
enters the San
valley east of
the KRF and (
on the KRF a
an area of app

1) That near-surface paleosols on the KRF, Tuolumne River fluvial fan (TRF) and Merced River fluvial fan (MRF) are laterally continuous features, on a regional scale.

2) Breaks exist in these near-surface paleosols, which can be attributed to distributary paleochannels that once carried outwash sediments over the fluvial fans surfaces; and the mean widths and geometries of these breaks can be estimated by combined analysis of GPR profiles and county soil survey maps.

In addition to the above hypotheses we also intend to discuss how the northern fluvial fans (TRF & MRF) and southern fluvial fans (KRF in particular) exhibit notable morphological differences that could be linked to a number of different factors, including but not limited to, regional basin subsidence differences, upland drainage area, location of data collection, and the amount of data collected on both fluvial fans.

STUDY AREA

The KRF, TRF, and MRF are stream-dominated fluvial fans ("losimean fan" to "braided river fan" after Stanistreet & McCarthy, 1993) that are located where their rivers leave the Sierra Nevada into the San Joaquin Valley, California (Figure 2.1). The KRF enters the San Joaquin Valley southeast of Fresno while the TRF and MRF enter the valley east of Modesto. All three fluvial fans are of low gradient (approximately 0.002 on the KRF and 0.003 on the TRF and MRF), with the drainage trending west to southwest on the KRF and MRF, and west on the TRF. The drainage basin above the KRF covers an area of approximately 4,334 km^2 (corrected drainage area from misprint in Weissmann et al. 2002). Al

km^2, while abo

(Drainage basin

area of approxi

covers an area o

hydrostratigraph

1997; Weissman

Weissmann, pers

Figure 2.1 Study
Tuolumne River
elevation models
thereof on the T

et al. 2002). Above the TRF the drainage basin covers an area of approximately 3,940 km^2, while above the MRF the drainage basin covers an area of approximately 2,685 km^2 (Drainage basin areas reported from USGS stream gauging stations). The KRF cover an area of approximately 3,150 km^2, the TRF covers and area of 576 km^2, while the MRF covers an area of 552 km^2. The KRF and TRF are both the sites of ongoing hydrostratigraphic characterization and groundwater modeling studies (Burow et al., 1997; Weissmann & Fogg, 1999; Weissmann et al., 1999, 2002b, *in press*; Burow & Weissmann, personal communication).

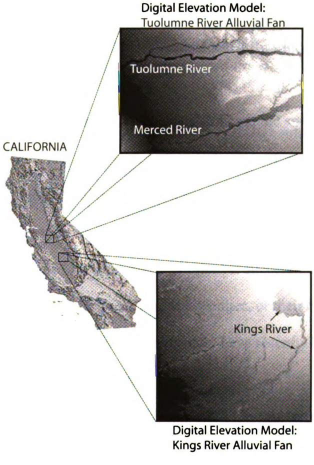

Figure 2.1 Study area location map, highlighting the locations of the Kings River fluvial fan, Tuolumne River fluvial fan, and the Merced River fluvial fan. Images of fans are 30m digital elevation models from the USGS. Note highly visible abandoned channels on KRF, and lack thereof on the TRF and MRF.

SEQ

Repeat

created recogn

1977; Hunting

Weissmann, 19

preserve those

2002a). Sequen

as soil mapping

with similar seq

(Helley, 1966; J

1987; Lettis 198

Weissma

the KRF. In this

the repeated Pleis

approach, stratig

where the sequen

related strata bou

conformities" (M

in the TRF (Weis

Sequence

cyclicity in the Si

interglacial period

occurred due to de

SEQUENCE STRATIGRAPHY OF FLUVIAL FAN DEPOSITS

Repeated glaciation and deglaciation of the Sierra Nevada during the Pleistocene created recognizable cycles (sequences) of sediment deposition (Janda, 1966; Marchand, 1977; Huntington, 1980; Marchand & Allwardt, 1981; Lettis 1982, 1988; Harden, 1987; Weissmann, 1999, Weissmann, et al. 2002a) with San Joaquin basin subsidence acting to preserve those fan deposits (Lettis, 1982; Lettis & Unruh, 1991; Weissmann et al., 2002a). Sequences have been recognized on the KRF through subsurface analysis as well as soil mapping (Huntington, 1971, 1980; Weissmann, 1999; Weissmann et al. 2002a), with similar sequences described on other eastern San Joaquin Valley fluvial fans (Helley, 1966; Janda, 1966; Marchand, 1977; Marchand and Allwardt, 1981; Harden, 1987; Lettis 1982, 1988).

Weissmann et al. (2002a) proposed a sequence stratigraphic conceptual model for the KRF. In this work, they related the episodes of aggradation and erosion on the KRF to the repeated Pleistocene glaciations of the Sierra Nevada (Figure 2.2). Using this approach, stratigraphic successions are framed within chronostratigraphic *sequences*, where the sequence is defined as "...a relatively conformable succession of genetically related strata bounded at its top and its base by unconformities, or their correlative conformities" (Mitchum, 1977, p.210). Similar sequences have recently been recognized in the TRF (Weissmann, personal communication).

Sequence development on these fluvial fans occurred in response to glacial cyclicity in the Sierra Nevada. At the end of glacial periods and the beginning of interglacial periods, fan incision as well as a basinward shift in the fan intersection point occurred due to declining sediment supply and stream discharge (Figure 2.2A & D).

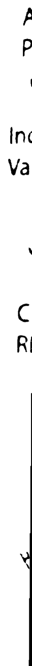

Figure 2.2 Sequen
2002a. (Modified

Stream in
fluvial fan, which
fan. During this t
soil development
in the production
the soils and the b
boundary.

Aggradati
supply and stream
allowing for the ag
Weissmann et al. 2
valley with a fining

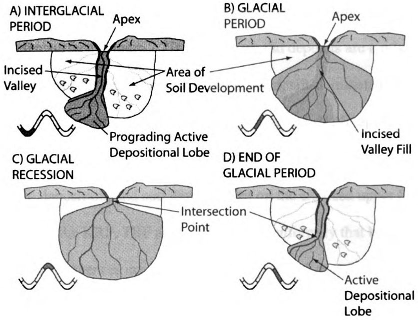

Figure 2.2 Sequence stratigraphic depositional cycle on the KRF as proposed by Weissmann et al. 2002a. (Modified from Weissmann et al., 2002a)

Stream incision created an incised valley in the middle and upper portion of the fluvial fan, which, therefore, confined deposition to more distal portions of the fluvial fan. During this time the middle and upper-portions of the fluvial fan were exposed to soil development and erosion, and/or eolian reworking. This time period then culminated in the production of an unconformity on the middle and upper-fan surfaces, marked by the soils and the bases of the incised valleys that represent the fluvial fan sequence boundary.

Aggradational events occur during glacial periods in response to higher sediment supply and stream discharge, with sediment supply out weighing stream discharge, thus allowing for the aggradation (Marchand and Allwardt, 1981; Lettis, 1982, 1988; Weissmann et al. 2002a). Increased aggradation during glacial periods filled the incised valley with a fining-upward succession of relatively coarse-grained channel and overbank deposits, and, (

over the fluvia

coarse-grained.

deposits. The e

decreases in se

basinward shift

In the ca

base of the sedi

fluvial fans duri

valleys whose c

development. F

recognized on t

1981; Lettis, 19

Lake, Riverban

Lettis, 1988) (F

TRF, and MRF

surface areas c

deposits. Henc

new glaciatio

tracking one c

separates the

deposits, and, once filled, the aggradation event led to relatively unconfined deposition over the fluvial fan surface (Figure 2.2B & C). Open fan deposits are a mix of discrete coarse-grained, channel-fill deposits within fine-grained, silt-dominated overbank deposits. The end of glaciation then led to a repetition of the stratigraphic cycle, with decreases in sediment supply and stream discharge that resulted in fan incision, basinward shift in deposition, and soil development on the exposed upper fan surface.

In the case of the KRF, TRF and MRF, the unconformity that bounds the top and base of the sediment sequences are represented by a paleosol that developed on the fluvial fans during waning glacial and interglacial periods, as well as the base of incised valleys whose channels flowed over the fluvial fan surface during the time of soil development. Five distinct episodes of aggradation and progradation have been recognized on the KRF (Marchand, 1977; Huntington, 1980; Marchand & Allwardt, 1981; Lettis, 1982, 1988). From oldest to youngest these include the Laguna, Turlock Lake, Riverbank, Modesto, and post-Modesto deposits (Marchand & Allwardt, 1981; Lettis, 1988) (Figure 2.3). Most of the land surface we see exposed today on the KRF, TRF, and MRF represents the post-Modesto interglacial period, with some upper fan surface areas containing outcrops of both Riverbank and Turlock Lake interglacial period deposits. Hence the soils developing today will later become a sequence boundary once a new glaciation begins. GPR allowed us to further analyze these sediment sequences by tracking one of its near-surface bounding unconformities, the Riverbank paleosol, which separates the Riverbank deposits from the more recent Modesto deposits (Figure 2.4).

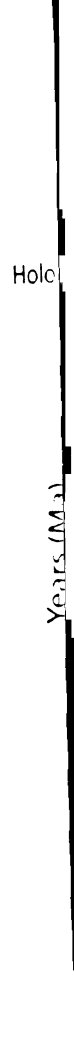

Figure 2.3 Stratigr
Marchand & Allwa

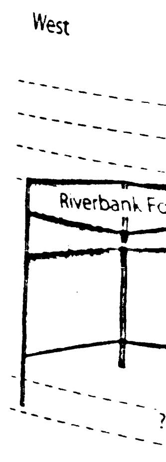

Figure 2.4 Cross-se
shows the proposed
Weissmann et al. 20

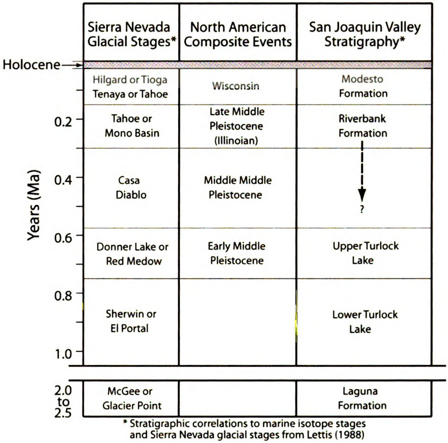

Figure 2.3 Stratigraphic column for the eastern San Joaquin Valley Quaternary deposits based on Marchand & Allwardt, (1981) and Lettis, (1988). (Modified from Weissmann et al., 2002a)

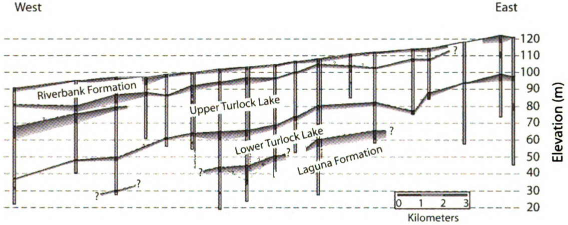

Figure 2.4 Cross-section through the upper KRF. Cross-section is parallel to depositional dip and shows the proposed laterally continuous sequence bounding paleosols. (Modified from Weissmann et al. 2002a)

GPR sy

the 80-1000 M

subsurface (Re

Figure 2.5 A) Simp
from Davis & Anna
repetitive moves of
GPR traces, highligh
a subsurface reflecto

GPR THEORY

GPR systems use short pulses of high frequency electromagnetic (EM) energy (in the 80-1000 MHz range) to detect inhomogeneities in electrical properties of the subsurface (Reynolds, 1997) (Figure 2.5).

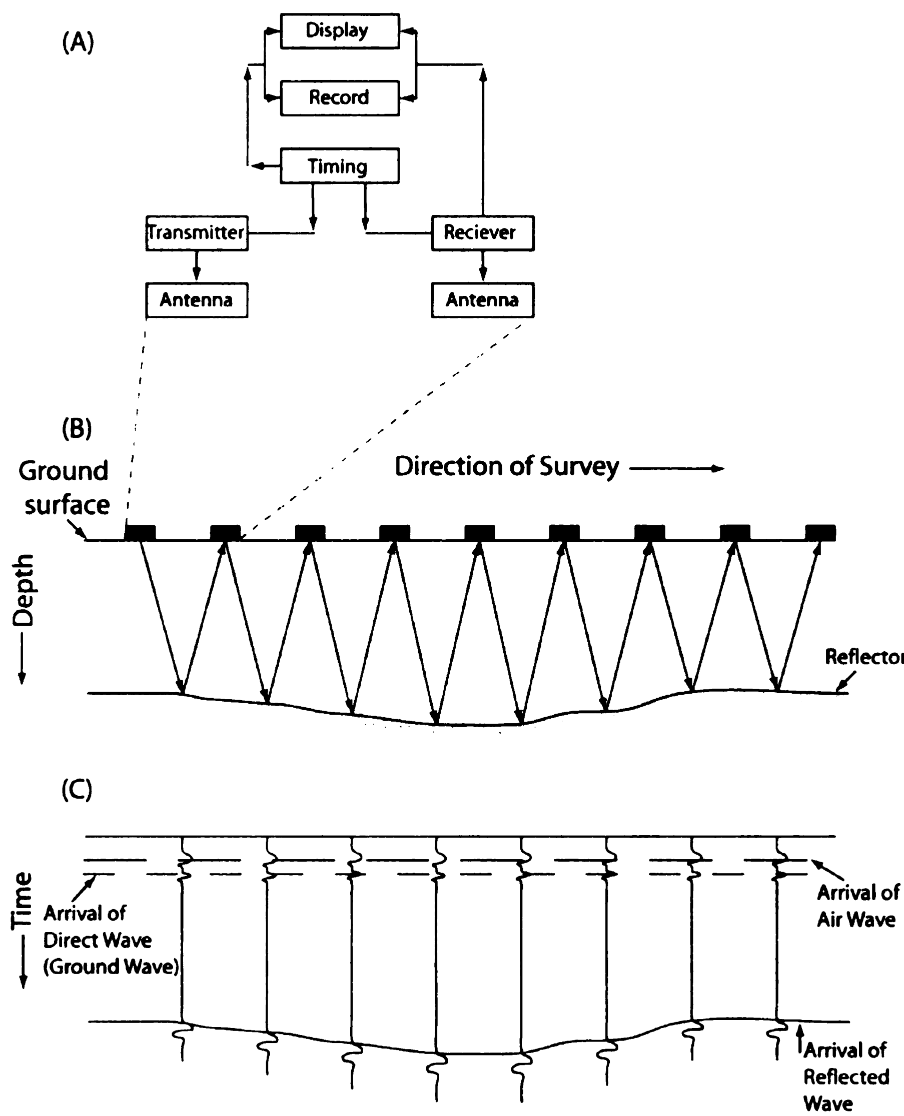

Figure 2.5 A) Simplified schematic diagram of the ground penetrating radar system. (Modified from Davis & Annan (1989)) B) Schematic procedure for GPR survey profiling, which involves repetitive moves of both the transmitter and receiver held at a constant spacing. C) Schematic GPR traces, highlighting the arrival of the air and ground wave pulses and a reflected wave from a subsurface reflector. ((B) & (C) Modified from Jol & Smith 1991)

When energy r

properties of th

the surface whi

Water content,

the electrical pr

Haeni et al., 19

recorded, proce

through the sub

way traveltime.

depth section on

calculated. Velo

(CMP) surveys (

show the hyperb

(Figure 2.6). This

scale for the rada

GPR ener

Attenuation in ge

as dry quartz sand

conductors such a

2.1 lists values of

A more complete

as effective radar r

(1984).

When energy radiated from the GPR antennae encounter changes in the bulk electrical properties of the materials it is penetrating, some of the energy is reflected back toward the surface while the rest is transmitted deeper into the subsurface (Reynolds, 1997). Water content, dissolved minerals, expansive clays and heavy mineral content all affect the electrical properties of geologic materials (Wright et al., 1984; Olhoeft, 1984, 1986; Haeni et al., 1987; Reynolds, 1997). The signal that returns to the surface is then recorded, processed, and displayed. A plot of the total traveltime for the signal to pass through the subsurface and return from a reflector is produced and represents the two-way traveltime, which is measured in nanoseconds. This plot can then be converted to a depth section once the radar wave velocities in the different subsurface layers have been calculated. Velocities in the near surface may be determined by common mid-point (CMP) surveys (Jol & Smith, 1991; Jakobsen & Overgaard, 2002). CMP experiments show the hyperbolic relationship between reflection arrival time and antenna separation (Figure 2.6). This allows for the establishment of wave velocity and, therefore, a depth scale for the radar profile. An example velocity calculation is shown in Figure 6.

GPR energy attenuation or absorption limits depth of penetration of EM waves. Attenuation in geologic materials is limited when probing poor electrical conductors such as dry quartz sand, but is much higher when attempting to penetrate good electrical conductors such as clay rich materials (Wright et al., 1984; Olhoeft, 1984, 1986). Table 2.1 lists values of conductivity and relative dielectric permittivity for selected materials. A more complete discussion of radar wave attenuation and propagation properties as well as effective radar range analysis is presented in Annan and Davis (1977) and Sheriff (1984).

Mat
Air
Pure water
Sea water
Fresh-water ic
Sand (dry)
Sand (saturate
Silt (saturated)
Clay (saturatec
Sandstone (we
Shale (wet)
Limestone (dry
Limestone (wet
Basalt (wet)
Granite (dry)
Granite (wet)

Table 2.1 Approx
materials. (Data fr

Figure 2.6 A) Com
of the electromagn
example of a CMP

Material	Conductivity (mhos per meter)	Relative dielectric permittivity
Air	0	1
Pure water	10^{-4} to 3 X 10^{-2}	81
Sea water	4	81
Fresh-water ice	10^{-3}	4
Sand (dry)	10^{-7} to 10^{-3}	4 to 6
Sand (saturated)	10^{-4} to 10^{-2}	30
Silt (saturated)	10^{-3} to 10^{-2}	10
Clay (saturated)	10^{-1} to 1	8 to 12
Sandstone (wet)	4 X 10^{-2}	6
Shale (wet)	10^{-1}	7
Limestone (dry)	10-9	7
Limestone (wet)	2.5 X 10^{-2}	8
Basalt (wet)	10^{-2}	8
Granite (dry)	10^{-8}	5
Granite (wet)	10^{-3}	7

Table 2.1 Approximate values of conductivity and relative dielectric permittivity for selected materials. (Data from Ulriksen, 1982). Modified from Beres & Haeni (1991).

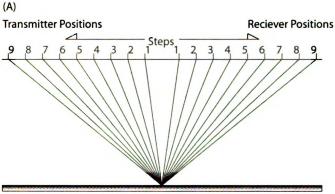

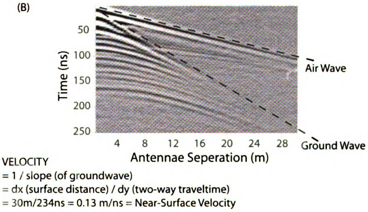

Figure 2.6 A) Common Mid Point (CMP) experiment used to calculate the propagation velocity of the electromagnetic GPR waves in the near-surface sediments (Modesto Formation). B) An example of a CMP used to determine the near-surface sediment velocity on the KRF.

We use

reflection surv

study areas. Int

were utilized.

of 1m at approx

Figure 2.7 Ground
console, laptop co
and 100 MHz ante
rechargeable 6-V
charge while doin

Each step locatio

time window of 8

triggered by an o

2.7). Profiles wer

EKKOMAPPER

GPR METHODOLOGY

We used the Sensors and Software Inc. pulseEKKO 100™ radar system in reflection survey mode with a 400V transmitter (pulser voltage) to collect data from the study areas. Interchangeable sets of antennae having 50 and 100 MHz center frequencies were utilized. The system was towed behind a car on a fiberglass GPR cart at a distance of 1m at approximately 5 km/hr (or approximately 3 mi/hr) (Figure 2.7).

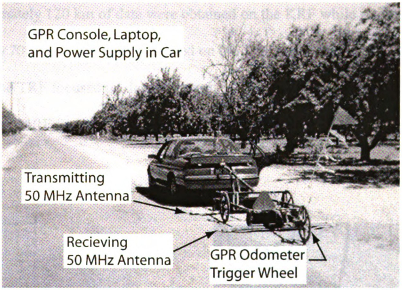

Figure 2.7 Ground penetrating radar system field setup in profiling mode. The system includes a console, laptop computer, 12-V battery power source (all located in car), and interchangeable 50 and 100 MHz antennae (50 MHz attached in photo). The GPR antennae were powered using two rechargeable 6-V batteries (chargers in trunk of car). Operational life of the batteries at full charge while doing long profiles (km length) averaged approximately 45 minutes.

Each step location (vertical trace) in reflection mode was stacked at least 8 times with a time window of 800 ps (1600 in some cases). GPR data were collected every 0.5 m, triggered by an odometer wheel, with the antenna separation maintained at 2 m (Figure 2.7). Profiles were processed and plotted with WINEKKO (version 1.0) and EKKOMAPPER (version 2). Processing was intentionally limited since interpretation of the data dic

decaying lo

reflections.

In or

velocity of (

conducted at

GPR

total, approx

approximatel

collected on t

collected on t

(A)

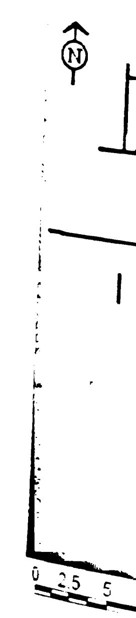

Figure 2.8 GPR pr
clustered in the sou
Background maps

the data did not require it. A dewow time filter was applied, which removes any slowly decaying low frequency “wow” which may be superimposed on high frequency reflections.

In order to develop depth scales for the GPR profiles, an averaged near-surface velocity of 0.14 m/ns was determined from fifteen common mid-point (CMP) surveys conducted at several sites on the both the KRF and the TRF (Figure 2.6).

GPR surveys were run along grids of roads on the fluvial fan surfaces and, in total, approximately 120 km of data were obtained on the KRF while a combined total of approximately 70 km of data were collected on the TRF and MRF (Figure 2.8). Data collected on the TRF focused on deposits south of the Tuolumne River, while data collected on the MRF focused on deposits north of the Merced River.

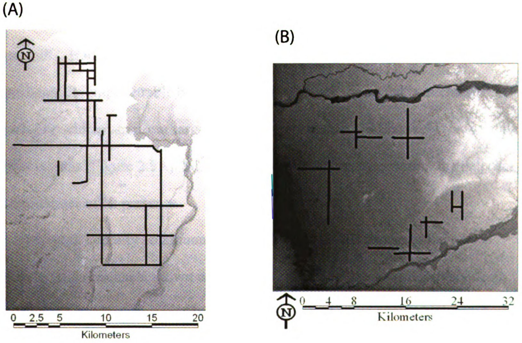

Figure 2.8 GPR profile location maps for (A) the KRF and (B) the TRF and MRF. Profiles clustered in the southeastern portion of (B) are located on Merced River deposits (See Figure 1). Background maps are 30m USGS seamless digital elevation models.

GPR p

conditions:

1) Lin

pal

2) Line

3) Line

the

abur

The near

known to have c

Harden, 1987; H

they are basicall

paleosols clay-ri

three fluvial fans

the key indicator

Althougl

dissected by pal

penetration. Are

penetration dept

continuity) (Figu

in character fron

GPR profile selection criteria consisted of locating lines that meet the following conditions:

1) Lines were located on the upper fluvial fan surface underlain by Riverbank paleosols, or were hypothesized to be underlain by Riverbank paleosols.
2) Lines were along roads that provide both long distance and straight paths.
3) Lines were along roads with low traffic volume and had limited potential for the contribution of significant sources of GPR signal interference (e.g. abundant overhead high-power lines as well as urban areas).

GPR RESULTS

The near-surface (Riverbank) paleosols observed on the KRF, TRF, and MRF are known to have clay rich B-horizons and exhibit hardpan development (Huntington, 1980; Harden, 1987; Harter et al., 1999; Weissmann, 1999; Weissmann et al. 2002a), therefore they are basically impenetrable by the GPR signal. Since the signal is attenuated in the paleosols clay-rich matrix, our large-scale survey was able to effectively track them on all three fluvial fans (Figure 2.9A). Shallow GPR signal attenuation within the paleosol was the key indicator of its presence.

Although laterally continuous, paleosols on the KRF appear to have been dissected by paleochannels shown on the GPR profiles by zones of relatively deep penetration. Areas along our profiles that showed notable increases in the signal penetration depth were interpreted as areas where the paleosol was missing (break in continuity) (Figure 2.9B). Channel incisions that removed the paleosol on the KRF varied in character from deep relatively narrow incisions (down to 10 m) to shallow wide lateral scou

2.9B

simi

wide

Figure 2.9
exposed a
below Mo
depth. B)
a deep pal
incision m
Stacked hy
narrow bar
irrigation d

scouring which simply removed the paleosol and rarely incised deeper then 6 m (Figure 2.9B). The Modesto incised valley fill, described by Weissmann et al. 2002a, has a similar character to breaks observed using GPR, but the incisised valley fill is much wider. Between channel incisions, the paleosol was observed to be laterally continuous.

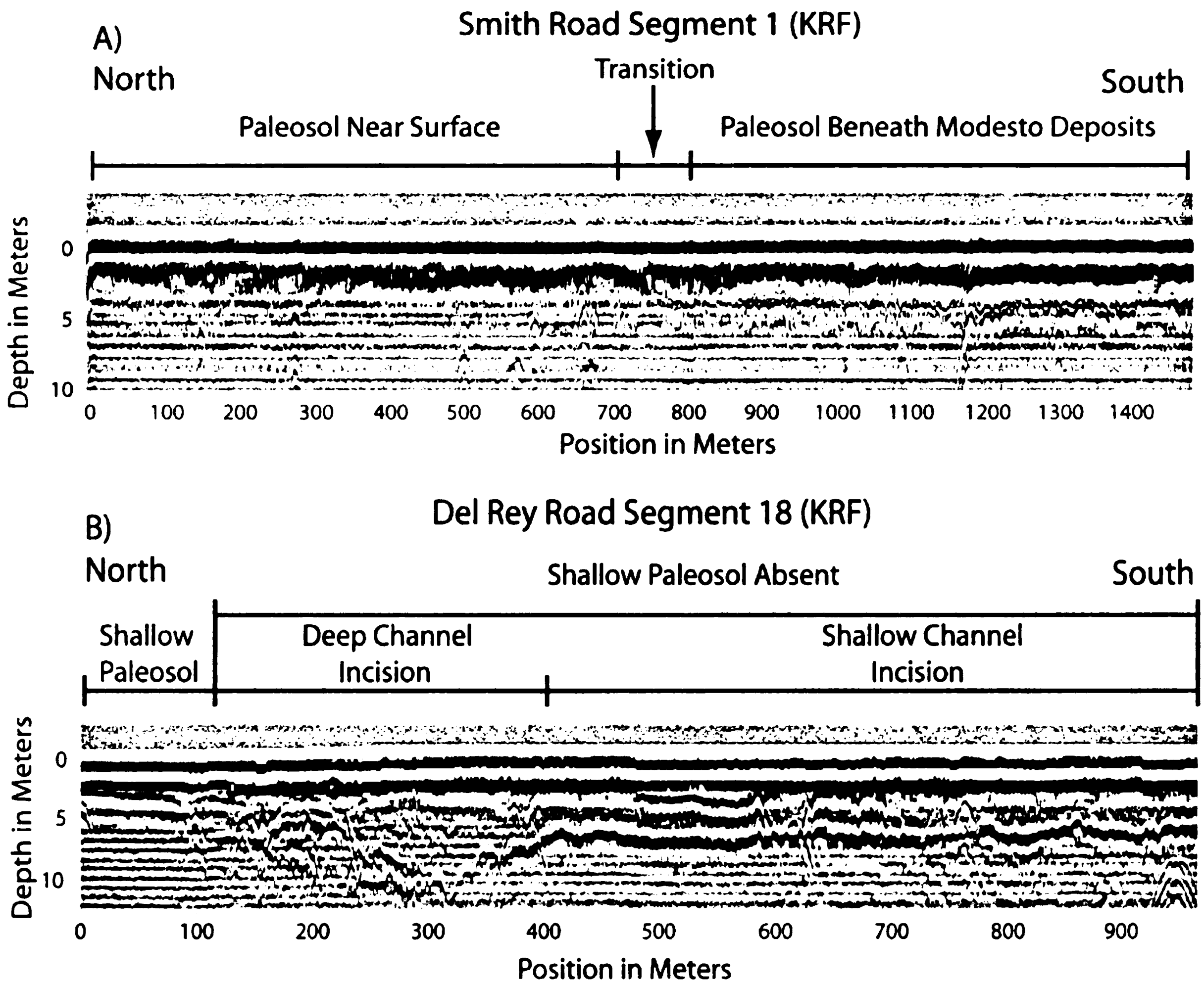

Figure 2.9 A) GPR profile on the KRF showing the typical paleosol reflection pattern when exposed at the surface as well as buried below Modesto deposits. Beyond 750 m paleosol is below Modesto deposits and is expressed as the tight dark band couplet at approximately 5 m depth. B) GPR profile on the KRF showing the typical reflection pattern observed when entering a deep paleochannel incision as well as an area that shows shallow channel incision. Shallow incision may be the result of lateral channel migration across the fan surface through time. Stacked hyperbola observed on both GPR profiles represent overhead power lines, while the deep narrow bands as observed at approximately 290 m on profile A and 380 m on profile B represent irrigation ditches.

Figure 2.10A M
the location of p
gray) on the KR
(yellow), shallov
blue and corrupt
figure is presente

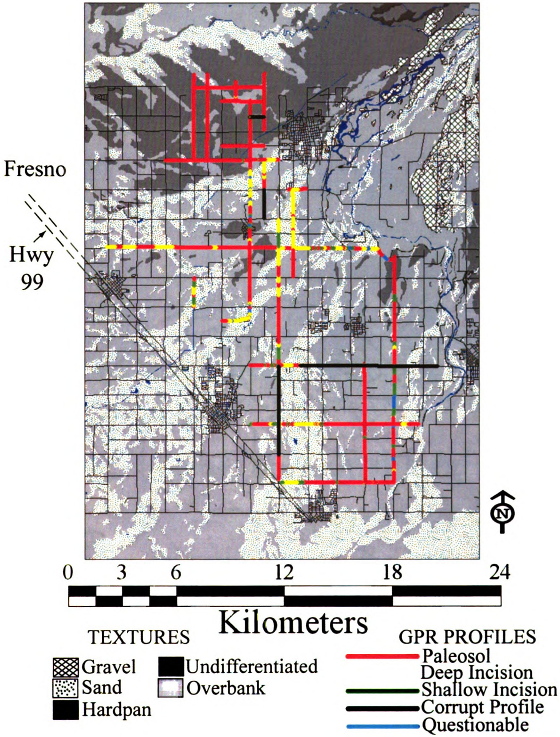

Figure 2.10A Map showing a portion of the upper KRF surface. C-horizon textures clearly show the location of paleochannels (stippled pattern), overbank deposits (light gray) and hardpan (dark gray) on the KRF. GPR profiles have been interpreted to highlight areas of deep channel incision (yellow), shallow channel incision (green), and paleosol (red). Questionable areas highlighted in blue and corrupt lines highlighted as black. (Soil map modified from Huntington, 1971) *This figure is presented in color.

Figure 2.10B Map
indicate location o
gray) on the TRF a
channel incision (y
areas highlighted a
presented in color.

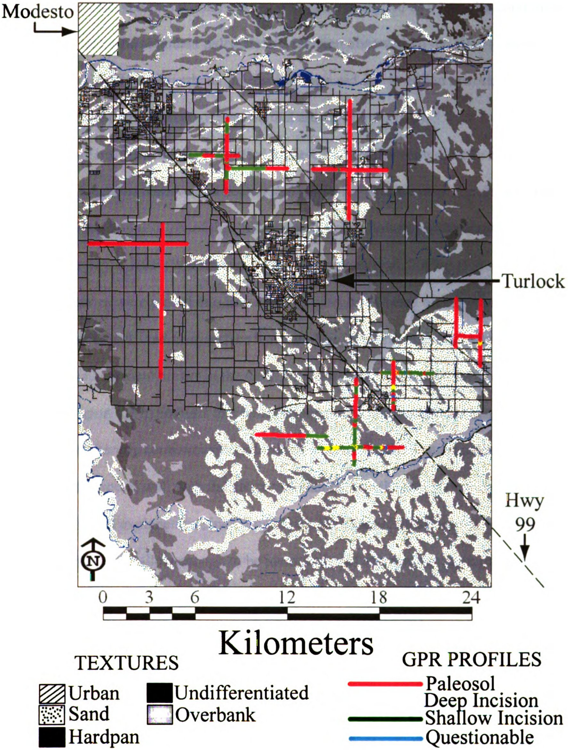

Figure 2.10B Map showing a portion of the upper TRF and MRF surfaces. C-Horizon textures indicate location of sands (stippled pattern), overbank deposits (light gray) and hardpan (dark gray) on the TRF and MRF. GPR profiles have been interpreted to highlight areas of deep channel incision (yellow), shallow channel incision (green), and paleosol (red). Questionable areas highlighted as light blue. (Soil map modified from Huntington, 1971) *This figure is presented in color.

On the

feature, yet it

2.10B). On th

sandy deposits

In man

paleochannel l

plotting the C-

paleochannels

Mapped soil s

gravel, sand, c

the GPR data.

soil survey su

sections of th

that did not c

number of di

the soil surv

(ripping), or

The

Once break

compared w

was observ

widths ther

channel bo

On the TRF, the Riverbank paleosol was again identified as a laterally continuous feature, yet it lacks the abundant paleochannel incision observed on the KRF (Figure 2.10B). On the MRF, the Riverbank paleosol is obscured due to eolian reworking of sandy deposits, which has created dunes in that area (Figure 2.10B).

In many instances breaks identified in the GPR profiles were directly correlated to paleochannel locations observed on county soil surveys. Previous work has shown that plotting the C-horizon textures of the different soil series allowed for the identification of paleochannels on the KRF (Weissmann, 1999; Weissmann et al. 2002a) (Figure 2.10A). Mapped soil series were placed into four separate categories based on C-horizon textures, gravel, sand, overbank, and near-surface hardpan. The resulting maps were compared to the GPR data. Coincident breaks in the GPR profiles with paleochannel locations on the soil survey support the hypothesis that paleochannels were responsible for removing sections of the laterally continuous Riverbank paleosol. Areas indicating paleosol breaks that did not correspond well with indications of channels on the soil survey could have a number of different explanations, including (1) a paleochannel that does not "outcrop" on the soil surveys (not shallow enough to be identified), (2) removal for agriculture (ripping), or (3) removal during road construction (if shallow enough).

The widths of paleochannels were approximated directly from the GPR profiles. Once break locations were identified and plotted, their widths were measured and compared with paleochannel locations observed on the soil surveys. A good correlation was observed, with paleochannels on the soil surveys tending to show slightly larger widths then the GPR profiles. GPR was therefore more effective at delineating the channel boundaries. Widths of the channels observed on the GPR profiles are apparent widths since t

correct for thi

surveys and th

calculate an es

KRF was appr

value was calc

breaks were ob

presence of du

OBS

Althou

KRF, there are

include overal

and the numbe

Draina

having the sli

relationship b

the result of in

though the dr

the KRF in te

fan size in the

and basin sub

widths since the GPR profiles tended to cross the paleochannels at an oblique angle. To correct for this, the orientation of the paleochannels was noted from the county soil surveys and the angle at which the GPR profile crossed the paleochannel was used to calculate an estimated width of the channel. The mean width of breaks identified on the KRF was approximately 320 m with a standard deviation of approximately 260 m. This value was calculated based on a total of 16 discrete breaks observed on the KRF. No breaks were observed on the TRF and breaks (if any) on the MRF are obscured by the presence of dunes in the study area.

OBSERVED DIFFERENCES BETWEEN THE KRF AND TRF

Although similar sequences have been observed and described on TRF, MRF and KRF, there are notable differences between the two fluvial fans. These differences include overall fan size, the apparent amount of Modesto deposits preserved on each fan, and the number of observed breaks in the underlying Riverbank paleosol.

Drainage basin areas above the TRF and KRF differ by 394 km^2, with the KRF having the slightly larger drainage basin area. Harvey (1989) has shown that there is a relationship between drainage basin area and fluvial fan area with the increase in fan area the result of increasing magnitude of sediment load with increasing drainage area. Even though the drainage areas are not significantly different, the TRF is much smaller then the KRF in terms of fan area. Therefore, drainage basin area does not appear to influence fan size in the San Joaquin Basin fans. We believe this indicates that stream base level and basin subsidence are potentially important controls on fan size.

Variab

have influenc

calculated the

regionally ext

subsiding fast

TRF, which li

KRF. Differin

in the fan morp

less accommod

fluvial fan.

Anothe

the timing of t

events during

(Weissmann et

Joaquin delta t

may have allo

to bypass the f

there is less vo

Modesto age c

Anothe

the two fluvial

number of GP

were observed

Variable subsidence rates for the northern and southern San Joaquin Valley may have influenced the morphology and sizes of the fluvial fans. Lettis & Unruh (1991) calculated the subsidence rate of the San Joaquin Basin using the Corcoran clay, a regionally extensive 600 ka lacustrine unit, and have shown that the southern valley is subsiding faster then the northern valley (0.4 m/ka and 0.2 m/ka respectively). Thus, the TRF, which lies further north, has been subjected to a slower subsidence rate then the KRF. Differing subsidence rates may therefore be one of the factors causing a difference in the fan morphologies, with the lower subsidence rate in the northern valley providing less accommodation space for sediments on the TRF, thus forcing sediment to bypass the fluvial fan.

Another possible reason for the morphology and size differences could be due to the timing of the fan aggradation with sea-level position. Timing of large sedimentation events during glacial events on the KRF coincides with low eustatic sea levels (Weissmann et al., 2002a). However, because the Tuolumne River is located near the San Joaquin delta the Tuolumne River may have been adjusted to the lower sea level. This may have allowed for the river to be held lower in its incised valley and for the sediment to bypass the fan system for a longer period of time. Evidence for this is exhibited in (1) there is less volume of Modesto sediments on the TRF and (2) there are no apparent Modesto age channels outside of the current channel location (Figure 2.10B).

Another factor that may have influenced the number of observed breaks between the two fluvial fans is the difference in the amount of data collected on each. The lower number of GPR profiles on the TRF could have resulted in a bias, where fewer breaks were observed.

Lastly

the identificat

developed by

Ground

of near-surfac

identify erosio

paleochannels

paleosol that w

the Riverbank

limited by the

penetration eff

Break widths i

the county soil

narrower then t

A differ

fluvial fans ma

northern fluvial

The KRF exhib

indicating that t

then the TRF an

periods may hav

Lastly, differences in the accuracy of the county soil surveys may have prevented the identification of paleochannels in the northern fluvial fans. The soil surveys were not developed by the same authors and may vary in their degree of accuracy.

CONCLUSIONS

Ground penetrating radar was able to effectively track the regional lateral extent of near-surface Riverbank paleosols on the KRF, TRF and MRF. GPR was also able to identify erosional breaks through the paleosol on the KRF, which were created as paleochannels switched across the upper fluvial fan surface during glacial periods. The paleosol that was tracked by our GPR surveys represented the top-bounding surface of the Riverbank Formation. Although the depth of penetration of the radar signal was limited by the Riverbank paleosol, discrete increases in the depth of GPR signal penetration effectively highlighted the location of erosional breaks through the paleosol. Break widths identified using GPR correlate with locations of paleochannels observed on the county soil surveys, yet the widths observed on the GPR profiles tended to be narrower then the widths observed on the county soil surveys.

A difference in the number of erosional breaks in the paleosol between the two fluvial fans may indicate that there are different controls on sedimentation between the northern fluvial fans (TRF and MRF) and the southern fluvial fans (KRF in particular). The KRF exhibits exceptionally more erosional breaks then the TRF and MRF, possibly indicating that the Kings River was more apt to aggrade and switch its channel location then the TRF and MRF. Factors that control channel aggradation/switching during glacial periods may have differed between the two fluvial fans. The ratio of sediment supply to discharge, dif

differing Sier

difference bet

discharge, differing valley subsidence rates (more in the south, less in the north), or differing Sierran drainage areas may be areas to focus further research to understand the difference between the two fluvial fans.

This chapter w

research:

•

•

•

Additionally

picking of th

Prev

along with

ground-pen

individual s

paleosol. It

Riverbank

To

groundtrut

CHAPTER THREE

OTHER GPR OBSERVATIONS

This chapter will focus on the following observations made during the course of this research:

- Observations leading to an attempt to identify radar facies above the Riverbank paleosol at the Kearney Agricultural Center, Orchard Site.
- Observations that provide ground truth information about the Riverbank paleosol at the Kearney Agricultural Center, Orchard Site.
- Observations of topography on the paleosol at the Kearney Agricultural Center Orchard Site and at the regional scale, as described in Chapter 2.

Additionally, a brief discussion is included that outlines an attempt to automate the picking of the paleosol breaks.

TESTS AT THE KEARNEY AGRICULTURAL CENTER

Previously collected core and detailed studies at the Kearney Agricultural Center, along with access to a former nectarine Orchard Site, allowed for the opportunity to use ground-penetrating radar (GPR) measurements as a tool to potentially differentiate individual sediment facies above the shallow regionally laterally continuous Riverbank paleosol. It also provided valuable ground truth about the reflection characteristics of the Riverbank paleosol.

To test our ability to recognize near-surface facies pattern as well as present groundtruth information that supports paleosol interpretations made in chapter 2, GPR data were col

University of

was formerly

rows of trees

been removed

investigations

Figure 3.1 Ma
former nectari
image from 30

data were collected at the Kearney Agricultural Center (KAC), an extension of the University of California, located southeast of Parlier, CA. The study area within the KAC was formerly an approximately one-hectare nectarine orchard plot that consisted of 15 rows of trees with 15 trees per row planted in 1975 (Figure 3.1). The trees have since been removed and the area is now the site of ongoing vadose zone hydrostratigraphic investigations (Harter et al., 1999).

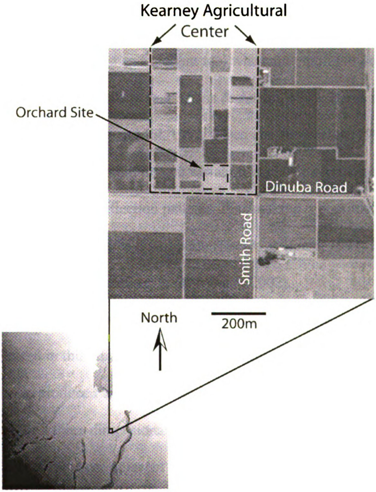

Figure 3.1 Map showing the location of the KAC on the KRF. Aerial photo shows location of former nectarine Orchard Site within the KAC. (Aerial photo from www.MapQuest.com, KRF image from 30m USGS Digital Elevation Model)

Kearney Agri

Interc

grown in resp

contaminant t

these sedimen

is controlled b

over the fluvia

GPR ha

distributions o

1991; Jol and S

1996; Van Ov

in lithology re

character (rada

1993; Van Ove

The co

GPR profiles c

of a reflection

Overmeeren, 1

whose characte

signatures (patt

summarized by

some problems

Huggenberger (

Kearney Agricultural Center: Radar Facies

Interest in the architecture and complexity of these fluvial fan sediments has grown in response to the need for an improved understanding of groundwater flow and contaminant transport in these fluvial fan aquifer systems. Hydraulic conductivities in these sediments are primarily controlled by sediment grain size and sorting, which in turn is controlled by the dynamic fluvial systems that selectively sort and distribute sediments over the fluvial fans of the Central Valley of California.

GPR has been shown to be an excellent tool when attempting to determine distributions of sedimentary structures (e.g. Davis & Annan, 1989; Beres and Haeni, 1991; Jol and Smith, 1991; Smith and Jol, 1992; Olsen and Andreasen, 1994; Jol et al., 1996; Van Overmeeren, 1998) and lithologic variation in clastic sediments. This variation in lithology results in differing reflection patterns, thus making it possible to relate radar character (radar facies) to lithofacies distributions (Beres & Haeni, 1991; Huggenberger, 1993; Van Overmeeren, 1988; Jakobsen & Overgaard, 2002).

The concept of radarfacies is implemented in the description and interpretation of GPR profiles collected in this study. This concept is defined as the sum of characteristics of a reflection pattern produced by a sedimentary unit (Beres and Haeni, 1991; Van Overmeeren, 1998) or a three-dimensional sedimentary unit composed of reflections whose characteristics differ from adjacent units (Huggenberger, 1993). Reflection signatures (patterns) that relate to lithologic and stratigraphic characteristics are summarized by Beres & Haeni (1991), yet Huggenberger (1993) shows that there may be some problems with the transferability and generalization of such signatures. Huggenberger (1993) explains that when attempting to identify radarfacies one must remember

Smith, 19

interpretin

events and

In

the KAC,

study (Har

summer of

cores dow

drilling tec

sediments

USDA-SC

grain-size a

sediment st

Turlock La

clay coatin

Five

silt silt loa

brief descri

see Harter

The

fragments,

remember that the reflection pattern depends on the central frequency applied (Jol & Smith, 1991). Additionally, the degree of saturation is an important factor when interpreting reflection patterns. Lastly, a single reflecting surface will produce multiple events and therefore care must be taken during interpretation.

In order to assess the ability of GPR to detect facies changes in the sediments at the KAC, detailed logs from core collected for use in a vadose zone nitrate contaminant study (Harter et al., 1999) were compared with GPR measurements collected during the summer of 2002. During the nitrate study by Harter et al. (1999), 59 continuous sediment cores down to a depth of 15.8 m below the surface were obtained using a direct-push drilling technique within the nectarine Orchard Site. Description of the fresh-drilled sediments focused on (1) the determination of the major textural classes according to the USDA-SCS 1994 Field Estimation, (2) color using the Munsell Soil Color Chart, (3) grain-size and degree of roundness for sands and gravels, and (4) description of the sediment structure (Harter et al., 1999). The Riverbank (Hardpan 1 in figures 5 & 6) and Turlock Lake (Hardpan 2 in figures 5 & 6) paleosols were identified by color, presence of clay coatings, root traces, aggregates, and cementation features (Harter et al., 1999).

Five textural units were distinguished from the cores: 1) sand, 2) sandy loam, 3) silt/silt loam/ loam/silty clay loam, 4) clay loam/clay, 5) paleosol (Harter et al., 1999). A brief description of each of these categories follows here; for a more in-depth description see Harter et al. (1999).

The *sand* is quartz-rich, with feldspar, muscovite, biotite, hornblende and lithic fragments, which is consistent with the granitic Sierran source (Harter et al., 1999). The grains are sub

medium grain

The *sa*

of the sandy lo

of color, prese

the sandy loan

sediments are

proximal flood

Silt, sil

floodplain dep

variable since t

to brownish gr

Root traces and

conditions duri

The *clay*

floodplains and

traces (< mm th

clay deposits (H

Paleosol

color developme

concretions, few

relatively mature

non-deposition d

grains are subangular to subrounded with sizes ranging from fine to coarse, but the fine to medium grain size are dominant (Harter et al., 1999).

The *sandy loam* is the most frequent category observed within the profiles. Some of the sandy loam deposits have been interpreted as weakly developed paleosols because of color, presence of root traces as well as aggregates (Harter et al., 1999). Sorting within the sandy loam is moderate to good with occasional thin (0.5-1 cm) clay layers. These sediments are assumed to have developed at the edge of channels, as levees, or as other proximal floodplain deposits near the channels (Harter et al., 1999).

Silt, *silt loam*, *loam* and *silty clay loam* are assumed to be the proximal to distal floodplain deposits of the KRF and are grouped together in well log descriptions as variable since they vary laterally (Harter et al., 1999). They are usually slight olive brown to brownish gray with bed thickness ranging from a few cm to dm (Harter et al., 1999). Root traces and rusty brown colored spots are quite common and indicate oxidizing conditions during some periods of time (Harter et al., 1999).

The *clay* and *clay loam* sediments are assumed to be deposits in the distal floodplains and in ponds that developed in abandoned channels (Harter et al., 1999). Root traces (< mm thick) as well as rusty brown spots are observed quite frequently in these clay deposits (Harter et al., 1999).

Paleosols exhibited different stages of maturity, typified by varying degrees of color development (Harter et al., 1999). Most exhibited aggregates, ferric nodules and concretions, few calcareous nodules and hard, cemented layers (Harter et al., 1999). The relatively mature paleosols formed during periods of stasis marked by non-erosion and non-deposition during the interglacial periods (Harter et al., 1999; Weissmann 1999;

Weissmann e

(Harter et al.,

Sedin

categories in t

of *sand, sand*

the scale of th

which is obse

GPR da

to match the ge

Figure 3.2 GPR gr
GPR profile locat
shown in figure 3.
a result of field co

Weissmann et al. 2002a). Paleosol thickness at this site ranges from 50 cm to about 2 m (Harter et al., 1999).

Sediments on top of the Riverbank paleosol have been separated into two categories in the well logs, the first of which is the variable category that contains a mix of *sand*, *sandy loam*, *silt*, *silt loam*, *loam*, or *silty clay loam*, all of which vary laterally at the scale of the study site. The second category is predominately *sand* to *sandy loam*, which is observed to be laterally continuous at the scale of the study site.

GPR METHODOLOGY

GPR data were collected along a grid that was established at the Kearney field site to match the geometry of the rows of nectarine trees once planted there (Figure 3.2).

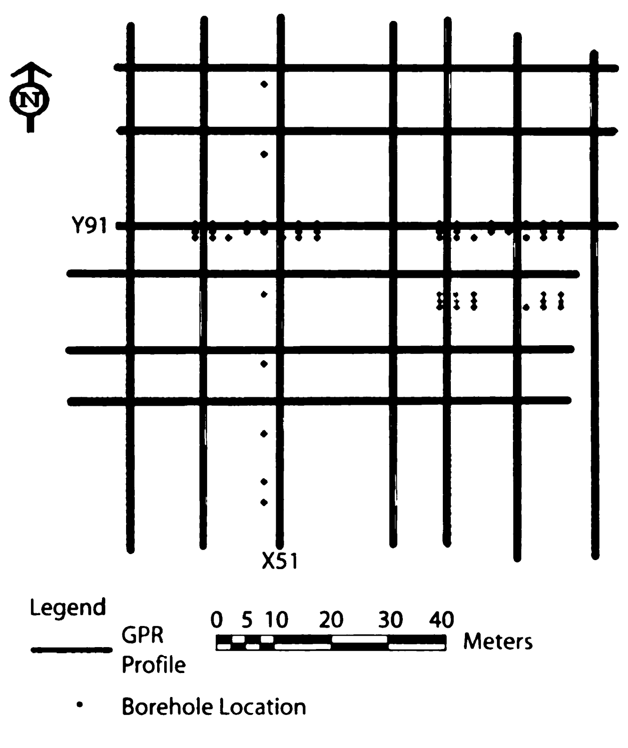

Figure 3.2 GPR grid established at the Kearney Agricultural Center Orchard Site. Lines represent GPR profile locations, and points represent well locations. The GPR profile from line Y91 is shown in figure 3.5, and the GPR profile from line X51 is shown in Figure 3.6. Offset in the lines a result of field conditions and equipment setup during the time of data collection.

This resulted

directions. T

Harter et al. (

The G

towed behind

Figure 3.3 Co
the back of th

The system

for Commo

antenna sepa

Antennas ha

analyses (50

surface GPR

profiles (Jol

WINEKKO

applied to th

slowly decay

frequency re

This resulted in a total of fourteen profiles, seven in both the south-north and west-east directions. The GPR profiles passed as close as possible to bore hole locations used in the Harter et al. (1999) nitrate study.

The GPR system employed in this survey was the pulseEKKO 100™, which was towed behind a tractor to facilitate rapid data collection (Figure 3.3).

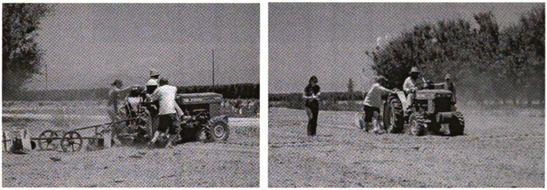

Figure 3.3 Collecting GPR data in the former nectarine Orchard Site. GPR equipment attached to the back of the tractor.

The system was operated in reflection survey mode with a signal stacking of 8 times (32 for Common mid-point (CMP)), a step size of 0.5 m (triggered by odometer wheel) and antenna separation of 2 m (maintained by a fiberglass GPR cart towed behind the tractor). Antennas having center frequencies of 50 and 100 MHz were utilized. Two CMP analyses (50 and 100 MHz) were completed, allowing for the estimation of the near-surface GPR wave velocity (0.14 m/ns) needed to develop depth scales for the GPR profiles (Jol and Smith, 1991) (Figure 3.4). Profiles were processed and plotted using WINEKKO (version 1.0) and EKKOMAPPER (version 2). Minimal processing has been applied to the raw GPR data, and consisted of dewow, a time filter which removes any slowly decaying low frequency "wow" which may become superimposed on higher frequency reflections.

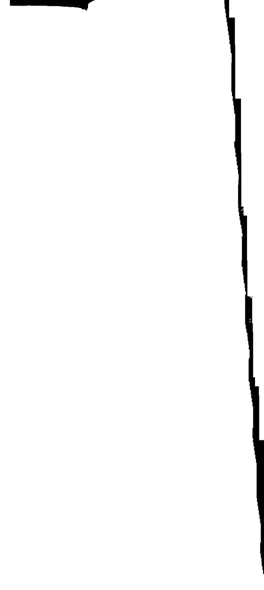

Figure 3.4 Cor
for a more in d

GPR Profile

In the

Both profiles

area. A prolo

relatively lo

retained son

the time of C

The

second profi

MHz (top) a

on both prof

within the n

Figure 3.4 Conducting a CMP experiment at the KAC Orchard Site study site (See chapter two for a more in depth description of CMP experiments).

GPR Profiles: Descriptions of Radar Facies

In the following section, two of the fourteen GPR profiles collected are presented. Both profiles contain data collected in the near-surface unsaturated zone of the study area. A prolonged period without rain in the Central Valley implied that there was relatively low water content in the unsaturated zone, yet fine-grained materials may have retained some degree of saturation. No measurements of water content were collected at the time of GPR data acquisition.

The first profile (Figure 3.4) is a west-east section that is 86 m in length. The second profile (Figure 3.5) is a south-north section that is 90 m in length. Both the 100 MHz (top) and 50 MHz (bottom) surveys are shown in each figure. Reflections observed on both profiles become less distinct with increasing depth due to signal attenuation within the near-surface, clay rich, Riverbank paleosol located between 3 and 5 m depth.

A)

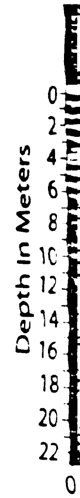

B)

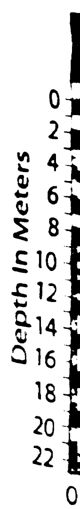

Figure 3
Dotted y
section (
19 and 4
analysis

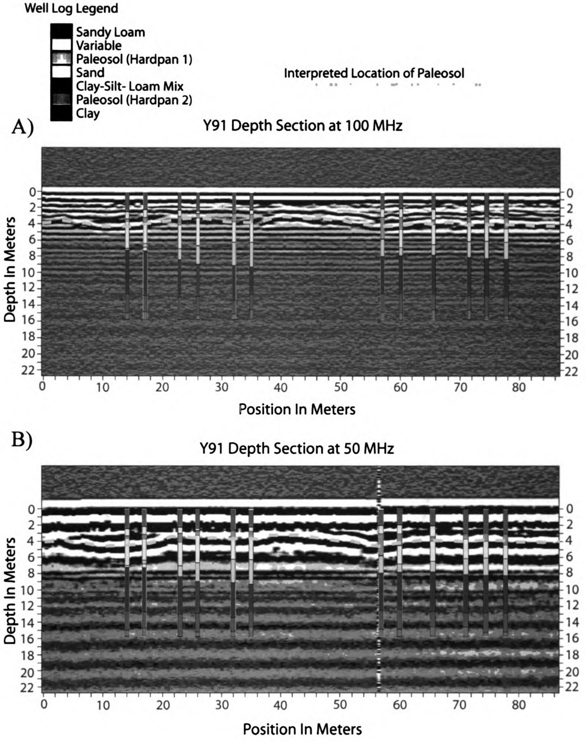

Figure 3.5 West-East GPR profile from the Orchard Site at the KAC with described well logs. Dotted yellow line sits on the reflector interpreted as the paleosol. Note that in the 50 MHz section (B) the ground wave arrival is overprinting the paleosol reflection between approximately 19 and 46 m. A velocity of 0.14m/ns was used in GPR profile depth correction from CMP analysis at the KAC. Profile locations are shown in figure 3.2. *This image is presented in color.

Well

A)

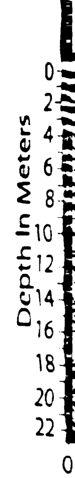

B)

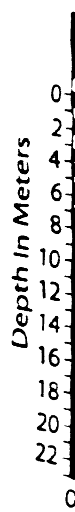

Figure 3
Dotted y
used in
in figure

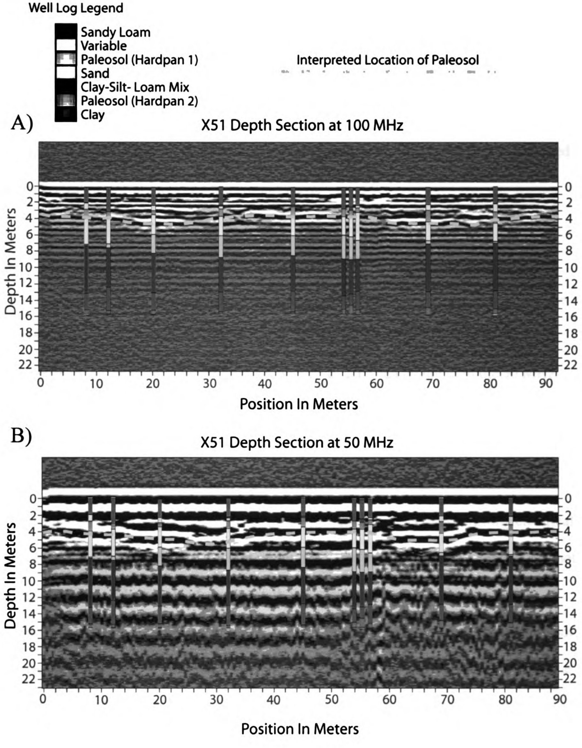

Figure 3.6 South-North GPR profile from the Orchard Site at the KAC with described well logs. Dotted yellow line sits on the reflector interpreted as the paleosol. A velocity of 0.14 m/ns was used in GPR profile depth correction from CMP analysis at the KAC. Profile locations are shown in figure 3.2. *This image is presented in color.

A vis

no indication

paleosol. Du

information i

by the arrival

The tw

Riverbank pal

changes in fac

sections wher

close to the su

What

occurring as a

properties, or

measured, the

boreholes rela

utilized, ident

current data se

channel-shape

present that ar

positioning rel

A visual comparison between the GPR profiles and the overlain well logs shows no indication of a correspondence between reflection patterns and the well logs above the paleosol. Due to the fact that the paleosol at the site is very shallow, limited signal information is preserved in the near surface since much of the signal is being overprinted by the arrival of the airwave and the ground wave.

RADAR FACIES CONCLUSIONS

The two categories as defined by Harter et al. (1999) for the sediments above the Riverbank paleosol, variable and sandy loam, appear to be too generalized to interpret changes in facies based on the GPR reflection signal. This can be noted in the 50 MHz sections where the airwave and ground wave are being overprinted on the reflection data close to the surface.

What can still be drawn from the GPR data collected is that reflections are occurring as a result of either a change in lithology between units of contrasting electrical properties, or a change of water content within the same unit. Since water content was not measured, the well logs lack adequate detail, uncertainty exists in the location of the boreholes relative to the GPR lines, and higher frequency antennae (>100 MHz) were not utilized, identification of radar facies at the KAC Orchard Site was not possible using the current data set. The GPR profiles, however, do contain elements that appear to be channel-shaped indicating potential channel facies, thus interpretable radar facies may be present that are not directly correlative to the boreholes due to uncertainty in their positioning relative to the GPR profiles. Future work attempting to identify radar facies at this

with

with

for a

at the

interpr

therefo

the larg

(1999)

and sub

the well

Site. Us

that follo

shows th

depth of

O

amount o

signal was

the KAC,

the paleosc

this site should include higher resolution antennae (200 MHz or higher) in combination with more rigorous groundtruth information in the form of accurately located well logs with highly detailed lithologic descriptions. Taking these steps would potentially allow for a more rigorous investigation into the identification of radar facies at this site.

PALEOSOL GROUNDTRUTH AT THE KAC

Although it was not possible to identify radar facies above the Riverbank paleosol at the KAC using the data collected, the data do provide the opportunity to make interpretations about the ability of GPR to identify the paleosol. The GPR data can therefore be used to provide reliable evidence that supports our interpretations made in the large-scale regional study discussed in chapter 2. Well logs collected by Harter et al. (1999) provided much needed groundtruth information about the depth to, thickness of, and subsurface character of the Riverbank paleosol. Referring back to figures 3.5 & 3.6, the well logs show the depth to and thickness of the Riverbank paleosol at the Orchard Site. Using the well logs as a guide it is possible to follow a nearly continuous reflection that follows the top of the paleosol identified in the well logs (Figures 3.5 & 3.6). This shows that the paleosol is providing a good reflection that can be traced and that the depth of signal penetration is limited due to the paleosol's clay-rich nature.

One observation that was made that was not expected at the Orchard Site was the amount of signal penetration into the paleosol. In our regional study we assumed the GPR signal was essentially fully attenuated once it had encountered the Riverbank paleosol. At the KAC, the GPR data seem to indicate that the signal penetrated into or slightly through the paleosol. This may be due to the fact that the GPR signal is not penetrating through roadbed mat

the surface. E

therefore pro

water from ir

high temperat

the paleosol a

made too soo

information ir

signature of th

Orchard Site s

supporting int

The las

scale and has i

incorporate the

surveys we not

developed fron

the paleosol is

that topographi

be locations wh

head at these lo

the paleosol int

roadbed material at the Orchard Site. Also, the paleosol at the KAC is relatively close to the surface. Being that it is close to the surface, it may have lost moisture content, therefore providing less signal attenuation then in other areas that may have received water from irrigation, or have been deep enough to avoid desiccation as a result of the high temperatures in the Central Valley of California. Conversely, our assumption that the paleosol attenuated our signal completely in the regional-scale study may have been made too soon and without adequate groundtruth information. Therefore, groundtruth information in the form of accurate well logs may be necessary to fully understand the signature of the paleosol in the regional scale study. Ultimately, the results from the Orchard Site show that it is possible to track a near-surface paleosol using GPR, supporting interpretations made in chapter 2.

PALEOSOL TOPOGRAPHY

The last observation made at the KAC Orchard Site was also made at the regional scale and has important implications for future groundwater modeling studies that aim to incorporate the effects of the regionally continuous paleosols into their models. In our surveys we noted that the paleosol surface exhibits subtle topography. Cross-sections developed from the KAC Orchard Site well logs as well as the GPR profiles indicate that the paleosol is not a perfectly planar feature. This observation therefore leads to the idea that topographic lows on a hydrostratigraphic-confining layer within the vadose zone will be locations where water/contaminants will migrate to and build up. Once the hydraulic head at these locations becomes high enough, water/contaminants will be forced through the paleosol into the deeper aquifer units (Figure 3.7). Jury et al. (1991) explain this phenomenon

unsaturated

layer to fill, t

observation c

developing g

topographic l

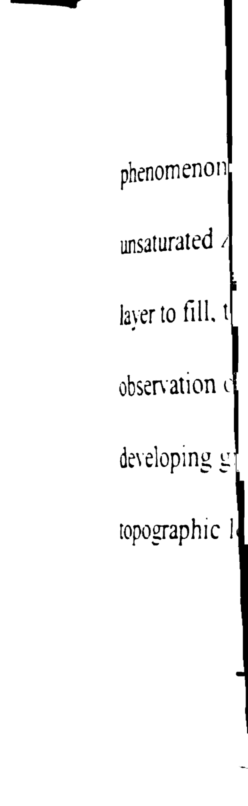

Figure 3.7 Sch
depressions in

CONCL

GPR

GPR to dete

the characte

as well as id

topography

surface.

Wit

MHz or gr

identify re

phenomenon in layered systems, whereby raising hydraulic head values in the unsaturated zone due to infiltration allows the pore spaces in the hardpan or clay rich layer to fill, thereby allowing flow through the paleosol to occur. Therefore, the observation of topography on the paleosol surface has significant implications when developing groundwater models to simulate fluid flow in these systems since these topographic lows will be spatially significant recharge locations.

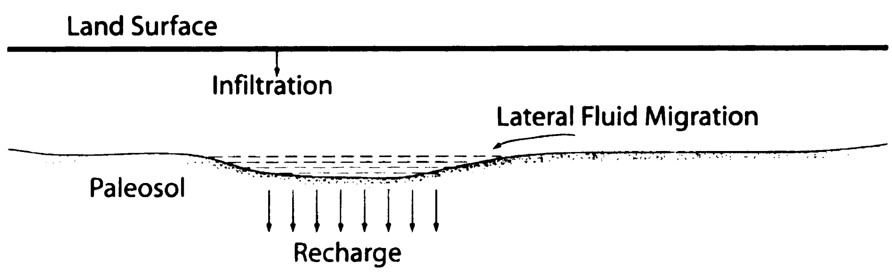

Figure 3.7 Schematic diagram depicting preferential recharge as a function of topographic depressions in the near-surface paleosols on Central Valley fluvial fans.

CONCLUDING REMARKS FOR FUTURE WORK ON RADAR FACIES

GPR data collected at the KAC provided the opportunity to explore the ability of GPR to detect facies changes in near-surface sediments, verify interpretations made about the character of the Riverbank paleosol in a setting with good ground truth information, as well as identify and explore the idea that the Riverbank paleosol exhibits subtle topography which may focus recharge to topographically low spots on the paleosol surface.

With regards to the identification of radar facies, higher frequency antennae (200 MHz or greater) combined with detailed lithologic well logs should provide the means to identify reflection patterns indicative of a facies change in the near surface. Considering the fact that

area in which

paleosol to b

different faci

profiles coul

in the near su

2) allow for t

intervals to in

near surface s

further resear

OUR

In an a

GPR profiles.

process. To do

value was assi

become noise.

using the "loes

were then plott

it was hoped th

location of area

the fact that the paleosol is so shallow at the KAC, it may also be advantageous to find an area in which the paleosol is slightly deeper. This will allow for more data above the paleosol to be collected in the hopes of better understanding the reflection patterns of the different facies observed. Lastly, establishing a highly detailed survey grid of GPR profiles could potentially allow for three-dimensional visualization of facies distribution in the near surface at the KAC. Newer software packages (e.g. EKKOMAPPER version 2) allow for the visualization of GPR block models that can then be sliced at various time intervals to image different portions of the subsurface. The KAC Orchard Sites variable near surface sediment distribution may provide an excellent area in which to conduct further research using GPR.

OUR ATTEMPT AT USING MATLAB TO PICK PALEOSOLS AND ASSOCIATED EROSIONAL BREAKS

In an attempt to expedite the process of interpreting approximately 190 km of GPR profiles, a MATLAB script was developed which attempted to automate the process. To do this, each GPR trace was normalized within MATLAB and then a cutoff value was assigned which represented the value at which the GPR signal had essentially become noise. Once all of these values had been calculated, the data were then smoothed using the "loess" smoothing function (quadratic fit) in MATLAB. The smoothed data were then plotted on top of the corresponding GPR profile (Figure 3.8). Once completed it was hoped that the smoothed data would show the depth to paleosol along with the location of areas of increased penetration depth along the GPR profiles.

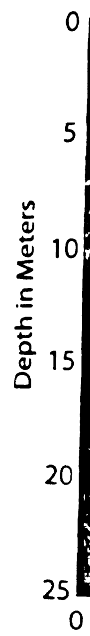

Figure 3.8 E
developed to
color.

As c

profile, a go

signals and

depth to pal

that were eit

script to ide

when it was

being made s

data failed to

fact that the

reached the c

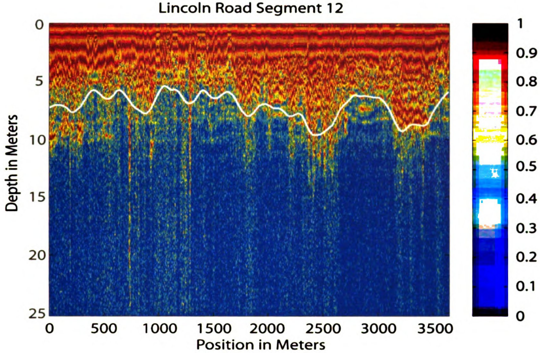

Figure 3.8 Example of smoothed data plotted on top of GPR profile using the MATLAB script developed to pick the trace values at which the signal goes to noise. *This figure presented in color.

As can be see in Figure 3.8, once the smoothed data was plotted onto the GPR profile, a good representation of the character of the interface between true reflected signals and noise was observed. With these data, we had hoped to assign a value for the depth to paleosol and use another MATLAB script to assign different categories to values that were either above or below the depth of paleosol, and then use the output from that script to identify erosional breaks in the paleosol. Difficulty arose during this process when it was noted that the smoothed data did not coincide with interpretations that were being made simply by eye. For instance, in figure 3.8 between 0 and 250m the smoothed data failed to envelope the obvious deep reflector in that interval. This resulted from the fact that the MATLAB script was not complicated enough to rule out values in traces that reached the cutoff threshold sooner then expected. It was also noted that assigning a constant val

or no break.

of missing s

paleosol, wo

time it was n

MATLAB sc

appendices a

research.

constant value for the depth to paleosol as a cutoff value for the interpretation of a break or no break, would, in the case of overestimation the depth to paleosol, have the potential of missing shallow breaks in the paleosol, and in the case of underestimating the depth to paleosol, would over estimate the true number and width of the breaks. Therefore, at this time it was more efficient and reliable to interpret the GPR profiles manually. The MATLAB script that was prepared to create the smoothed data is included in the appendices as are other MATLAB scripts that were developed during the course of this research.

PAL

I

multipl

2002a).

mid- an

possible

deposits

unable t

regional

EROS

C

observed

breaks c

survey m

that radia

through t

KRF.

F

features.

CHAPTER FOUR

THESIS CONCLUSIONS

PALEOSOLS AS REGIONALLY LATERALLY CONTINUOUS FEATURES

Fluvial fan deposits within the San Joaquin Valley of California consist of multiple sediment sequences separated by unconformable surfaces (Weissmann et al., 2002a). The unconformable surfaces can be identified by paleosols that formed on the mid- and upper-fluvial fan surface during times of depositional hiatus. Using GPR, it was possible to trace the lateral continuity of the uppermost paleosol, capping the Riverbank deposits in the subsurface of the KRF, TRF and MRF. Unfortunately, at this time we are unable to ascribe an accurate depth to the paleosol based on the GPR data due to a lack of regional scale groundtruth information.

EROSIONAL BREAKS IN THE LATERALLY CONTINUOUS PALEOSOLS

On the KRF discrete breaks in the continuity of the Riverbank paleosol were observed on GPR profiles collected across the mid- and upper fluvial fan surface. These breaks correlate well with observed paleochannel locations noted on digitized county soil survey maps that highlight c-horizon textures. Therefore, it appears that paleochannels that radiated from the apex of the KRF during the deposition of the Modesto unit incised through the Riverbank paleosol, thus interrupting the continuity of this paleosol on the KRF.

Further north on the TRF and MRF, we had expected to observe similar erosional features. Yet on the TRF the paleosol appears to be missing these erosion features. This seems to be

the most rec

River appea

ability to ero

On th

eolian depos

obscure pote

from paloch

RAD

Fifty-

orchard at the

profiles (seve

attempt ident

sediments abo

to directly co

Complication

descriptions,

evaluate facie

GPR profiles.

seems to be due to minimal lateral migration of the Tuolumne River paleochannel during the most recent glacial outwash event (e.g. Modesto deposition). Since the Tuolumne River appears to have maintained its channel position during Modesto deposition, its ability to erode through the Riverbank paleosol was limited.

On the MRF, erosion breaks were difficult to identify due to relatively thick eolian deposits in the area in which the GPR data were collected. The dunes tended to obscure potential erosional breaks due to the fact that they could not be differentiated from palochannel deposits on the MRF county soil surveys.

RADAR FACIES AT THE KEARNEY AGRICULTURAL CENTER

Fifty-eight continuously cored and described wells within a former nectarine orchard at the Kearney Agricultural Center (KAC) combined with a grid of 14 GPR profiles (seven west-east and seven south-north profiles) provided the opportunity to attempt identification of characteristic radar reflection patterns for various facies in sediments above the Riverbank paleosol (see Chapter 3). Unfortunately, we were unable to directly correlate any facies changes observed in the well logs with the GPR data. Complications with radar facies interpretations were the result of (1) generalized well log descriptions, (2) GPR antenna frequency, which was too low for the detail necessary to evaluate facies so close to the surface, (3) inaccurate borehole location with respect to GPR profiles.

The f

near v

geoph

used t

that th

identi

corres

by the

their G

data in

at this

a good

own st

nectarin

the opp

describe

reflectio

exact de

the digit

and that

PALEOSOL GROUNDTRUTH INFORMATION

Groundtruth information for this study was obtained at two different locations. The first being data collected for a USGS study by Burrow et al. (1997) that was located near where we had collected GPR data for this study. Burrow et al. (1997) collected geophysical data in the form of continuous seismic profiling, and GPR data that were used to identify laterally continuous fine-grained layers (unknown at the time was the fact that they were tracking sequence bounding paleosols). In their study they successfully identified a laterally continuous subsurface reflector on their GPR profiles that corresponds to the Turlock Lake paleosol, which in most cases in our study was obscured by the presence of the Riverbank paleosol that sits above it. We were able to compare their GPR results and well log groundtruth information to our own since we had collected data in the same vicinity. Assuming that we are correctly identifying the depth to paleosol at this site (assumed to be the point at which the signal is completely attenuated), we see a good correlation between the Turlock Lake paleosol observed in USGS study and our own study.

The second site at which we have groundtruth information is at the KAC nectarine orchard site. At the KAC, continuously collected and described core provided the opportunity to groundtruth our observations of the paleosol on the GPR profiles with described borehole data. This work showed that it was possible to identify the paleosol reflection within the GPR profiles. Yet, we remain uncertain about our ability to show the exact depth of the paleosol reflector. Correlation between the observed paleochannels on the digitized soil surveys and the GPR profiles supports the hypothesis that breaks exist and that GPR data were able to identify these features, therefore we feel that we were also able to

this time.

COMP

The

which were

obvious of t

3,150 km^2, v

km^2. Fan are

when compa

fans (approx

assume that

suggested h

level, theref

to bypass th

Lake Sub-b

change.

The

data. The r

differed, w

major eros

deposits,

GPR data

also able to trace the extent of the laterally continuous paleosols but not the true depth at this time.

COMPARE AND CONTRAST BETWEEN THE THREE FLUVIAL FANS

The three fluvial fans studied exhibit notable morphological differences, some of which were observed in the county soil surveys and the GPR data collected. The most obvious of these differences is fan size, with the KRF being the largest with an area of 3,150 km^2, while the TRF has an area of 576 km^2, and the MRF having an area of 552 km^2. Fan area has been described as a function of drainage basin area (Harvey, 1989), yet when comparing drainage basin areas it is noted that little difference exists between these fans (approximately 394 km^2 between the KRF and TRF) (see Chapter 2). Therefore, we assume that the fan areas differ due to a control other then drainage basin area. It is suggested here that TRF and possibly the MRF may have been adjusted to eustatic sea level, therefore allowing sediment that would have been deposited on the TRF and MRF to bypass these systems by way of the San Joaquin delta. The KRF adjusted to the Tulare Lake Sub-basin to the south and appears not have been affected by eustatic sea level change.

The last obvious difference between the fluvial fans was observed in the GPR data. The number of erosional breaks through the paleosol observed on the fluvial fans differed, with the KRF having the largest occurrence of breaks. The TRF lacked any major erosional breaks, while MRF paleochannel identification was difficult due to eolian deposits, which complicated our ability to make accurate interpretations without further GPR data and well log information.

FUTURE CONSIDERATIONS

Future work that may further support the conclusions reached here would include collection of additional groundtruth information then was provided in this study. Due to the large-scale nature of this study, it was impossible during acquisition of the GPR data to collect physical subsurface groundtruth information. The GPR profiles include questionable areas that could not be interpreted without further information about the character of the subsurface. If core had been collected in those areas, fewer questionable areas might exist along our GPR profiles and our understanding of these fluvial fans systems might be greatly enhanced.

Another consideration to further enhance the results of this study would be the use of higher GPR frequencies. This may have provided more detail in both the regional study and our attempt to identify radar facies at the KAC orchard site. Since the paleosol observed on the fluvial fans is a relatively shallow feature, more information could be collected about the character of the sediments above the paleosol using higher frequency antenna. Although we used 50 MHz antennae to maximize depth of penetration when we encountered a deep erosional incision, it limited valuable near surface detail in the GPR profiles thereby hindering the interpretation of radar facies and paleosol reflection character. In many instances, the ground wave and airwave tended to overprint their signatures on top of data that would have shown the paleosol or facies changes.

APPENDICIES

Appendix A

Kings River Fluvial Fan GPR Profiles

Smith Road Merged Profiles 34-39

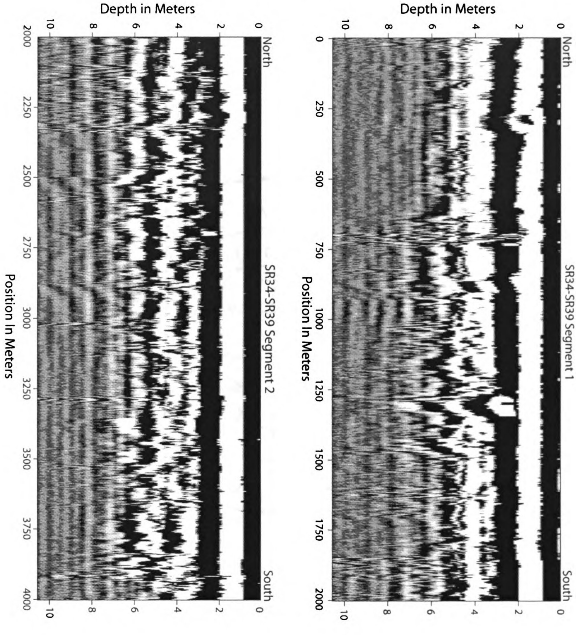

Figure A1 Segments 1 & 2 of merged Smith Road profiles 34-39.

Smith Road Merged Profiles 34-39 (Cont.)

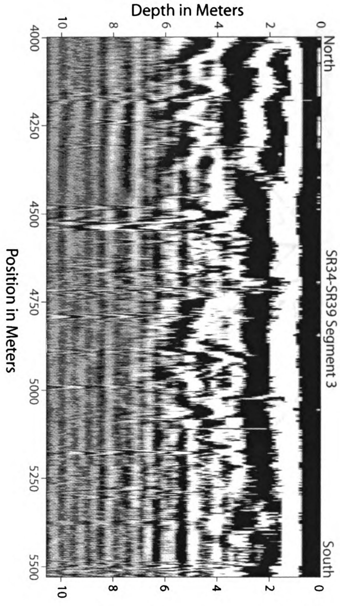

Figure A2 Segment 3 of merged Smith Road profiles 34-39.

Smith Road Merged Profiles 40-43

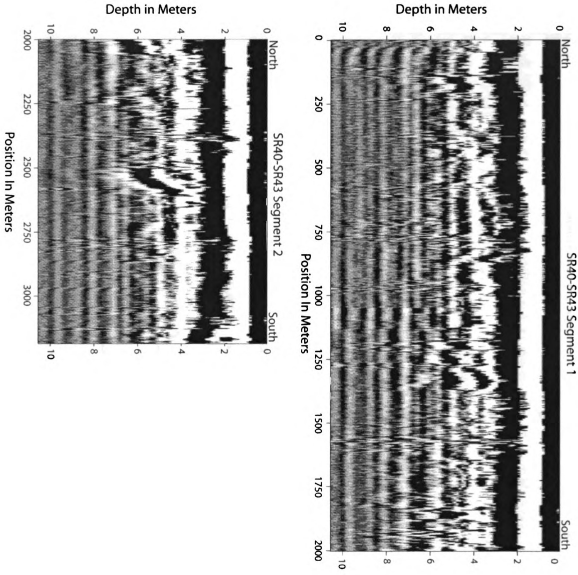

Figure A3 Segments 1 & 2 of merged Smith Road profiles 40-43.

Smith Road 1 & 2 Merged

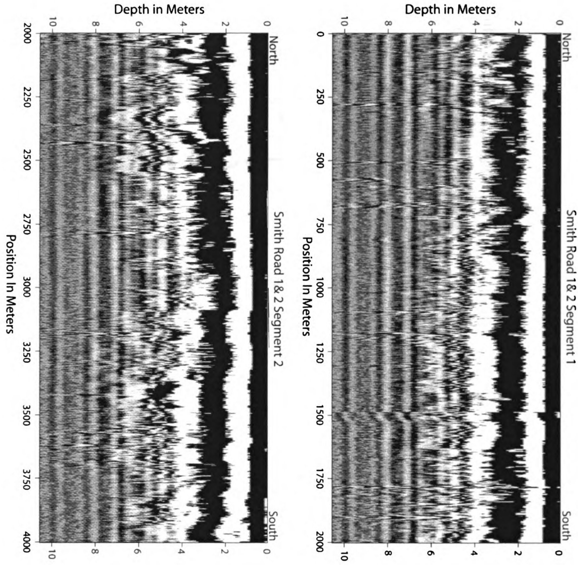

Figure A4 Segments 1 & 2 of merged Smith Road profiles 1 & 2.

Smith Road 1 & 2 Merged (Cont.)

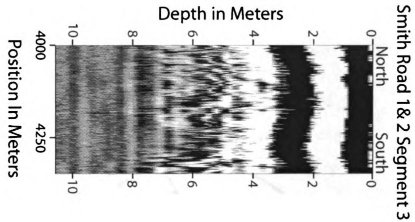

Figure A5 Segment 3 of merged Smith Road profiles 1 & 2.

Del Rey Road Merged Profiles 11-15

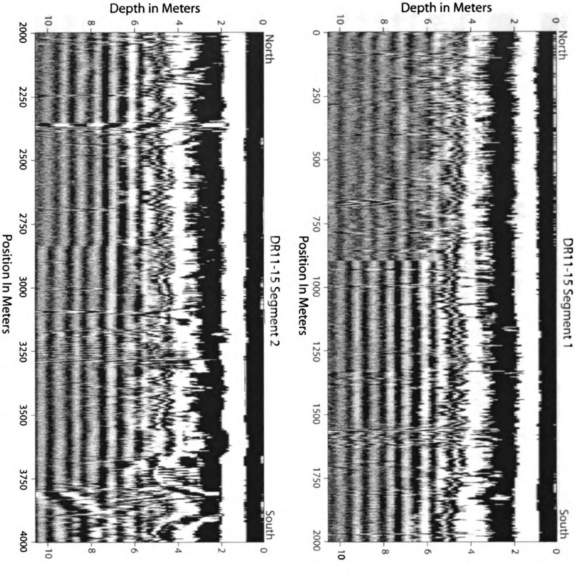

Figure A6 Segments 1 & 2 of merged Del Rey Road profiles 11-15.


6000
6250
Position In Meters

Del Rey Road Merged Profiles 11-15 (Cont.)

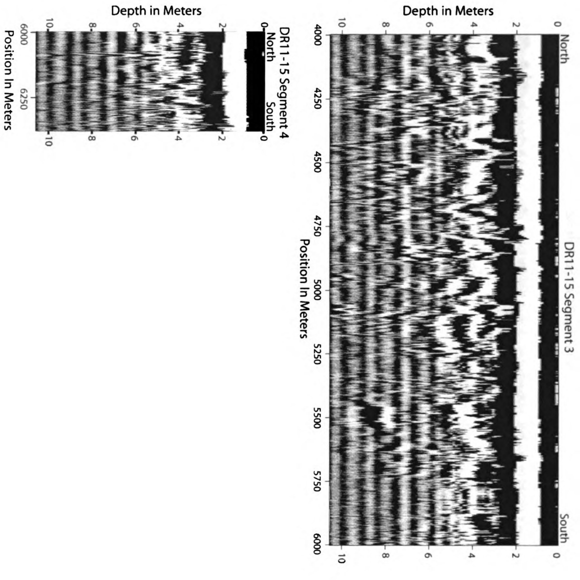

Figure A7 Segments 3 & 4 of merged Del Rey Road profiles 11-15.

Del Rey Road Merged Profiles 16-20

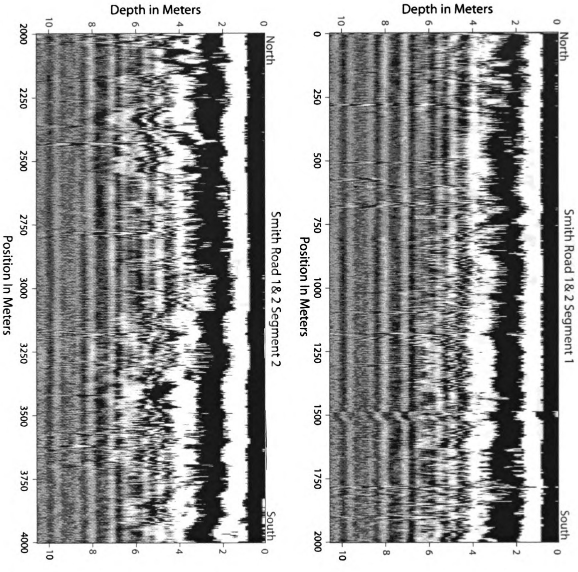

Figure A8 Segments 1 & 2 of merged Del Rey Road profiles 16-20.

Del Rey Road Merged Profiles 16-20 (Cont.)

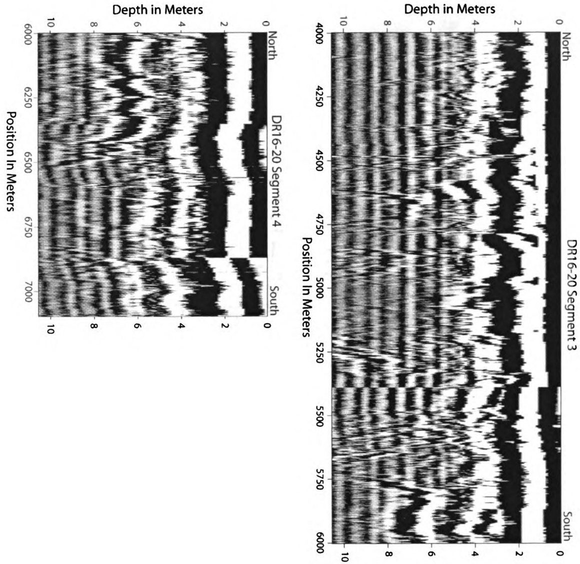

Figure A9 Segments 3 & 4 of merged Del Rey Road profiles 16-20.

Highland Road Profile

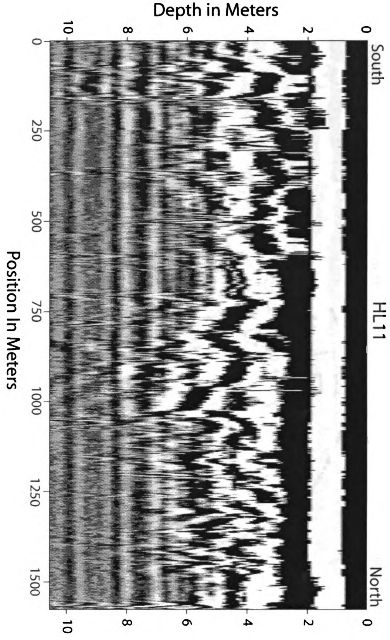

Figure A10 Highland Road Profile (HL11).

Del Rey Road Merged Profiles 31-33

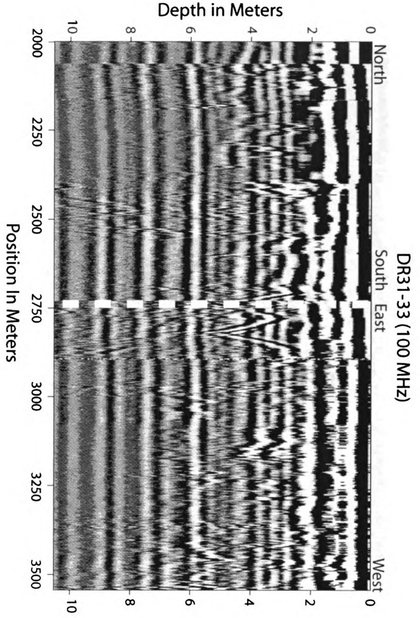

Figure A11 Del Rey Road Merged Profiles 31-33 (100 MHz).

Lincoln Road Merged Profiles 11-13

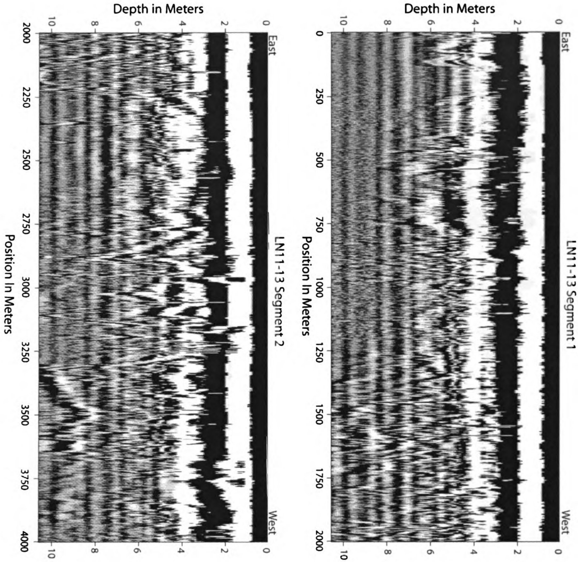

Figure A12 Segments 1&2 of Lincoln Road Merged Profiles 11-13.

Lincoln Road Merged Profiles 11-13 (Cont.)

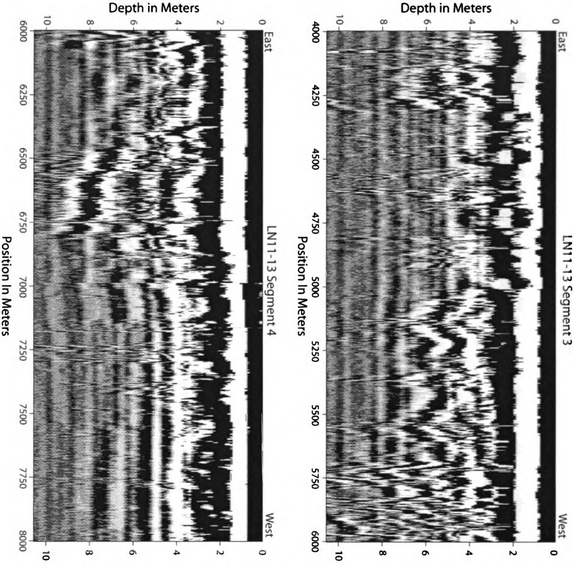

Figure A13 Segments 3&4 of Lincoln Road Merged Profiles 11-13.

Lincoln Road Merged Profiles 11-13 (Cont.)

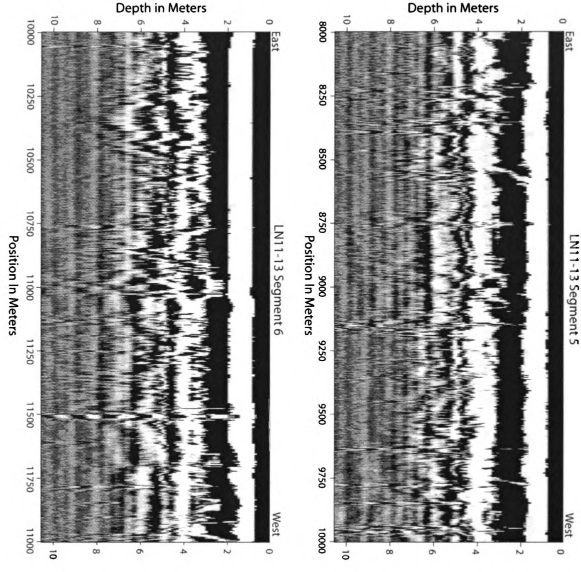

Figure A14 Segments 5&6 of Lincoln Road Merged Profiles 11-13.

Lincoln Road Merged Profiles 11-13 (Cont.)

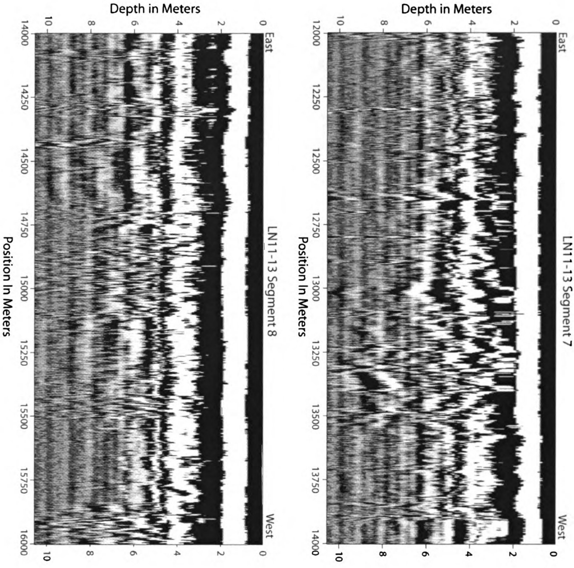

Figure A15 Segments 7&8 of Lincoln Road Merged Profiles 11-13.

Lincoln Road Merged Profiles 11-13 (Cont.)

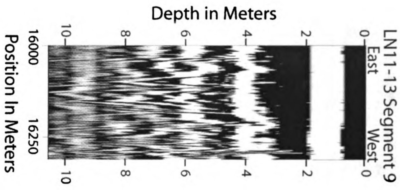

Figure A16 Segment 9 of Lincoln Road Merged Profiles 11-13.

Bethel Road Merged Profiles 2-3

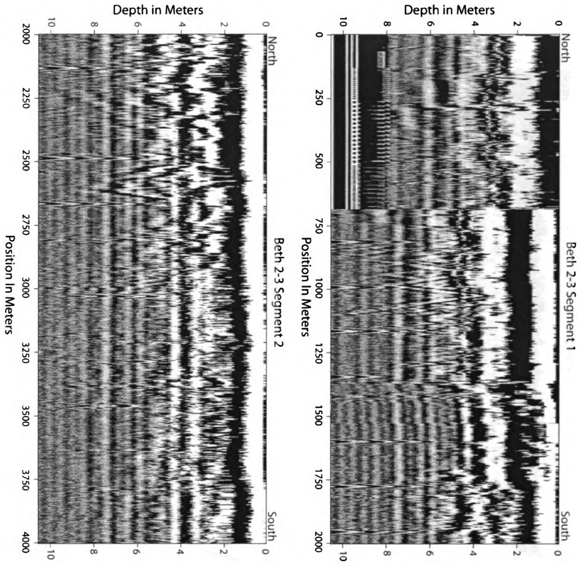

Figure A17 Segments 1&2 of Bethel Road Merged Profiles 2-3. Segment two (0-660m) corrupt.

Bethel Road Merged Profiles 2-3 (Cont.)

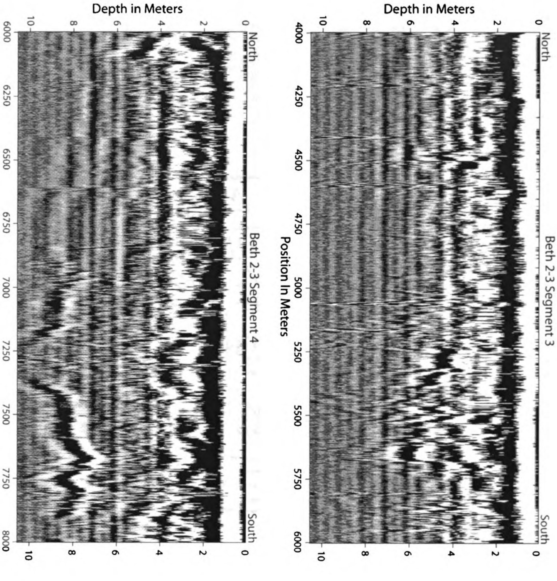

Figure A18 Segments 3&4 of Bethel Road Merged Profiles 2-3.

Bethel Road Merged Profiles 2-3 (Cont.)

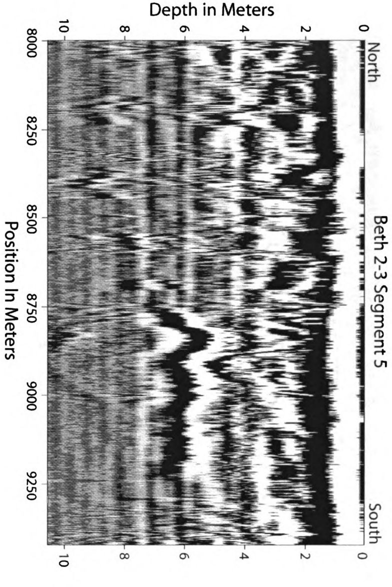

Figure A19 Segment 5 of Bethel Road Merged Profiles 2-3.

Dinuba Road Profile 3

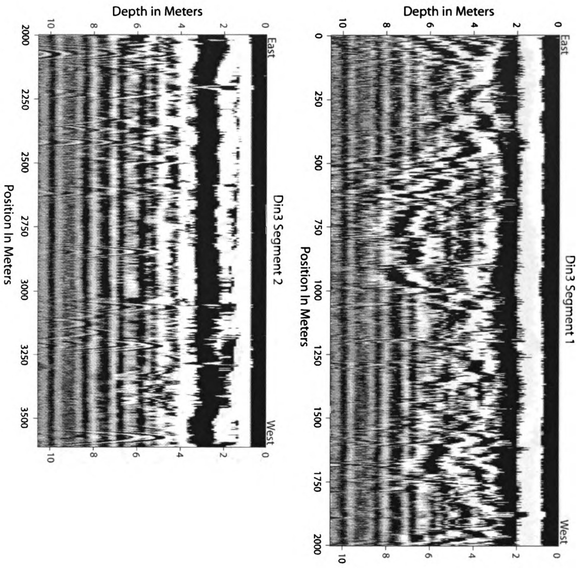

Figure A20 Segments 1&2 of Dinuba Road Profile 3.

North Road Profile 1

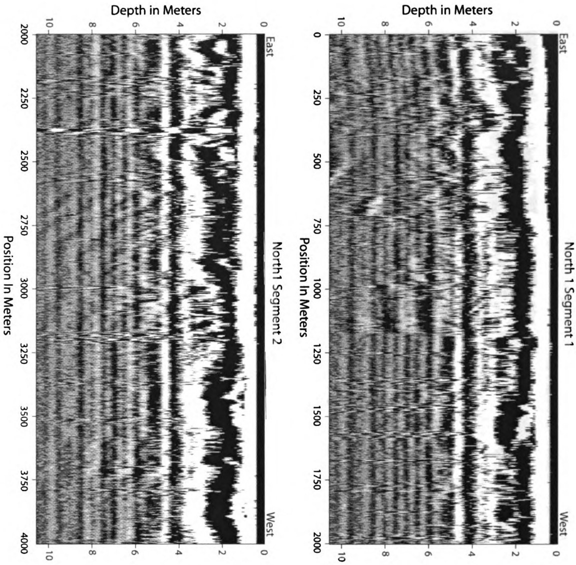

Figure A21 Segments 1&2 of North Road Profile 1.

North Road Profile 1 (Cont.)

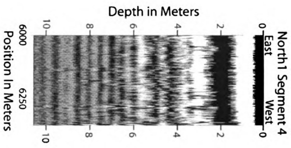

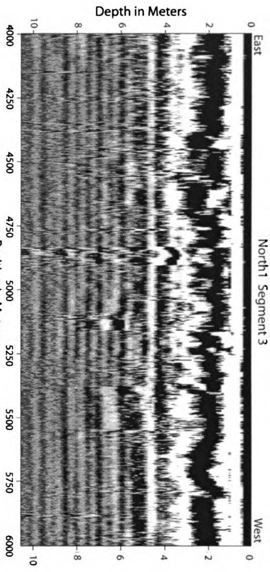

Figure A22 Segments 3&4 of North Road Profile 1.

Indianola Road Profile 3

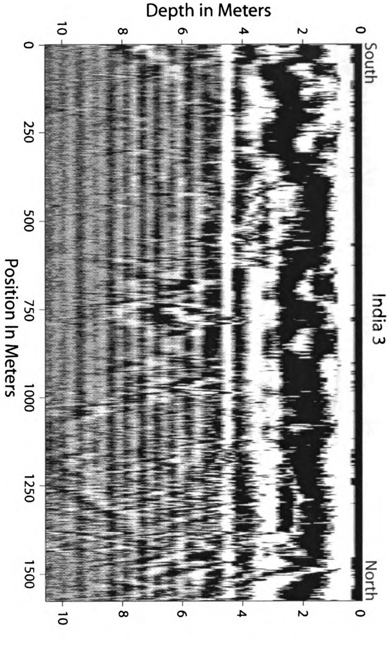

Figure A23 Indianola Road Profile 3.

Annadale Road Profile 1

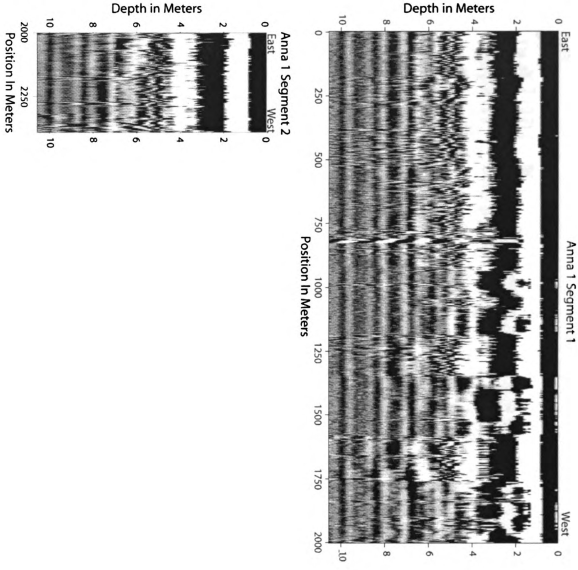

Figure A24 Segments 1&2 of Annadale Road Profile 1.

Green Road Merged Profiles 1-2

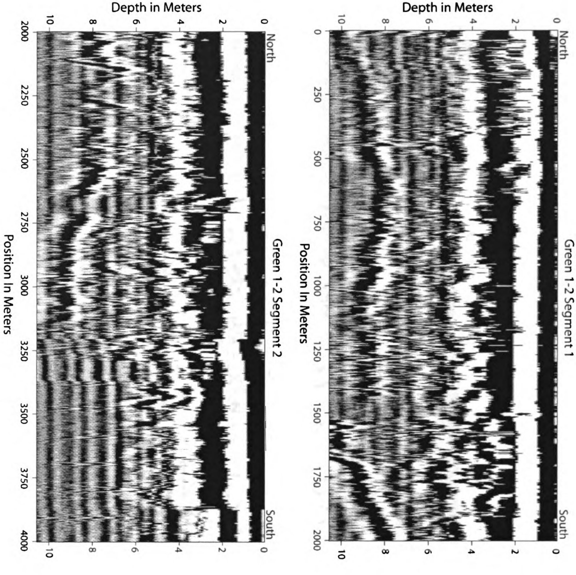

Figure A25 Segments 1&2 of Green Road Merged Profiles 1-2.

Green Road Merged Profiles 1-2 (Cont.)

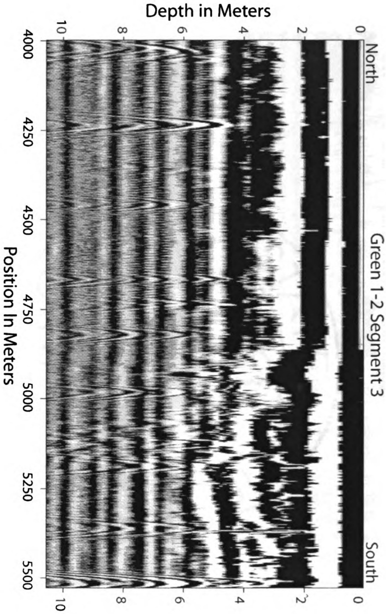

Figure A26 Segment3 of Green Road Merged Profiles 1-2.

Highland Road Profile 1 (High1)

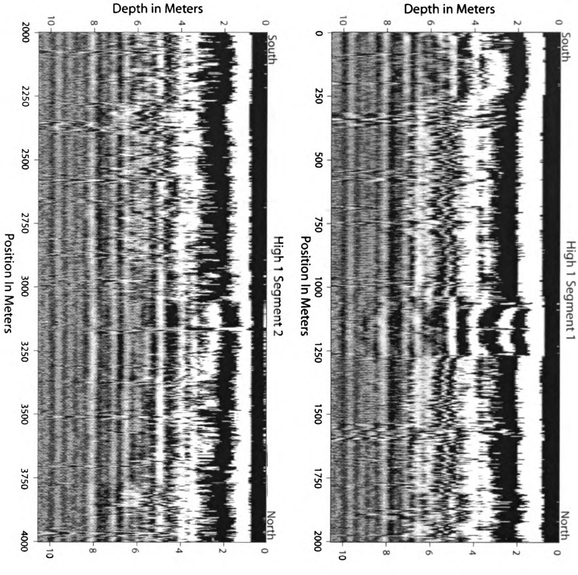

Figure A27 Segments 1&2 of Highland Road Profile 1.

Highland Road Profile 1 (High1) (Cont.)

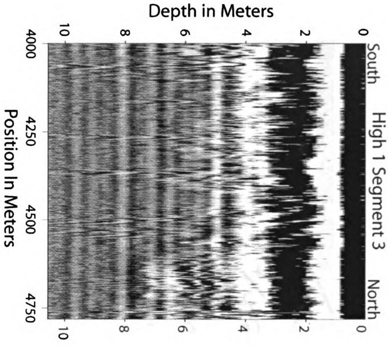

Figure A28 Segment 3 of Highland Road Profile 1.

Central Avenue Merged Profiles 1-2

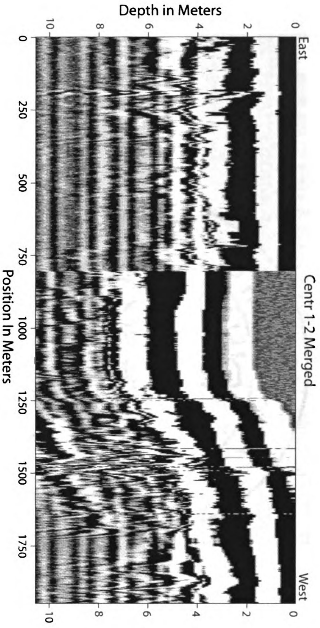

Figure A29 Central Avenue Merged Profiles 1&2. Segment 2 is corrupt.

Butler Road Profile 1

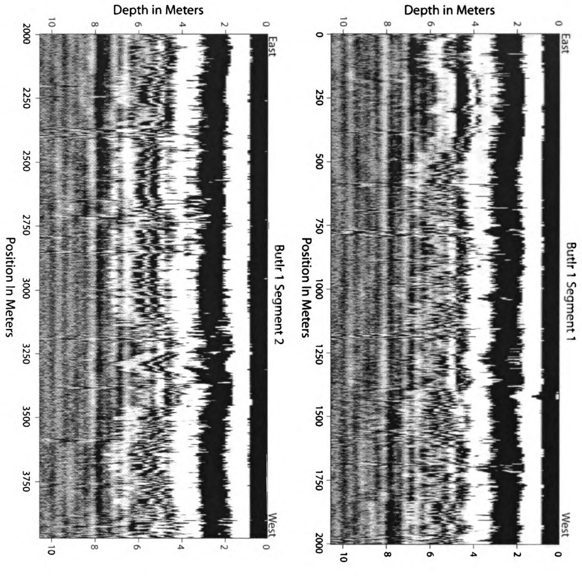

Figure A30 Segments 1&2 of Butler Road Profile 1.

California Road Profile 1

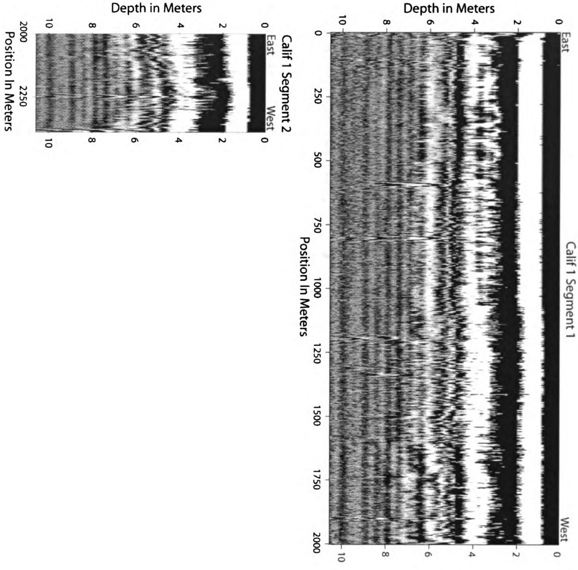

Figure A31 Segments 1&2 of California Road Profile 1.

Church Road Profile 1

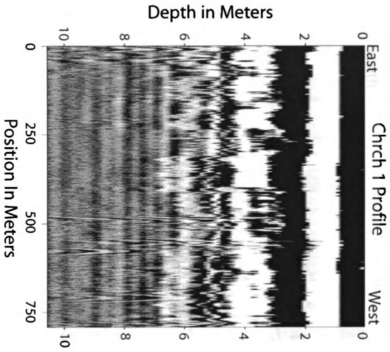

Figure A32 Church Road Profile 1.

Dockery Road Profile 1

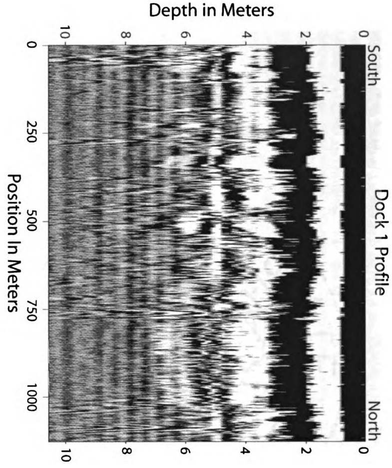

Figure A33 Dockery Road Profile 1.

Indianola Road Profile 21 (Indi21)

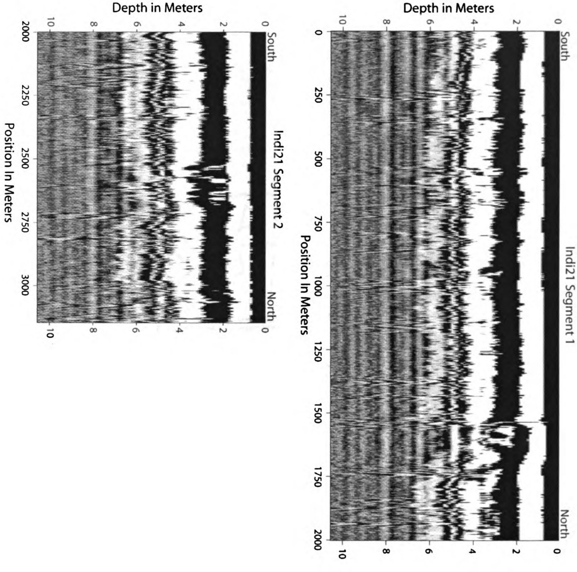

Figure A34 Segments 1&2 of Indianola Road Profile 21.

Thompson Road Profile 1 (Thom1)

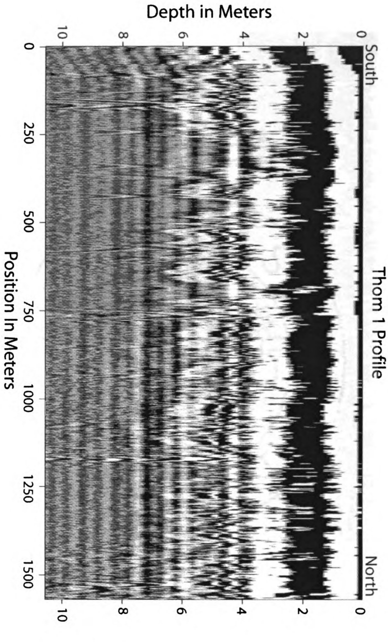

Figure A35 Thompson Road Profile 1.

Thompson Road Profile (Thom21)

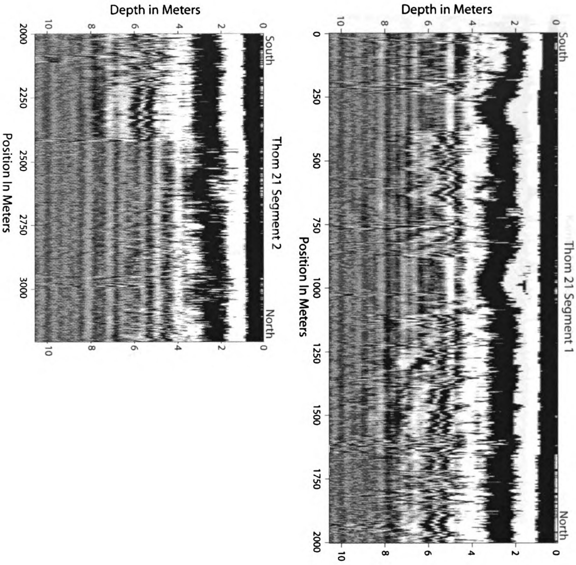

Figure A36 Segments 1&2 of Thompson Road Profile 21 (Thom21).

Kamm Road Merged Profiles 1-2

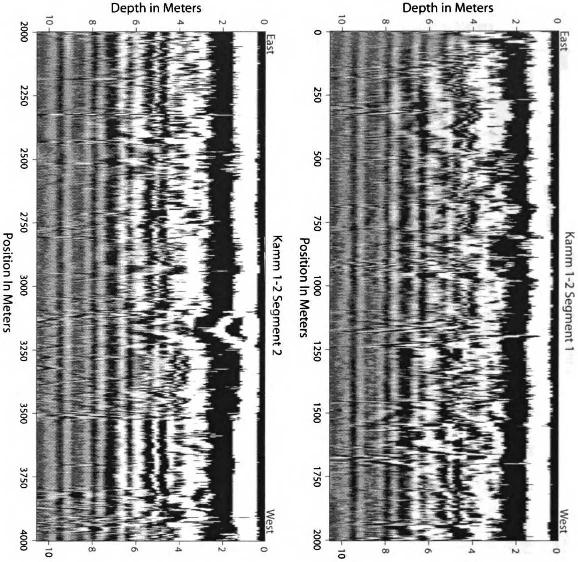

Figure A37 Segments 1&2 of Kamm Road Merged Profiles 1&2.

Kamm Road Merged Profiles 1-2 (Cont.)

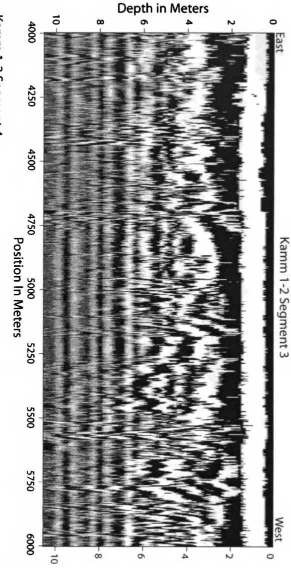

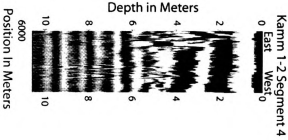

Figure A38 Segments 3&4 of Kamm Road Merged Profiles 1-2.

Nebraska Road Merged Profiles 1-3

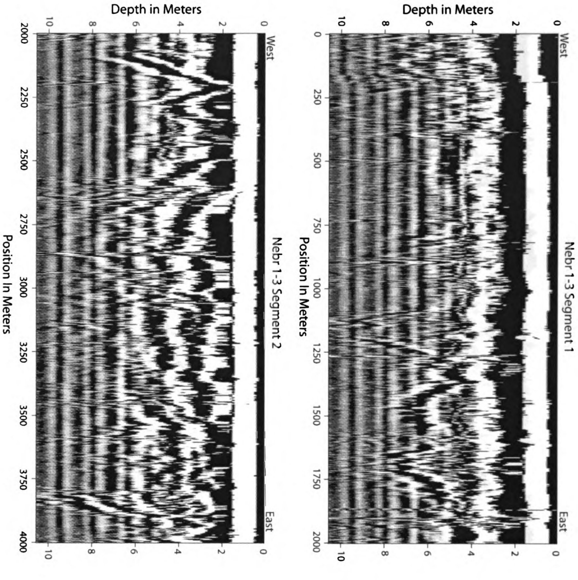

Figure A39 Segments 1&2 of Nebraska Road Merged Profiles 1-3.

Nebraska Road Merged Profiles 1-3 (Cont.)

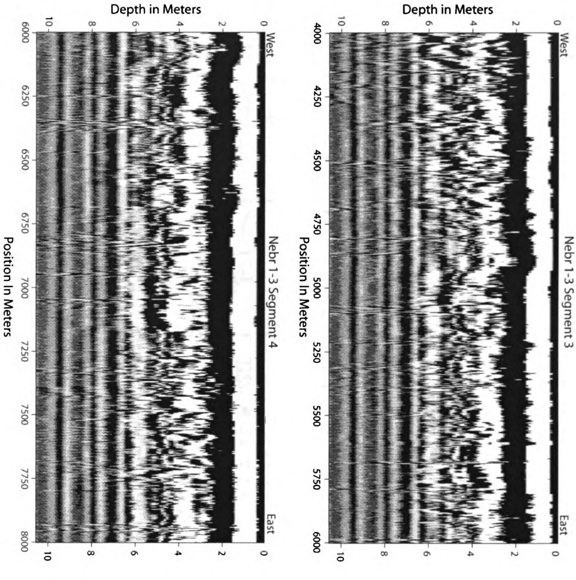

Figure A40 Segments 3&4 of Nebraska Road Merged Profiles 1-3.

Nebraska Road Merged Profiles 1-3

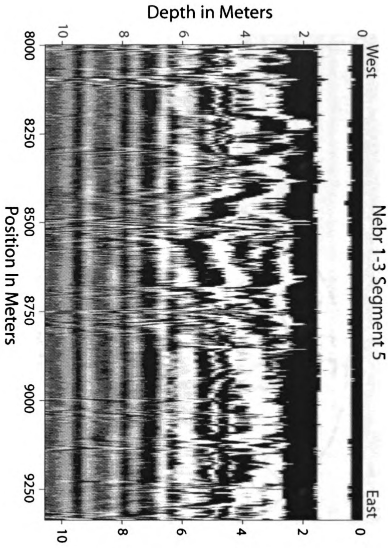

Figure A41 Segment 5 of Nebraska Road Merged Profiles 1-3.

Zediker Road Profile 1

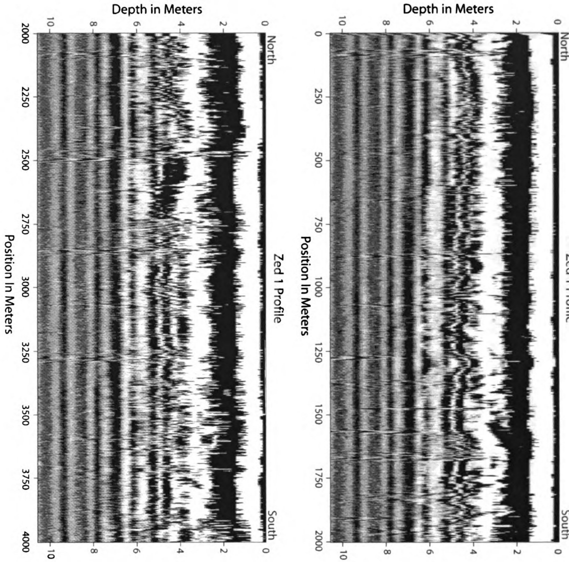

Figure A42 Segments 1&2 of Zediker Road Profile 1.

Zediker Road Profile 1 (Cont.)

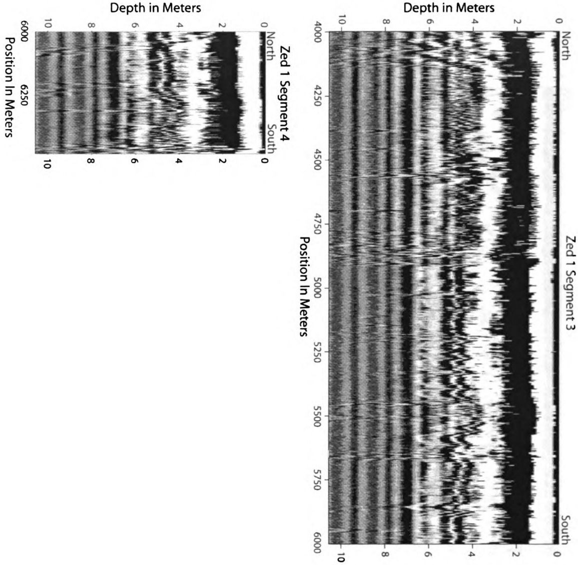

Figure A43 Segments 3&4 of Zediker Road Profile 1.

Tuolumne and Merced River Fluvial Fan GPR Profiles

Bradbury Road Profile 1

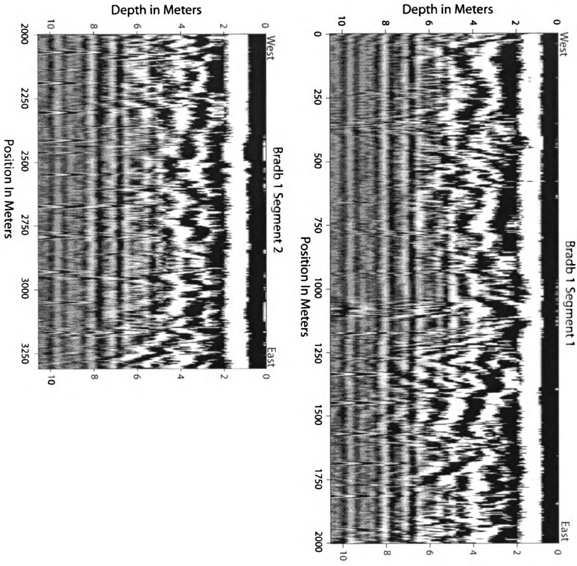

Figure A44 Segments 1&2 of Bradbury Road Profile 1.

Merced Road Merged Profiles 1-2

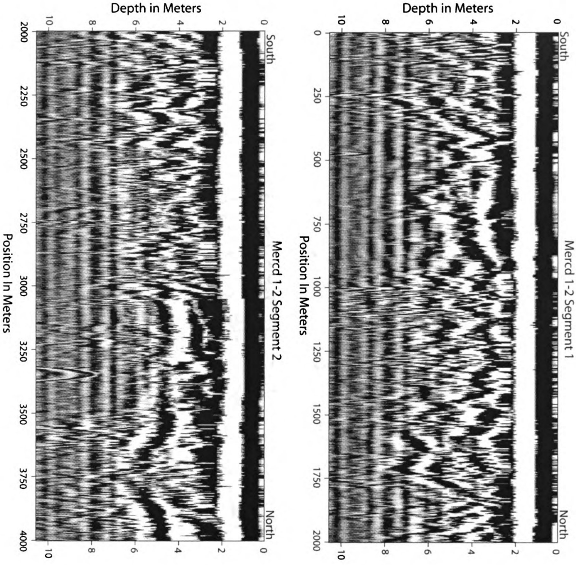

Figure A45 Segments 1&2 of Merced Road Merged Profiles 1-2.

Merced Road Merged Profiles 1-2 (Cont.)

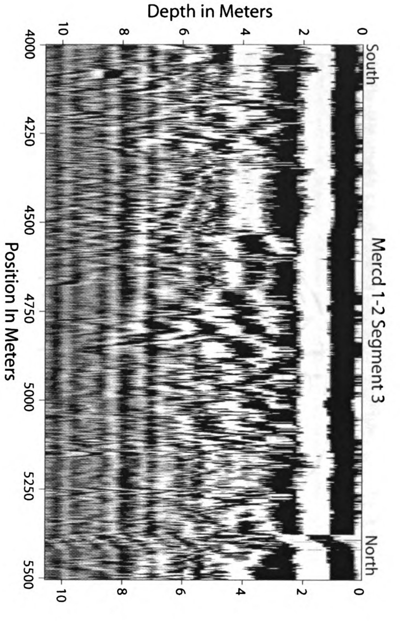

Figure A46 Segment 3of Merced Road Merged Profiles 1-2.

Palm Road Merged Profiles 1-2

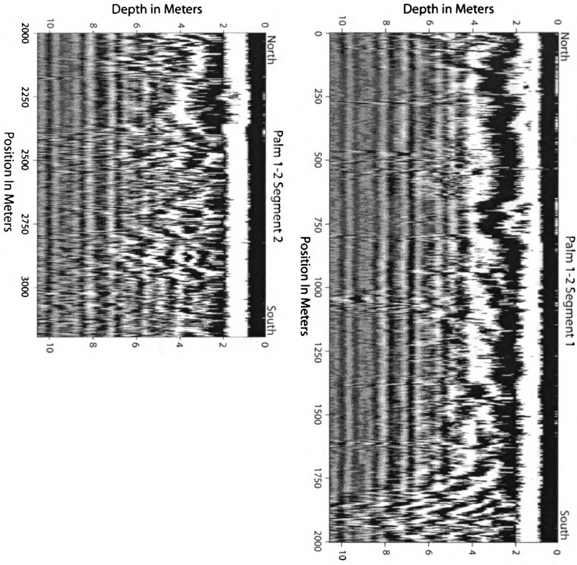

Figure A47 Segments 1&2 of Palm Road Merged Profiles 1-2.

Bloss Road Merged Profiles 1-3

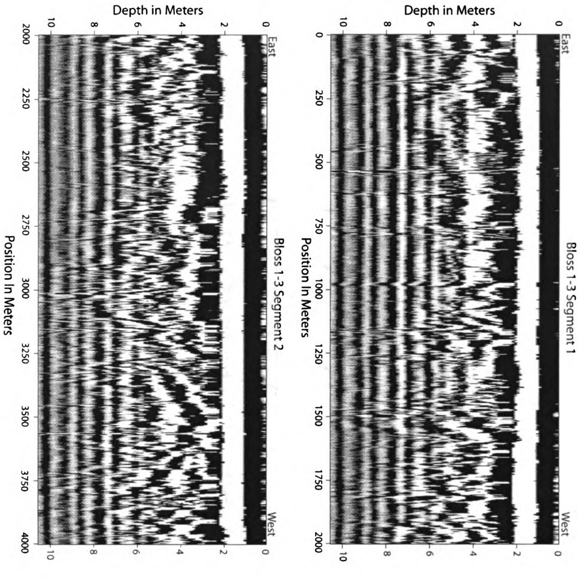

Figure A48 Segments 1&2 of Bloss Road Merged Profiles 1-3.

Bloss Road Merged Profiles 1-3 (Cont.)

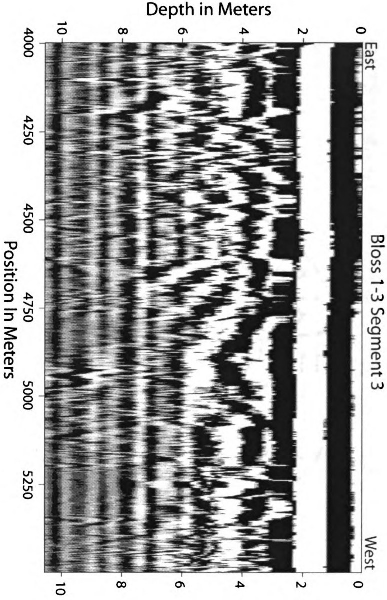

Figure A49 Segment 3 of Bloss Road Merged Profiles 1-3.

American Avenue Profile 1

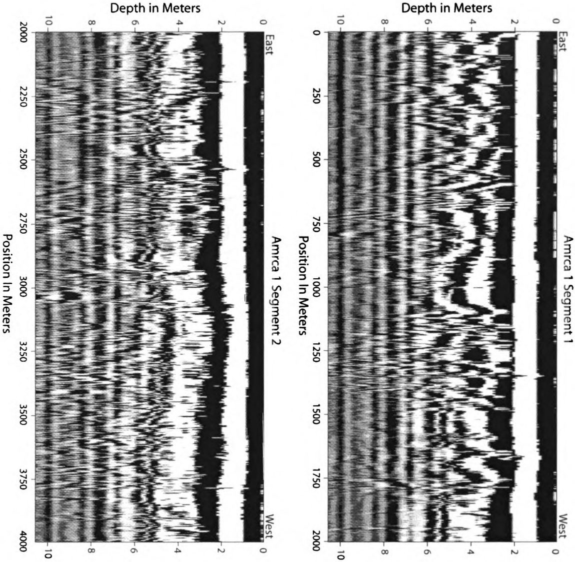

Figure A50 Segments 1&2 of American Avenue Profile 1.

American Avenue Profile 1 (Cont.)

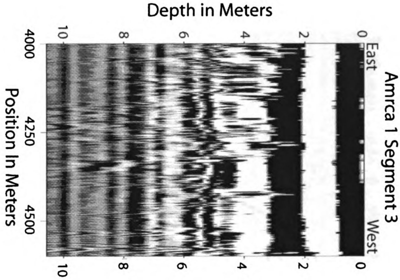

Figure A51 Segment 3 of American Avenue Profile 1.

Pepper Road Profile 1

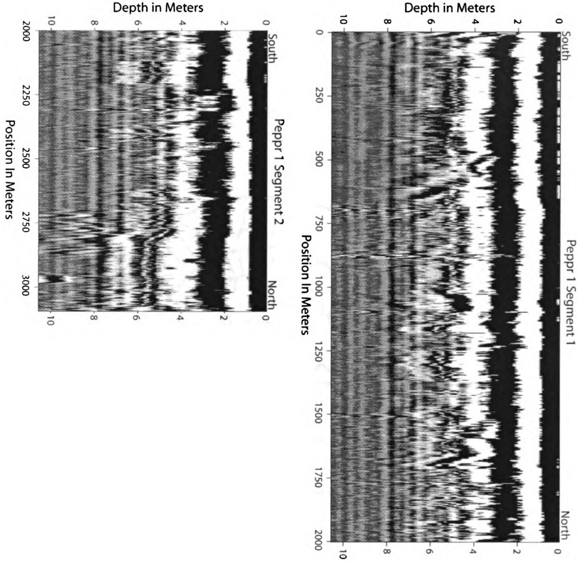

Figure A52 Segments 1&2 of Pepper Road Profile 1.

Sunny Acres Road Profile 1

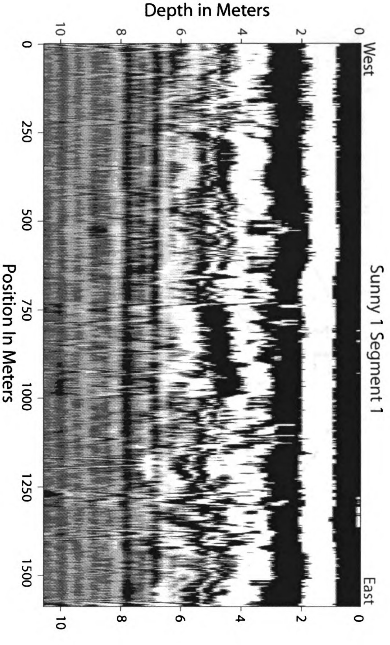

Figure A53 Sunny Acres Road Profile 1.

Newport Road Profile 1

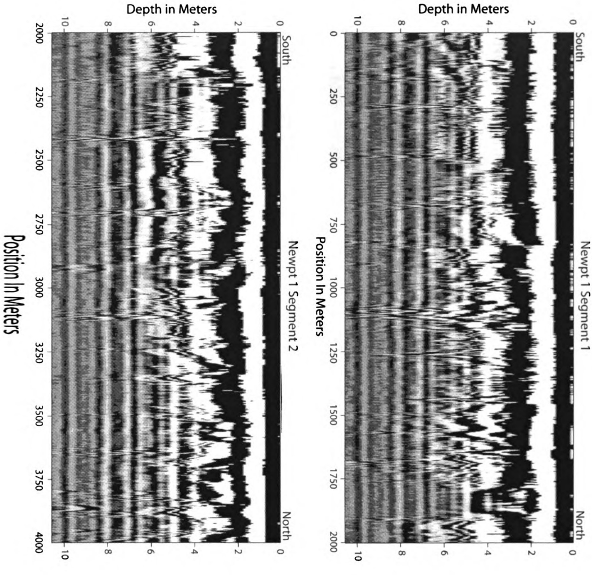

Figure A54 Segments 1&2 of Newport Road Profile 1.

Newport Road Profile 1 (Cont.)

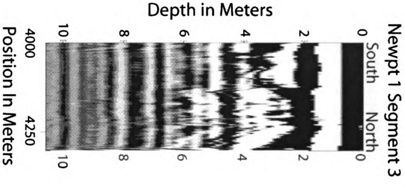

Figure A55 Segment 3 of Newport Road Profile 1.

Sperry Road Profile 1

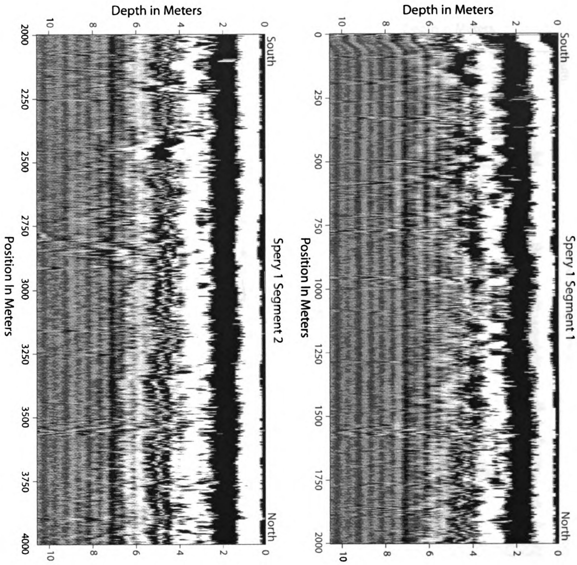

Figure A56 Segments 1&2 of Sperry Road Profile 1.

Sperry Road Profile 1 (Cont.)

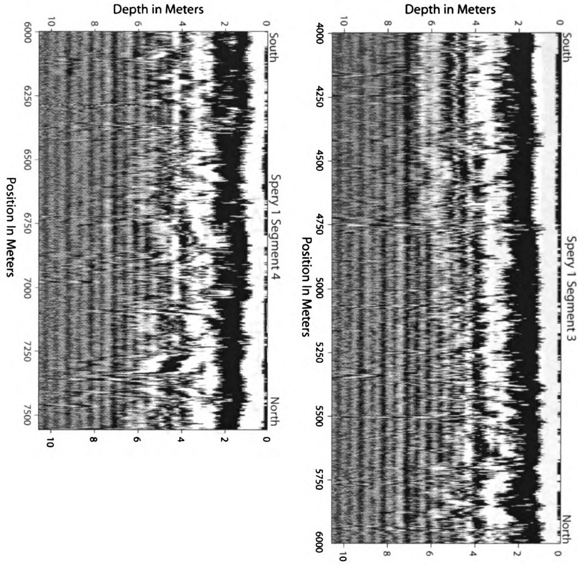

Figure A57 Segments 3&4 of Sperry Road Profile 1.

Grayson Road Profile 1 (Grays1)

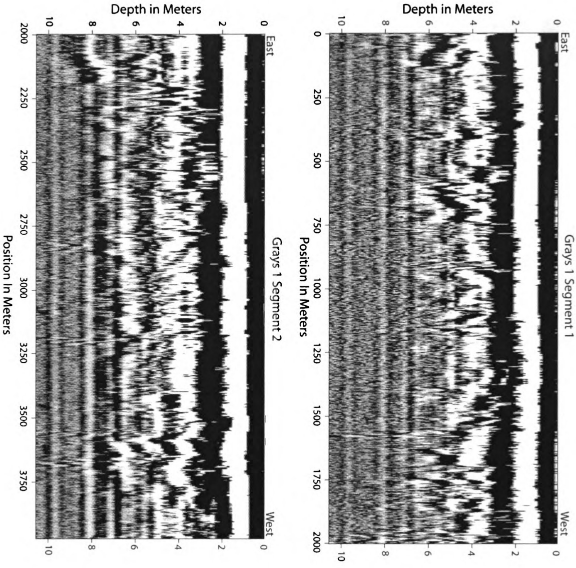

Figure A58 Segments 1&2 of Grayson Road Profile 1 (Grays1).

Pioneer Road Profile 1

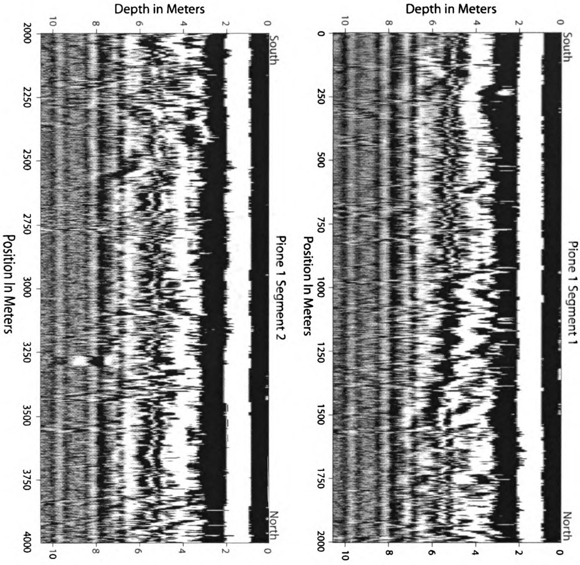

Figure A59 Segments 1&2 of Pioneer Road Profile 1.

Pioneer Road Profile 1 (Cont.)

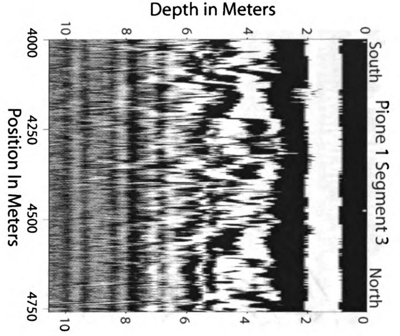

Figure A60 Segment 3 of Pioneer Road Profile 1.

Redwood Road Profile 1

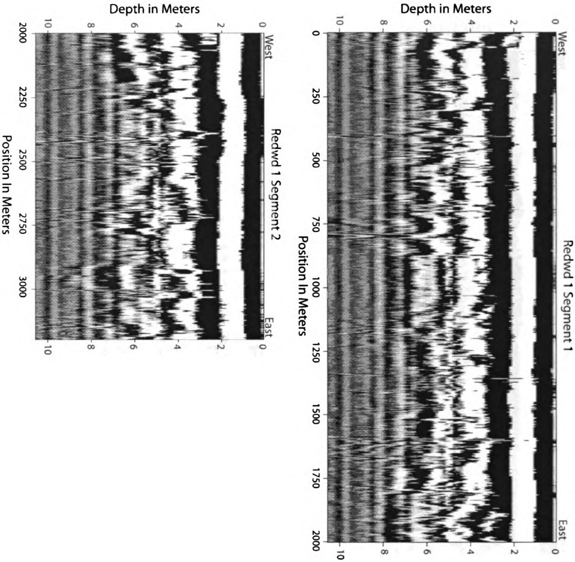

Figure A61 Segments 1&2 of Redwood Road Profile 1.

Monte Vista Road Profile 1

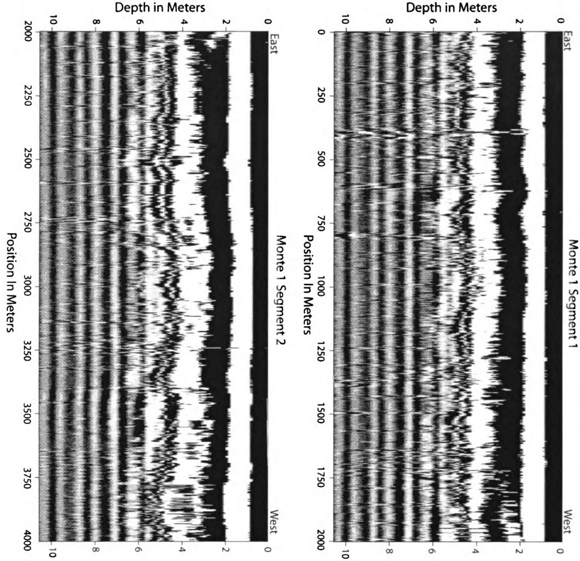

Figure A62 Segments 1&2 of Monte Vista Road Profile 1.

Monte Vista Road Profile 1 (Cont.)

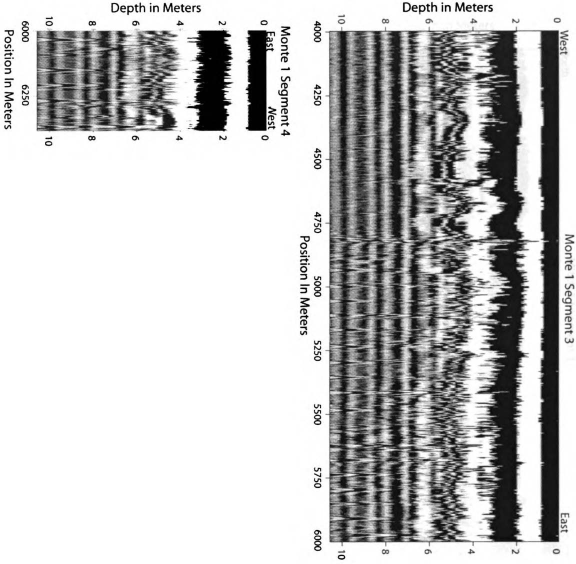

Figure A63 Segments 3&4 of Monte Vista Road Profile 1.

Mitchell Road Profile 1

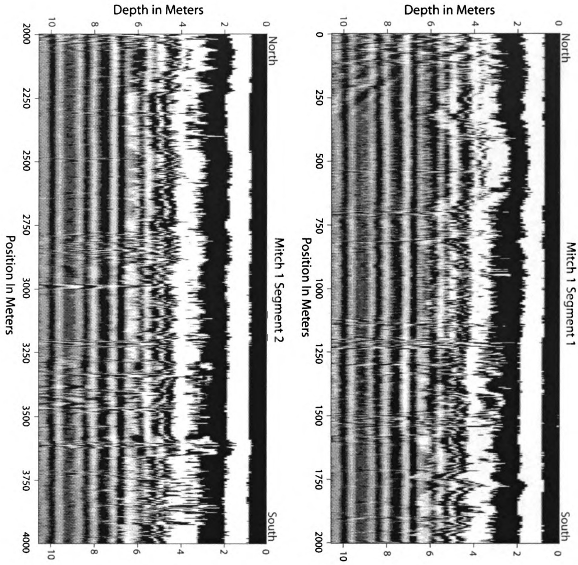

Figure A64 Segments 1&2 of Mitchell Road Profile 1.

Mitchell Road Profile 1 (Cont.)

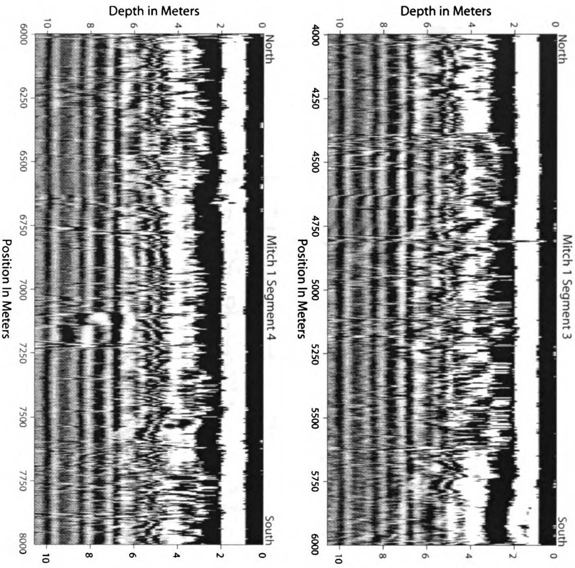

Figure A65 Segments 3&4 of Mitchell Road Profile 1.

Mitchell Road Profile 1 (Cont.)

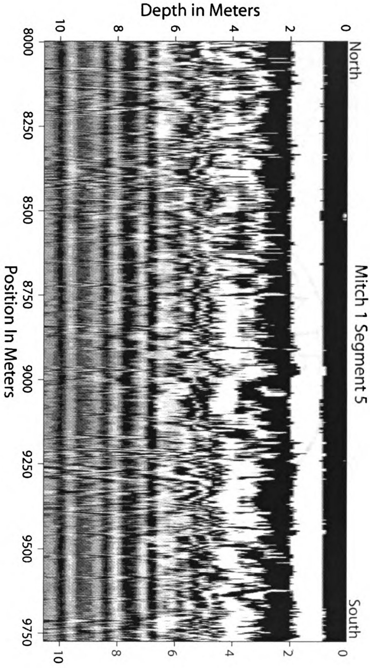

Figure A66 Segment 5 of Mitchell Road Profile 1.

Grayson Road Profile 1 (Grson1)

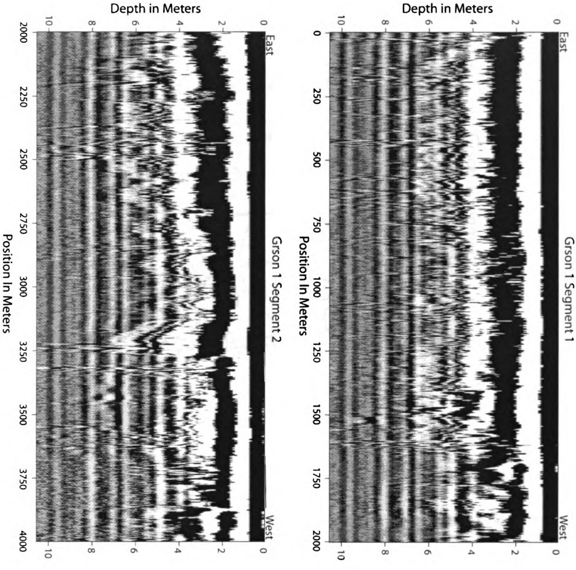

Figure A67 Segments 1&2 of Grayson Road Profile 1 (Grson1).

Grayson Road Profile 1 (Grson1) (Cont.)

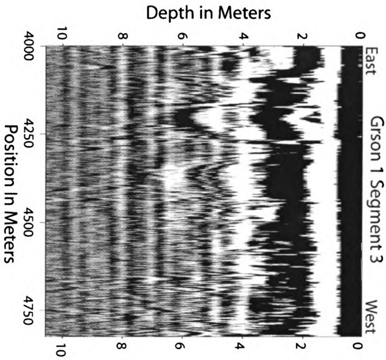

Figure A68 Segment 3 of Grayson Road Profile 1 (Grson1).

Appendix B

Kearney Orchard Site GPR Profiles

This section presents all of the GPR data collected at the Kearney Agricultural Center (KAC). GPR profiles were collected using both 100 and 50 MHz antennas.

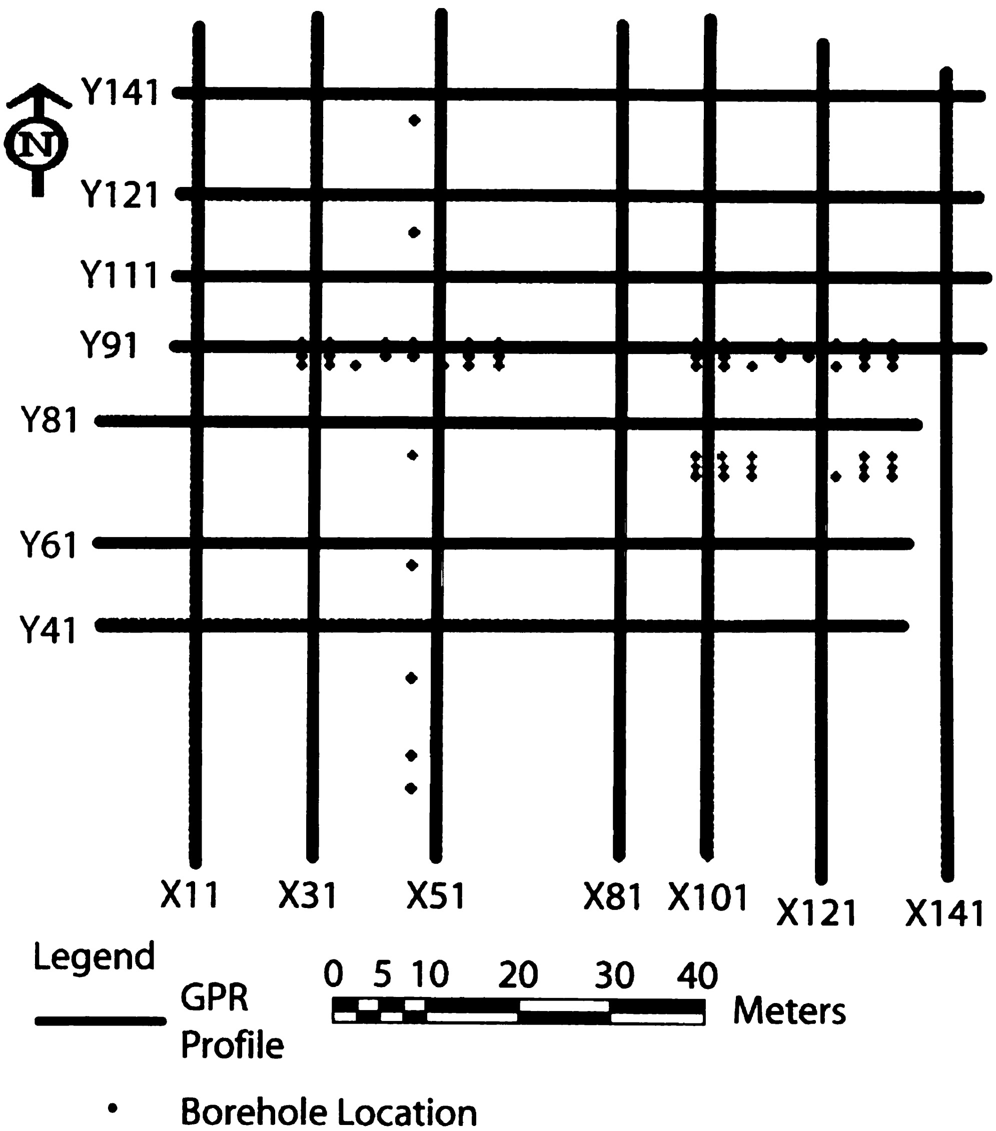

Figure B1 Kearney Agricultural Center orchard site GPR grid map. Geoprobe borehole locations used to groundtruth the GPR data are also shown.

50MHz Y-Direction Profiles

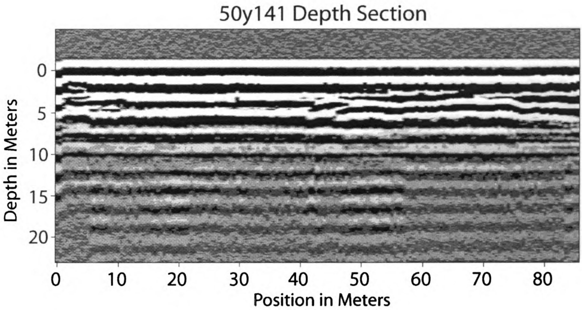

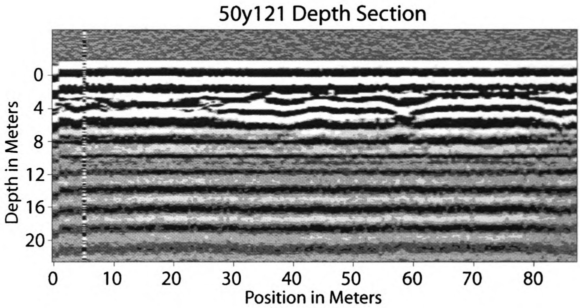

Figure B2 50y141 depth section.

Figure B3 50y121 depth section.

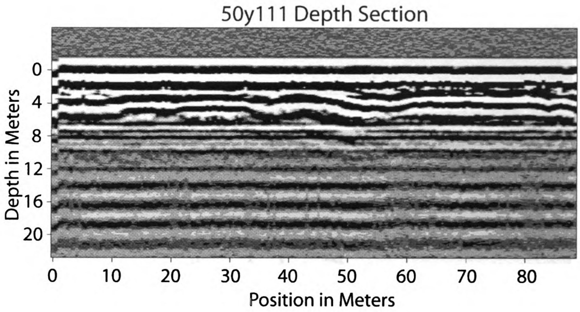

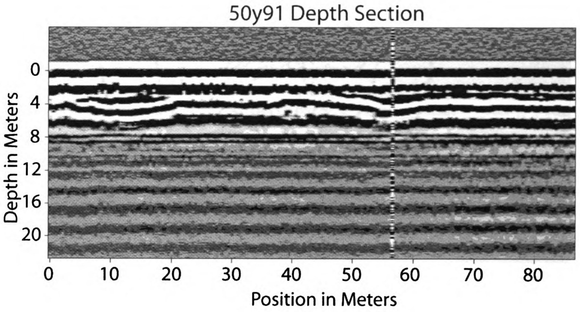

Figure B4 50y111 depth section.

Figure B5 50y91 depth section.

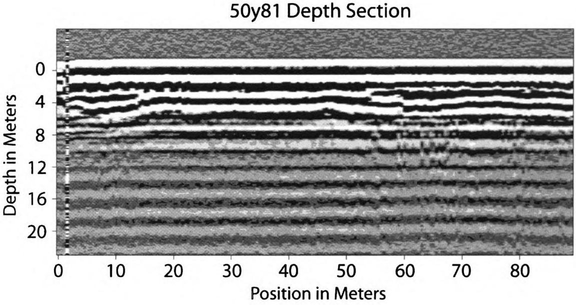

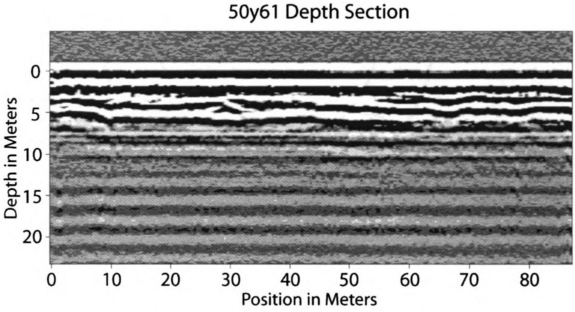

Figure B6 50y81 depth section.

Figure B7 50y61 depth section.

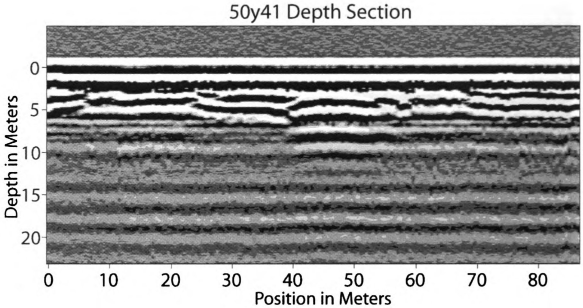

50MHz X-Direction Profiles

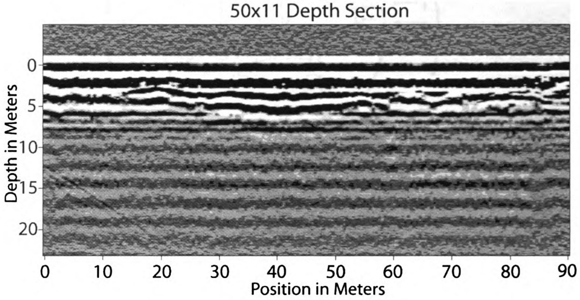

Figure B8 50y41 depth section.

Figure B9 50x11 depth section.

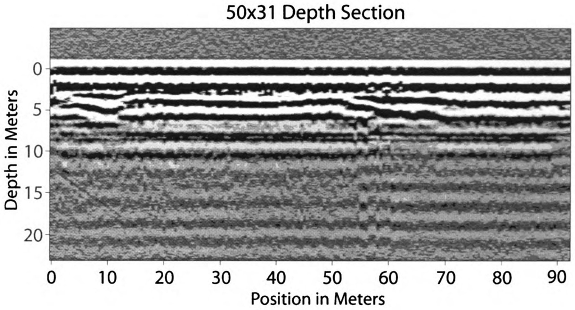

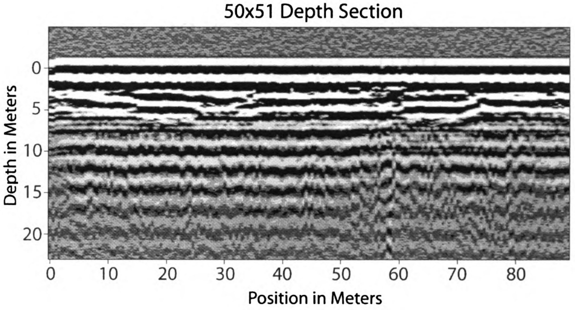

Figure B10 50x31 depth section.

Figure B11 50x51 depth section.

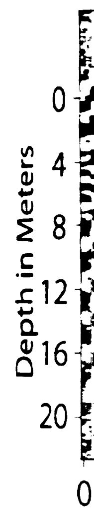

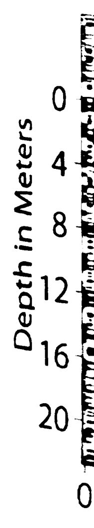

Figure B

Figure B

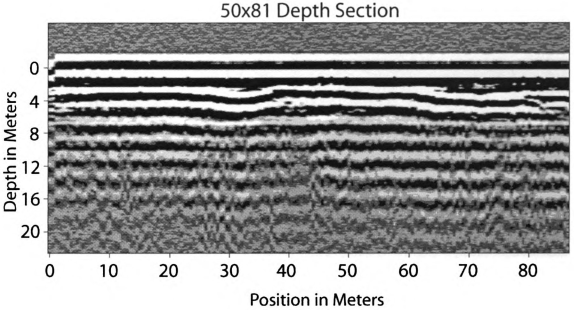

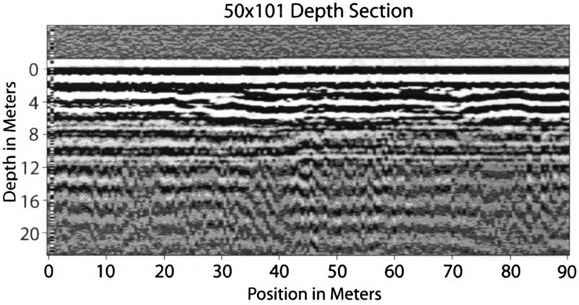

Figure B12 50x81 depth section.

Figure B13 50x101 depth section.

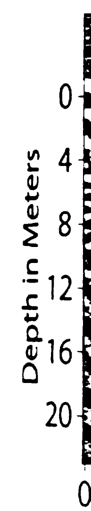

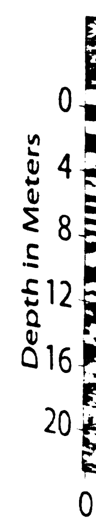

Figure B1

Figure B1

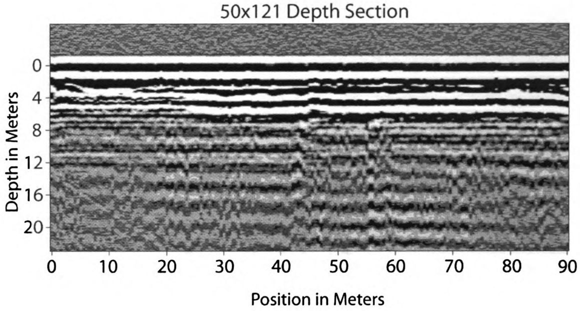

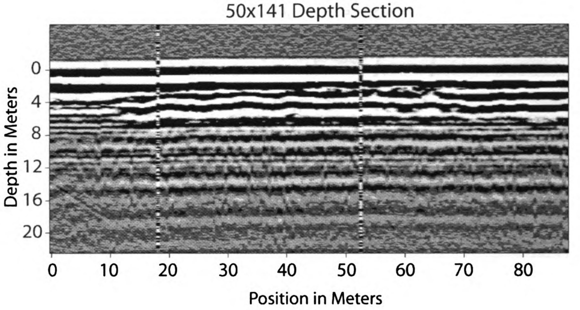

Figure B14 50x121 depth section.

Figure B15 50x141 depth section.

100MHz Y-Direction Profiles

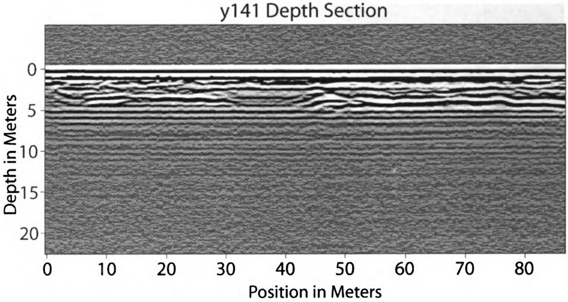

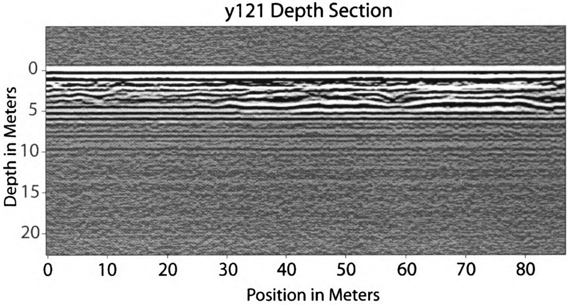

Figure B16 y141 depth section.

Figure B17 y121 depth section.

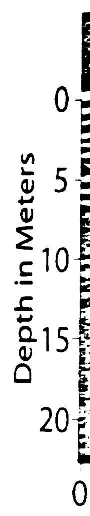

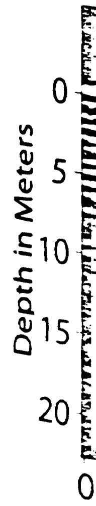

Figure B

Figure B

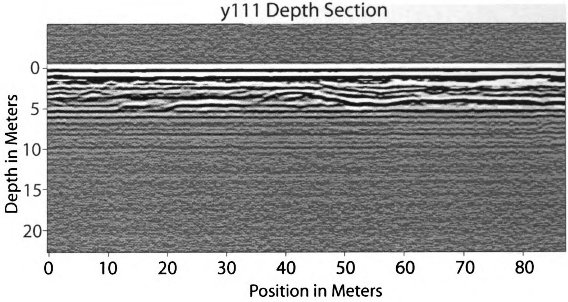

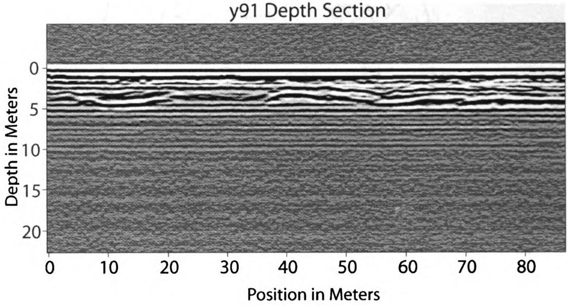

Figure B18 y111 depth section.

Figure B19 y91 depth section.

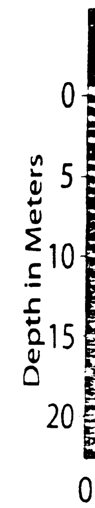

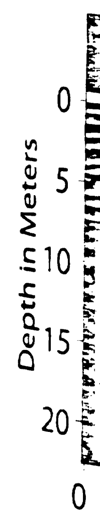

Figure B2

Figure B2

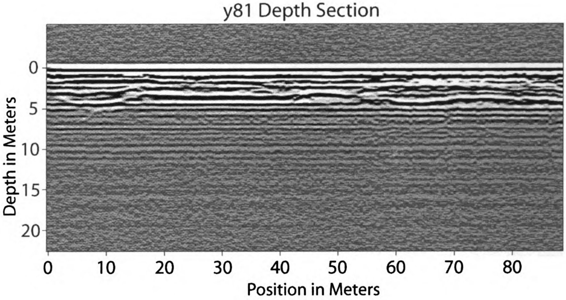

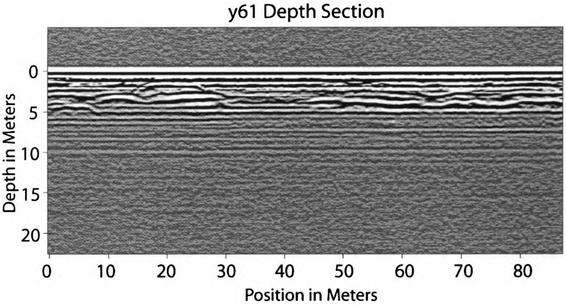

Figure B20 y81 depth section.

Figure B21 y61 depth section.

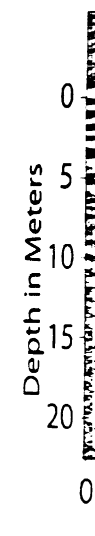

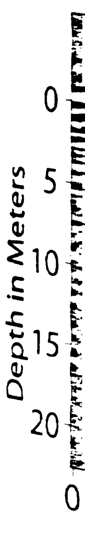

Figure B2

Figure B2

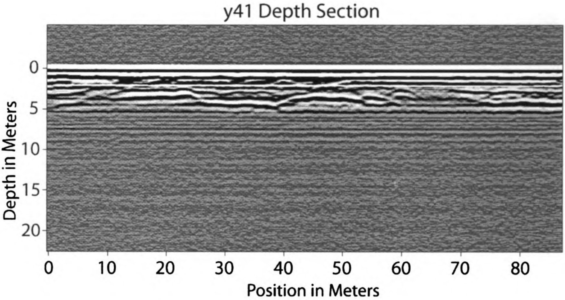

100MHz X-Direction Profiles

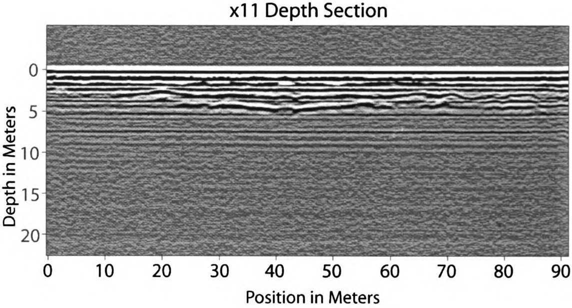

Figure B22 y41 depth section.

Figure B23 x11 depth section.

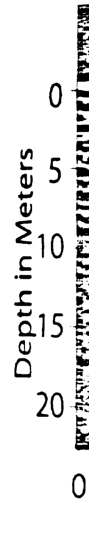

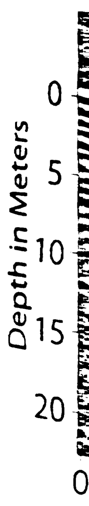

Figure B

Figure B

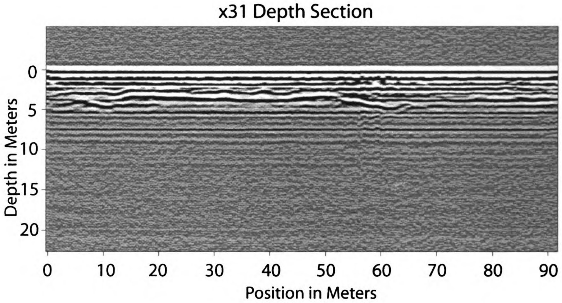

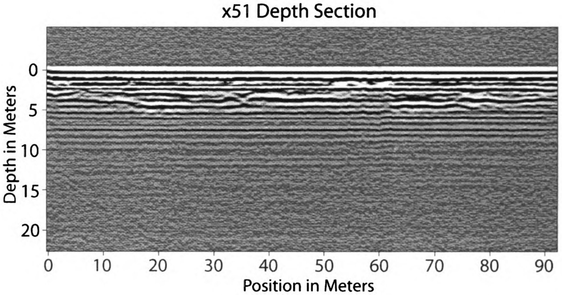

Figure B24 x31 depth section.

Figure B25 x51 depth section.

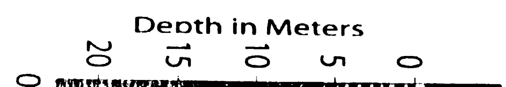

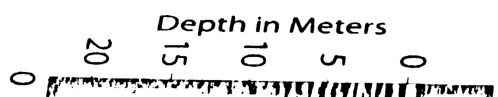

Figure B2

Figure B2

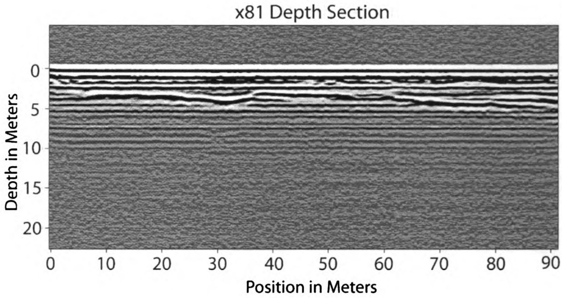

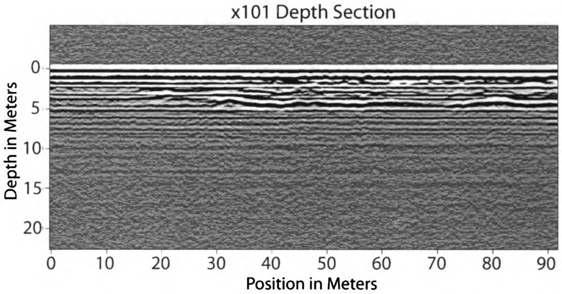

Figure B26 x81 depth section.

Figure B27 x101 depth section.

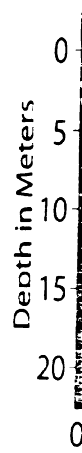

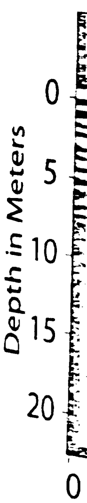

Figure B28

Figure B29

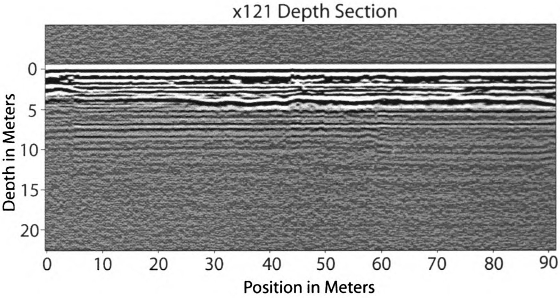

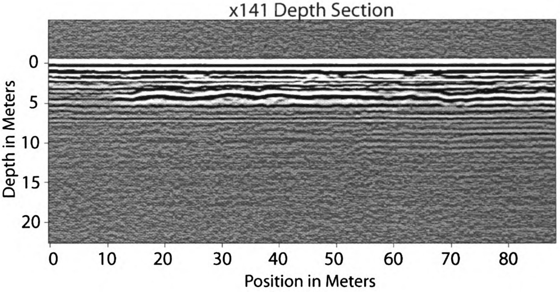

Figure B28 x121 depth section.

Figure B29 x141 depth section.

Appendix C

CMP Experiments

In order to develop depth scales for our GPR profiles, common-mid point experiments (CMP's) were conducted at various points across the upper KRF, TRF, and MRF surfaces. Presented here are the results of the CMP experiments. First a table that contains the calculated near-surface velocity for each CMP experiment along with the location listed in decimal degrees is given below. Second, all CMP images are presented along with a location map showing the location of each CMP.

CMP Name	Calculated Near Surface Velocity	Location in Degrees, Decimal Minutes
DRCMP1 (50 MHz)	No Value Calculated	N 36d 43.261' W 119d 35.467'
HLCMP1 (50 MHz)	0.16 m/ns	N 36d 37.327' W 119d 37.636'
HLCMP2 (100MHz)	No Value Calculated	N 36d 37.327' W 119d 37.636'
LNCMP1 (50 MHz)	0.14 m/ns	N 36d 38.561' W 119d 30.103'
LNCMP2 (50 MHz)	0.12 m/ns	N 36d 38.951' W 119d 40.829'
PLCMP1 (100 MHz)	0.13 m/ns	N 36d 36.752' W 119d 35.631'
PLCMP2 (50 MHz)	0.13 m/ns	N 36d 36.752' W 119d 35.631'
KRCMP1 (50 MHz)	No Value Calculated	N 36d 35.450' W 119d 30.179'
KRCMP2 (100 MHz)	0.14 m/ns	N 36d 35.450' W 119d 30.179'
DNCMP2 (50 MHz)	0.14 m/ns	N 36d 35.406' W 119d 33.760'
BLCMP1 (50 MHz)	0.14 m/ns	N 37d 24.301' W 120d 45.537'
MHCMP1 (50 MHz)	No Value Calculated	N 37d 31.437' W 120d 56.366'
NPCMP1 (50 MHz)	0.14 m/ns	N 37d 28.020' W 120d 42.139'
PMCMP1 (50 MHz)	No Value Calculated	N 37d 26.859' W 120d 45.980'
RWCMP1 (50 MHz)	0.16 m/ns	N 37d 34.383' W 120d 53.208'

Table C1 Table listing all CMP experiments by name as well as calculated near surface velocity and location in Degrees Decimal Minutes.

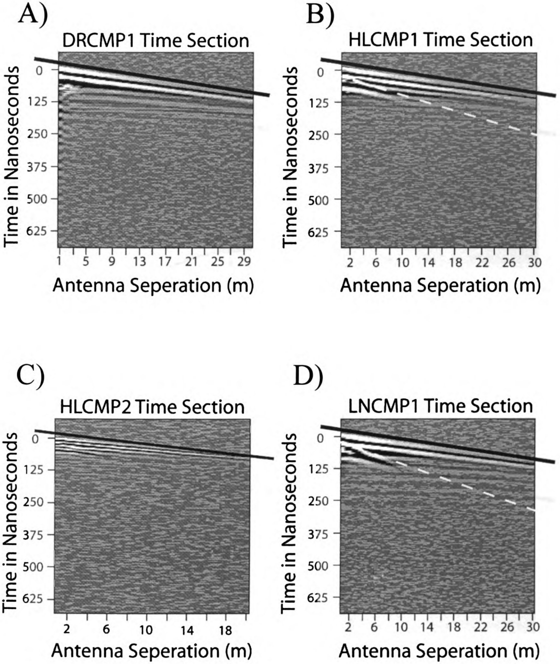

Figure C1 A) Del Rey Road CMP B) Highland Road 1 CMP C) Highland Road 2 CMP (100MHz) D) Lincoln Road 1 CMP

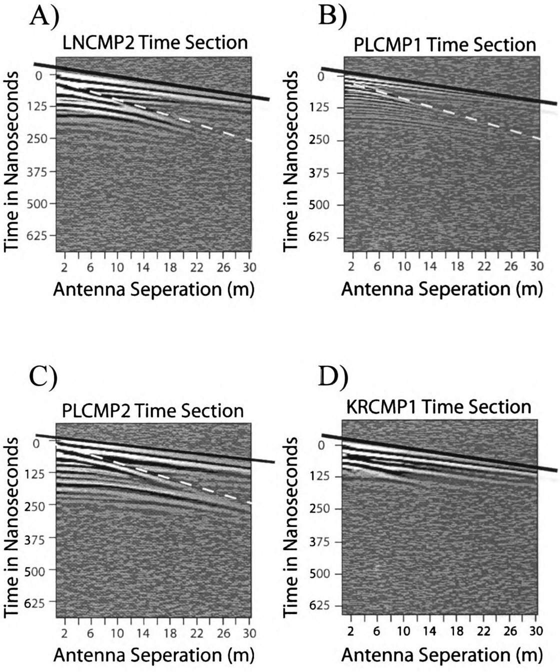

Figure C2 A) Lincoln Road 2 CMP B) Parlier Road 1 CMP (100MHz) C) Parlier Road 2 CMP D) Kearney Orchard Site 1 CMP

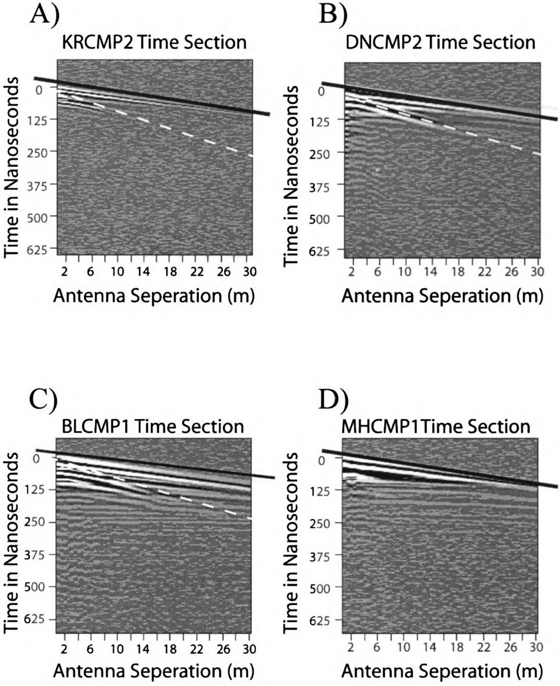

Figure C3 A) Kearney Orchard Site 2 CMP (100 MHz) B) Dinuba Road 2 CMP C) Bloss Road 1 CMP D) Mitchel Road 1 CMP

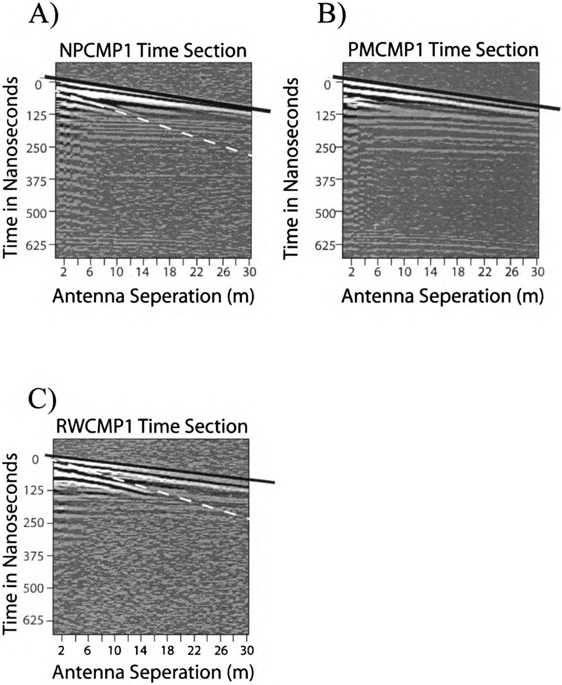

Figure C4 A) Newport Road 1 CMP B) Palm Road 1 CMP C) Redwood Road 1 CMP

CMP Location Maps

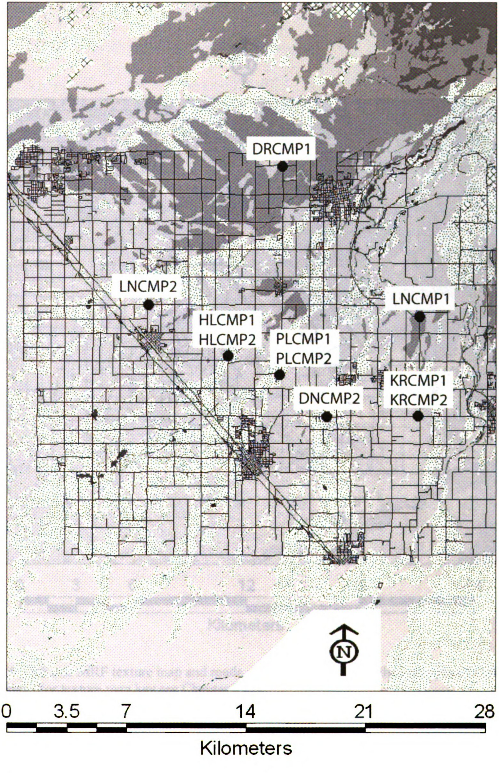

Figure C5 KRF texture map and roads coverage highlighting the locations of CMP experiments. For texture map key see Chapter Two.

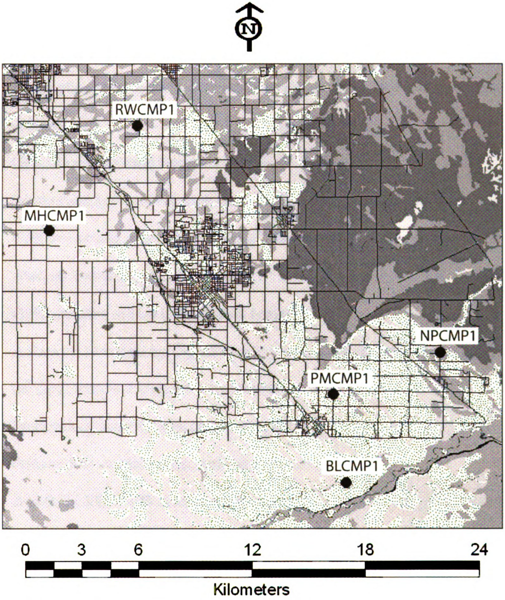

Figure C6 TRF and MRF texture map and roads coverage highlighting the locations of CMP experiments. For texture map key see Chapter Two.

Appendix D

GPR System Components

- Sensors and Software Inc. pulseEKKO 100 GPR system
- 50 MHz and 100MHz center frequency antennae
- Transmitting and receiving antenna modules
- Fiber optic cables connected transmitting and receiving antennae to the main GPR console.
- GPR triggering/sound box
- Sensors and Software Inc. Fast Port (facilitates faster data acquisition)
- GPR system was attached to Gateway Solo laptop computer (Pentium II) that acted as recording/processing device.
- GPR operating software installed on computer
- A deep cycle marine trolling 12V battery was used to power both the laptop and the GPR console during data acquisition.
- Transmitting and receiving units were each powered by two 12V – 2.3AH rechargeable camcorder type batteries.
- A pulseEKKO 100/IV fiberglass antenna cart
- Odometer trigger wheel which attaches to antenna cart

Steps to Setup GPR System

- Build fiberglass antenna cart
- Attach antenna cart to car
- Attach antennae to antenna cart

- Attach transmitting and receiving modules to antennae (transmitting in front, receiving in back)
- Attach odometer trigger to GPR antenna cart
- Connect antennae modules and odometer trigger to GPR console using fiber optic cables
- Connect GPR console to Gateway Solo laptop computer with serial cable
- Connect manual trigger/sound box to GPR console
- Connect fast port to GPR console and laptop
- Connect GPR and laptop computer to deep cycle 12V battery
- Place 12V – 2.3AH batteries in transmitter and receiver and turn components on
- Turn on laptop and GPR console
- Start GPR software on laptop computer (note: computer and GPR system performed best when computer was run in DOS mode rather then in the windows environment)
- Test system by finding time zero with test shot
- Enter data which will define the GPR profile and mode of operation: Starting latitude and longitude, line name (road name), antenna separation, operation mode (reflection or CMP), number of stacks, time window, data output characteristics (wiggle trace, color, etc.)

Common Problems

Skipped Traces

A common problem we encountered while collecting our GPR data was skipped traces. This typically occurred when our speed exceeded approximately 6 kilometers per hour (4 mph). Traces were also skipped when the system trigger (odometer wheel) who sway excessively due to uneven road conditions or wind gusts. To correct for this common error in our data sets we used the processing software (WINEKKO Version 3) to fill gaps.

Dos Mode vs. Windows Environment

Early on in the collection of our GPR data it was noted that when attempting to use the "fast port" and operating the system software in the Windows environment (Windows 98 running Sensors & Software pulseEKKO V 4.22) the system was very prone to console errors that would force us to restart the system. This prevented the collection of GPR profiles of substantial length. Eventually it was realized that the software was much older then the operating system and ran smoother in a basic DOS environment rather then the Windows environment. Therefore, running the GPR operating software in the DOS environment allowed for the collection of long uninterrupted GPR profiles without the frequent console errors encountered early on in our data collection.

GPR Data Processing

Processing of the GPR data was intentionally limited due to the fact that interpretation did not require it. Yet in some instances some filters were applied in an attempt to enhance specific features. For instance, a background subtraction filter was at times applied that acted to enhance areas of increased depth of penetration. This filter did show these areas well, but in the end it was noted that the same interpretation could be made without the addition of the filter. The only filter that was consistently applied was made without the addition of the filter. The only filter that was consistently applied was the "dewow" filter, which acted to remove any low frequency "wow" from the data which may become superimposed on high frequency reflections.

GPR Data Analysis

Data analysis was done manually and consisted of looking at each GPR profile and placing specific sections along the profile into specific categories. The categories chosen for this interpretation are as follows:

1) Areas of significantly deep signal penetration (> then 9 m).
2) Areas of relatively deep signal penetration (> 5 m but < 9 m).
3) Areas of very shallow signal penetration, which signaled the presence of paleosol (generally 5 m or less).
4) Questionable area due to excessive noise or unclear reflection characteristics.

Once all of the profiles had been categorized data base file was created for each GPR profile, which contained the category codes and trace locations along each profile. Using this database file, the interpreted profiles could then be imported into ArcMap and joined with the corresponding profile line coverage and plotted on top of the digitized county soil surveys thus allowing for the visualizations presented in Chapter Two.

Appendix E

MATLAB SCRIPTS

Point Define Auto Script

In order to allow for the comparison of our GPR profiles with digitized county soil surveys we needed to create a way to digitize our GPR profiles trace by trace. What was developed was a MATLAB script entitled PointDefineAuto that took the GPR readings obtained in the field (start and end) and output a text file that contained an x,y location for every trace along the GPR profile. With this file, point coverages could be established in ARC GIS (Geographic Information System) for each GPR profile that would allow for it to be correctly plotted in space on top of the digitized soil surveys.

PointDefineAuto:

```
%MATLAB script that takes an input file containing start/end GPS pts, the number of
traces and a line ID %and creates an output file for a GPR profile that contains (x,y)
locations along that line at a set interval.

%Written February 2003
%George L. Bennett V

format long g;

[lineid,start_east,start_north,end_east,end_north,tracesbetween,flag,tracesafterend]=
textread('input.txt','%s %f %f %f %f %d %d %d');

dybetween = (start_north - end_north);   % Calculates the difference between start and
end northing
dxbetween = (start_east - end_east);     % Calculates the difference between start and
end easting

northing_step = dybetween/tracesbetween;   % Calculates the step interval
easting_step = dxbetween/tracesbetween;    % Calculates the step interval

true_disbetween = tracesbetween * .5;

m = ((end_north - start_north)/(end_east - start_east));
b = end_north - (m * end_east);
```

```
theta = atan(m);
opposite = ((sin(theta))*true_disbetween);
adjacent = ((cos(theta))*true_disbetween);

delnorth = (start_north - end_north);
calc_line_dis = abs(delnorth/sin(theta));
error = abs(calc_line_dis - true_disbetween);
out = [error,calc_line_dis,true_disbetween];
fid = fopen('input_err','w');
fprintf(fid, '%6.2f %6.2f %6.2f',out);
fclose(fid);

tracebetween = (1:tracesbetween)';

for n = (1:tracesbetween)                          % For loop that assigns a northing
for every trace
  northingbetween(n) = start_north - (northing_step*n);
end
for n = (1:tracesbetween)                          % For loop that assigns an easting
for every trace
    eastingbetween(n) = start_east - (easting_step*n);
end
northbetween = (northingbetween)';
eastbetween = (eastingbetween)';
finaloutbetween = [tracebetween,eastbetween,northbetween];
final = (finaloutbetween)';
fid = fopen('input','w');                        % opens file and creates it if it does not
already exist
fprintf(fid, '%6.5f\t %6.5f\t %6.5f\n',final);     % writes data to file
fclose(fid);                                   % closes file


% Calculates points after last know end point if flag is equal to 1
if flag == 1
  true_disafter = tracesafterend * .5;
  dxadj=(cos(theta)*(.5));
  dyopp=(sin(theta)*(.5));
  dxafterend = dxadj;
  dyafterend = dyopp;
  adjacentend=(cos(theta)*(true_disafter));
  tracesafterend = (1:tracesafterend)';
  if end_east > start_east
    eastingafter = (end_east+dxadj:dxadj:end_east+adjacentend);
    else
    east = (end_east-adjacentend:dxadj:end_east-dxadj);
    eastingafter = fliplr(east);
```

```
  end
y = (m * eastingafter) + b;
eastafter = (eastingafter)';
northafter = (y)';
finaloutafterend = [tracesafterend,eastafter,northafter];
finalafter = (finaloutafterend)';
fid = fopen('input2','w');          % opens file and creates it if it does not already exist
fprintf(fid, '%6.5f\t %6.5f\t %6.5f\n',finalafter);          % writes data to file
fclose(fid);                                                   % closes file
else
end
```

GPR2 Script

In an attempt to automate the process of interpreting our GPR profiles a MATLAB script was developed that attempted to pick the depth at which the GPR signal in each trace went to noise. The script would then mark this depth in each GPR trace and the values could then be connected to plot on top of the GPR profile showing locations of increased depth of penetration relative to areas in which the GPR signal had been attenuated. To do this a text file containing all of the numerical GPR data values was extracted from TRANSFORM (GPR data display program). This data was then normalized within MATLAB and a trace energy value was chosen that would correspond to the value at which the signal had gone to noise. Once the depth to noise values had been calculated the resulting information was smoothed using the loess (quadratic fit) smoothing function and the data were plotted on top of the GPR profiles. (See Chapter 3)

GPR2:

```
%MATLAB script that normalizes and reads each trace in a GPR profile and attempts to
define the point at %which the GPR signal goes to noise. Script then takes the depth to
noise values and smoothes this data %and plots it on top of the GPR data for comparison.


%Written September 2003
%Phanikumar Mantha & George L. Bennett V

function gpr2
epsilon=0.30;                       % Sets cutoff noise cutoff value
load input.txt;                      % Text file that contains numerical GPR data
a=input;
depth=a(:,1);                       % Identifies and labels depth values in the numerical
GPR data.
i_neg=max(find(depth < 0));
[nrow,ncol]=size(a);

% Truncates the negative depth values at the top of the file-------
for j=1:ncol
   temp=a(:,j);
```

```
    temp(1:i_neg,:)='';
    aa(:,j)=temp;
end
a=aa;
depth=a(:,1);
[nrow,ncol]=size(a);

for k = 2:ncol
  dist(k)=(k-1)*0.5;
end

ratio = max(dist)/max(depth);

% Normalizes GPR data
for i=2:ncol
     temp=a(:,i);
     amax=max(temp);
     amin=min(temp);
     diff=amax-amin;
     a_norm(:,i) = (temp - amin)./diff;
end

a_norm(:,1)=depth;

% Plots normalized GPR data
figure(2);
a_norm2=a_norm;
a_norm2(:,1)='';
h=imagesc(dist,depth,a_norm2);
colorbar;
hold on;

for j=2:ncol
   signal=a_norm(:,j);
   [ijk] = find_depth(signal,epsilon);
   icrit(j)=ijk;
end

for j=2:ncol
   if(isnan(icrit(j)))
      crit_depth(j) = nan;
   else
      crit_depth(j) = depth(icrit(j));
   end
end
```

```
crit_depth(1)=nan;
critd = flipud(crit_depth);
critd_smooth = smooth(dist,crit_depth,0.1,'loess');
cds = critd_smooth';
mat = [dist; cds]';
% save critd_smooth.txt cds -ASCII;
save critd_smooth.txt mat -ASCII;          % Saves smoothed data into text file

plot(dist,critd_smooth,'w-','linewidth',3);
ccd = crit_depth';
cds = critd_smooth';
save crit_depth.txt -ASCII  ccd;           % Saves crit_depth values to text file

% Plots GPR data which will be background for smoothed data.
figure(3)
h=imagesc(dist,depth,a_norm2);
colorbar;

function [icrit] =  find_depth(signal,epsilon)
nd=length(signal);

for i=40:nd
   if (signal(i) < epsilon)   icrit=i;
     return
   else
     icrit=nan;
   end
end
```

REFERENCES

REFERENCES

Annan, A.P., and Davis, J.L., 1977, Radar range analysis for geological materials: Report of Activities, Geological Survey of Canada, Paper 77-1B, pp. 117-124.

Arkley, R.J., 1962, The geology, geomorphology, and soils of the San Joaquin Valley in the vicinity of the Merced River, California: California Division of Mines and Geology, Bulletin 182, pp. 25-31.

Beres, M., Green, A., Huggenberger, P., and Horstmeyer, H., 1995, Mapping the architecture of glaciofluvial sediments with three-dimensional georadar: Geology, v. 23, pp. 1087-1090.

Beres, M., and Haeni, F.P., 1991, Application of ground-penetrating-radar methods in hydrogeologic studies: Ground Water, v. 29, pp. 375-386.

Burow, K.R., Weissmann, G.S., Miller, R.D., and Placzek, G., 1997, Hydrogeologic facies charaterization of an alluvial fan near Fresno, California, using geophysical techniques: U.S. Geological Survey Open-File Report 97-46.

Davis, J.L., and Annan, A.P., 1989, Ground-penetrating radar for high resolution mapping of soil and rock stratigraphy: Geophysical Prospecting, v. 37, pp. 531-551.

Haeni, F.P., McKeegan, D.K., and Capron, D.R., 1987, Ground-penetrating radar study of the thickness and extent of sediments beneath Silver Lake, Berlin and Meriden, Connecticut: U.S. Geological Survey Water Resources Investigation, v. 85-4108, 19 p.

Harden, J.W., 1987, Soils developed in granitic alluvium near Merced, California: United States Geological Survey Bulletin, v. 1590-A, 65 p.

Harter, T., Heeren, K., Weissmann, G.S., Horwath, W.R., and Hopmans, J., 1999, Field scale characterization of a heterogeneous, moderately deep vadose zone: The Kearney Research Site: Proceedings, Characterization and Measurement of the Hydraulic Properties of Unsaturated Porous Media, United States Salinity Laboratory, Riverside, California, pp. 415-426.

Harvey, A.M., 1989, The occurance and role of arid zone alluvial fans: *in* Thomas D.G. (ed.), Arid Zone Geomorphology: Halstead Press, Belhaven, pp. 136-158.

Helley, E.J., 1966, Sediment transport in the Chowchilla River Basin: Mariposa, Madera, and Merced Counties, California: Berkeley, University of California, Ph.D. thesis, 189 p.

Huggenberger, P., 1993, Radar facies: recognition of facies patterns and heterogeneities within Pleistocene Rhine gravels, NE Switzerland: Geological Society Special Publication, pp. 163-176.

Huntington, G.L., 1971, Soil survey, eastern Fresno area, California: U.S. Department of Agriculture, Soil Conservation Service, U.S. Government Printing Office, 323 p.

Huntington, G.L., 1980, Soil-land form relationships of portions of the San Joaquin River and Kings River alluvial depositional systems in the Great Valley of California [unpublished Ph.D. Dissertation]: University of California at Davis, 147 p.

Jakobsen, P.R., and Overgaard, T., 2002, Georadar facies and glaciotectonic structures in ice marginal deposits, northwest Zealand, Denmark: Quaternary Science Reviews, v. 21, pp. 917-927.

Janda, R.J., 1966, Pleistocene history and hydrology of the upper San Joaquin River, California: [unpublished Ph.D. Dissertation]: University of California, Berkeley, 293 p.

Janda, R.J., and Croft, M.G., 1967, The stratigraphic significance of a sequence of noncalcic brown soils formed on the Quaternary alluvium of the northeastern San Joaquin Valley, California: *in:* Quaternary Soils, International Association for Quaternary Research Congress, 7th, Reno, Nev., 1967, Proceedings, v. 9, pp. 158-190.

Jol, H.M., and Smith, D.G., 1991, Ground-penetrating radar of northern lacuatrine deltas: Canadian Journal of Earth Sciences, v. 28, pp. 1939-1947.

Jol, H.M., Young, R., Fisher, T.G., Smith, D.G., and Meyers, R.A., 1996, Ground penetrating radar of eskers, kame terraces, and moraines: Alberta and Saskatchewan, Canada: In: Proceedings Sixth International Conference on Ground Penetrating Radar., v. September 30-October 3, 1996, Sendai, Japan, pp. 167-172.

Jury, W.A., Gardner, W.R., and Gerdner, W.H., 1991, Soil Physics, 5th ed., John Wiley & Sons, Inc. New York, 328 p.

Lettis, W.R., 1982, Late Cenozoic stratigraphy and structure of the western margin of the central San Joaquin Valley, California: U.S. Geological Survey Open-File Report 82-526, 194 p.

Lettis, W.R., 1988, Quaternary geology of the Northern San Joaquin Valley: *in* Graham, S.A., ed., Studies of the Geology of the San Joaquin Basin: SEPM, Pacific Section, v. 60, pp. 333-351.

Lettis, W.R., and Unruh, J.R., 1991, Quaternary geology of the Great Valley, California: *in* Morrison R.B., ed., Quaternary Nonglacial Geology: Conterminous U.S.: Geological Society of America, Geology of North America, v. K-2, pp. 164-176.

Marchand, D.E., 1977, The Cenozoic history of the San Joaquin Valley and the adjacent Sierra Nevada as inferred from the geology and soils of the eastern San Joaquin Valley: *in* Singer, M.J., ed., Soil Development, Geomorphology, and Cenozoic History of the North-eastern San Joaquin Valley and Adjacent Areas, California: University of California Press. Guidebook for Joint Field Session, Soil Science Society of America and Geological Society of America, pp. 39-50.

Marchand, D.E., and Allwardt, A., 1981, Late cenozoic stratigraphic units, northeastern San Joaquin Valley, California: U.S. Geological Survey, Bulletin 1470, 70 p.

Mitchum, R.M., Jr., 1977, Seismic stratigraphy and global changes of sea level; part 11, Glossary of terms used in seismic stratigraphy *in* C.E. Payton, ed., Seismic stratigraphy- applications to hydrocarbon exploration: Memoir - American Association of Petroleum Geologists, v. 26, pp. 205-212.

Olhoeft, G.R., 1984, Applications and limitations of ground-penetrating radar [abs.]: Society of Exploration Geophysicists, 54th Annual International Meeting, Atlanta, GA, pp. 147-148.

Olhoeft, G.R., 1986, Direct detection of hydrocarbon and organic chemicals with ground-penetrating radar and complex resistivity: Proceedings of the NWWA Conference on Petroleum Hydrocarbons and Organic Chemicals in Ground Water, Houston, TX.

Olsen, H., and Andreasen, F., 1994, Sedimentology and ground-penetrating radar characteristics of a pleistocene sandur deposit.: Sedimentary Geology, v. 99, pp. 1-15.

Reynolds, J.M., 1997, An introduction to applied and environmental geophysics: New York, John Wiley and Sons Ltd, 690 p.

Sheriff, R.E., 1984, Encyclopedic dictionary of exploration geophysics, 2nd ed. Society of Exploration Geophysicists, Tulsa, OK. p. 323.

Smith, D.G., and Jol, H.M., 1992, Ground-penetrating radar investigation of a Lake Bonneville delta, Provo level, Brigham City, Utah: Geology, v. 20, pp. 1083-1086.

Stanistreet, I.G., and McCarthy, T.S., 1993, The Okavango Fan and the classification of subaerial fans: Sedimentary Geology, v. 85, pp. 114-133.

Ulriksen, P.F., 1982, Application of impulse radar to civil engineering. [Ph.D. thesis]: Lund, Sweden, Lund University of Technology.

Van Overmeeren, R.A., 1998, Radar facies of unconsolidated sediments in the Netherlands: a radar stratigraphic interpretation method for hydrogeology: Journal of Applied Geophysics, v. 40, pp. 1-18.

Weissmann, G.S., 1999, Toward new models of subsurface heterogeneity: an alluvial fan sequence stratigraphic framework with transition probability geostatistics: unpublished Ph.D. Dissertation, University of California, Davis, 279 p.

Weissmann, G.S., and Fogg, G.E., 1999, Multi-scale alluvial fan heterogeneity modeled with transition probability geostatistics in a sequence stratigraphic framework: Journal of Hydrology, v. 226, pp. 48-65.

Weissmann, G.S., Mount, J.F., and Fogg, G.E., 2002a, Glacially driven cycles in accumulation space and sequence stratigraphy of a stream dominated alluvial fan, San Joaquin Valley, California, U.S.A.: Journal of Sedimentary Research, v. 72, pp. 240-251.

Weissmann, G.S., Zhang, Y., LaBolle, E.M., and Fogg, G.E., 2002b, Dispersion of groundwater age in an alluvial aquifer system: Water Resources Research, v. 38, pp. 1198-1211.

Weissmann, G.S., Yong, Z., Fogg, G.E., and Mount, J.F., *in press*, Influence of incised valley fill deposits on hydrogeology of a glacially-influenced, stream-dominated alluvial fan, *in* Bridge, J., and Hyndman, D.W., Aquifer Characterization, SEPM Special Publication 80, publication expected Spring 2004.

Wright, D.L., Olhoeft, G.R., and Watts, R.D., 1984, Ground-penetrating radar studies on Cape Cop, *in* Neilsen, D.M., and Curl, M., eds., Surface Borehole Geophysical Methods in Groundwater Investigations: Worthington, Ohio, National Water Well Association, pp. 666-680.